Electronic Supplementary Information

Ruthenium complexes of redox non-innocent aryl-azo-oximes in catalytic α -alkylation of ketones and synthesis of 2-substituted quinolines

Supriyo Halder[a†], Srijita Naskar[a†], Debashis Jana[a], Gopal Kanrar[b], Kausikisankar Pramanik[a*], Sanjib Ganguly[b*]

[a]Department of Chemistry, Jadavpur University, Kolkata – 700032, India

[b]Department of Chemistry, St. Xavier's College (Autonomous), Kolkata – 700016, India

[†]Authors contributed equally to this work

kpramanik@hotmail.com   Tel: +91 33 2457 2781

*To whom correspondence should be addressed.

icsgxav@gmail.com   icsg@sxccal.edu   Tel: +91 33 2255 1266

Index

Table S1: Crystallographic details of **1a**, **2a**, **3a** and **4a**

	1a	2a	3a	4a
Empirical formula	$C_{50}H_{40}N_3ClO_2P_2Ru$	$C_{50}H_{39}N_3ClFO_2P_2Ru$	$C_{50}H_{38}N_3ClF_2O_2$ P_2Ru	$C_{50}H_{40}N_3ClO_3P_2Ru$
T/K	273.15	273.15	273.15	273.15
fw	913.35	931.30	949.29	929.31
Crystal system	Monoclinic	Monoclinic	Monoclinic	Monoclinic
Space Group	P 1 21 1	P 1 21/n 1	P 1 21/c 1	P 1 21/c 1
a/Å	11.0288(4)	10.5558(3)	12.2380(5)	20.1633(17)
b/Å	16.7801(6)	21.1187(7)	18.6710(7)	12.2066(10)
c/ Å	12.7714(4)	19.2437(6)	20.9395(8)	18.6526(16)
$α$/deg	90	90	90	90
$β$/deg	113.194(1)	94.6440(10)	99.9840(10)	109.084(3)
$γ$/deg	90	90	90	90
V/ Å³	2172.50(13)	4275.8(2)	4712.1(3)	4338.6(6)
Z	2	4	4	4
D_c/Mgm^{-3}	1.396	1.447	1.338	1.423
$μ$/mm^{-1}	0.540	0.553	0.506	0.543
F(000)	934.685	1904	1936	1904
cryst size/mm³	0.6×0.4×0.3	0.4×0.2×0.1	0.5×0.3×0.2	0.35×0.26×0.18
$θ$/deg	2.35–30.05	2.163–25.715	1.690–28.422	2.585–29.177
Measured reflns	41211	115966	160291	98620
Unique reflns	12639	8138	11794	11679
[a]GOF on F^2	1.027	1.249	1.142	1.086
R1[b], wR2[c][$I>2σ(I)$]	0.0296, 0.0722	0.0552, 0.0948	0.0496, 0.1068	0.0342, 0.0781
R1, wR2	0.0329, 0.0736	0.0655, 0.0989	0.0606, 0.1126	0.0460, 0.0887

[a]GOF = $\{\Sigma[w(F_o{}^2-F_c{}^2)2]/(n-p)\}^{1/2}$. [b]R1 = $\Sigma\ [|F_o|-|F_c|]/\ \Sigma\ |F_o|$.
[c]wR2 = $[\Sigma\ [w(F_o{}^2-F_c{}^2)^2]/\ \Sigma\ [w(F_o{}^2)^2]]^{1/2}$ where w = $1/[\ σ^2(F_o{}^2)+(aP)^2+bP]$, P = $(F_o{}^2+2F_c{}^2)/3$.

Table S2: Crystallographic and theoretical metrical parameters for complexes **1a**, **2a**, **3a**, **[3a]·⁻** and **4a**

Metrical Parameters	1a Expt.	1a Theo.	2a Expt.	2a Theo.	3a Expt.	3a Theo.	[3a]·⁻ Theo.	4a Expt.
Ru1–N1	2.0871(19)	2.132	2.083(3)	2.135	2.076(2)	2.140	2.144	2.0959(17)
Ru1–N3	2.0408(18)	2.089	2.052(3)	2.080	2.042(2)	2.103	2.147	2.0300(16)
Ru1–C1	1.881(2)	1.900	1.878(4)	1.903	1.881(3)	1.899	1.884	1.886(2)
Ru1–Cl1	2.4386(5)	2.519	2.4213(11)	2.528	2.4239(8)	2.515	2.554	2.4239(5)
Ru1–P1	2.4238(5)	2.502	2.4283(11)	2.515	2.4257(7)	2.507	2.475	2.4225(6)
Ru1–P2	2.4120(5)	2.520	2.4075(11)	2.512	2.4223(7)	2.538	2.514	2.4103(16)
N2–N3	1.317(3)	1.285	1.303(4)	1.282	1.301(3)	1.286	1.347	1.296(2)
N1–O2	1.274(3)	1.254	1.265(4)	1.257	1.267(3)	1.253	1.296	1.302(2)
C1–O1	1.148(3)	1.148	1.147(5)	1.147	1.139(4)	1.147	1.155	1.137(3)
C2 –N1	1.359(3)	1.359	1.349(5)	1.357	1.343(4)	1.354	1.362	1.337(3)
C2– N2	1.330(4)	1.350	1.352(5)	1.352	1.349(4)	1.342	1.318	1.364(3)
C9–N3	1.483(3)	1.436	1.445(5)	1.435	1.444(4)	1.435	1.395	1.448(2)
C2–C3	1.487(4)	1.479	1.475(5)	1.477	1.477(4)	1.482	1.488	1.482(3)
N1–Ru1–N3	76.34(8)	75.26	76.40(12)	75.33	76.20(9)	75.42	75.93	75.69(7)
N1–Ru1–P1	89.55(5)	88.72	88.55(9)	88.49	89.24(7)	89.32	89.44	89.75(5)
N1–Ru1–P2	85.85(5)	89.42	91.98(9)	88.59	90.63(6)	92.02	90.12	90.12(5)
N3–Ru1–P1	91.14(5)	92.88	89.41(9)	91.85	93.88(6)	93.34	90.79	91.77(5)
N3–Ru1–P2	91.22(5)	93.82	90.41(9)	91.55	92.42(6)	94.41	91.90	93.57(5)
C1–Ru1–Cl1	87.56(6)	89.10	88.59(13)	87.28	86.97(11)	90.34	88.73	87.58(6)
C1–Ru1–P1	93.73(6)	93.36	93.50(13)	94.57	91.99(9)	91.83	90.75	91.32(6)
C1–Ru1–P2	91.13(6)	89.21	85.96(13)	88.71	88.67(9)	87.58	89.78	89.34(6)
Cl1–Ru1–P1	86.272(19)	86.89	89.89(4)	86.13	86.70(3)	87.58	89.97	86.787(18)
Cl1–Ru1–P2	90.770(18)	85.93	90.39(4)	90.02	86.85(3)	84.65	87.16	87.741(17)
N1–Ru1–Cl1	97.11(6)	96.64	93.36(9)	97.98	97.72(7)	95.33	93.50	93.36(9)
N3–Ru1–C1	99.11(9)	98.97	101.66(15)	99.46	99.09(12)	98.87	101.82	97.93(5)
P1–Ru1–P2	174.190(18)	172.33	179.39(4)	174.81	173.48(3)	172.21	177.07	174.454(17)

Physical measurements:

NMR spectra (^{1}H, ^{13}C, ^{31}P and ^{19}F) of all complexes were obtained from Brucker FT 300 and 400 MHz spectrometer. Elemental analysis (C, H, N) was done on a Perkin Elmer 2400 series II Analyzer. Cyclic voltametric experiment was performed on BASi Epsilon-EC using dichloromethane/acetonitrile (9:1 v/v) solution containing 0.2M tetrabutylammonium

hexafluorophosphate as supporting electrolyte. Glassy Carbon electrode as working electrode, Platinum wire as Auxiliary Electrode and Ag/AgCl reference electrode were used for electrochemical experiment. Electron-transfer ability of the synthesized complexes were monitored by cyclic voltammetry in dichloromethane : acetonitrile (1:9 v/v) (supporting electrolyte is 0.2 M Bu_4NPF_6) by means of a glassy carbon working electrode and the reported potential is referenced to Ag/AgCl electrode.

Infrared spectra were acquired from PerkinElmer L-0010 spectrometer. The absorption spectra were recorded using PerkinElmer LAMDA 25 spectrometer with solute concentration about 10^{-5} M. Electron Paramagnetic Resonance (EPR) spectrum was taken for the sample in standard quartz EPR tubes using a JEOL JES-FA200 X-band spectrometer. Instrument settings: microwave frequency, 9.458 GHz; microwave power, 0.998 mW; modulation frequency, 100 kHz.

Table S3: Electrochemical data of Ru(II)-complexes with respect to Ag/AgCl

Complex	$E_{1/2}/V$ ($\Delta E^a/mV$)	
	Oxidation	**Reduction**
1a	+1.23(75^a)	-0.63 (E_p^2/V), -1.08 (E_p^2/V)
2a	+1.24(87^a)	-0.61(E_p^2/V), -1.09(E_p^2/V)
3a	+1.35(70)	-0.59 (110mV)V, -1.09(E_p^2/V)
4a	+1.16(116), 0.68(E_p^1/V)	-0.65(E_p^2/V), -0.97(E_p^2/V)
E_P^1 = anodic peak potential; E_p^2 = cathodic peak potential, ^{a}peak-to-peak separation		

X-Ray crystallography:

The suitable crystals of all complexes were placed on Bruker D8 QUEST SC-XRD Diffractometer equipped with graphite monochromator (Mo Kα, λ = 0.71073 Å) the crystals were kept at steady *T*= 273K during data collection. SAINT[1] crystallographic programme was utilized to integrate and scale the intensity data. SADABS[2] program was employed to process and rectify the integrated

data. Data collection, reduction, absorption corrections were performed. The structure solution was carried out with SHELXT 2014/5[3] solution programme using iterative method and Olex2 1.5-dev[4] as the graphical user interface. The SHELXL 2018/3[3] programme was utilised to refine the model structure using full matrix least square minimisation on F^2. Lastly, the consistency regarding thermal parameters, bond distances and estimated standard deviation (ESD) within respective atoms were accomplished using suitable commands in SHELXL programme. All non-hydrogen atoms were refined anisotropically. Riding model was applied to determine the position of H atoms geometrically and refined. ORTEP plot was used to draw the molecular structure using Olex2 1.5-dev as GUI. Crystallographic and refinement data of both complexes are given in Table S1. Additional refinement data can be found in CIF files.
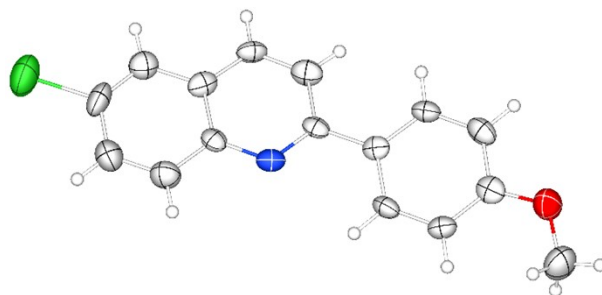
Figure S1: ORTEP view of **6-chloro-2-(4-methoxyphenyl)quinoline (10t)** (Thermal ellipsoids are set at 40% probability)
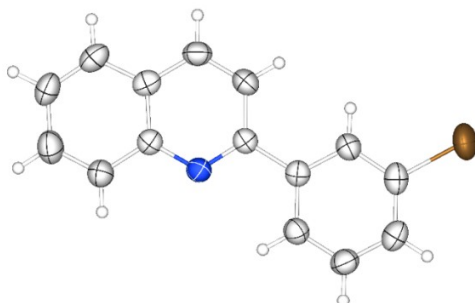
Figure S2: ORTEP view of **2-(3-bromophenyl)quinoline (10i)** (Thermal ellipsoids are set at 40% probability)

Computational Study:

The singlet ground state (S_0) and excited state molecular geometries of synthesised complex **1a**, **2a** and **3a** were computed by DFT method by employing (R)B3LYP[5,6] while for complex **[3a]**[•−] (U)B3LYP which is incorporated in GAUSSIAN 09[7] programme package. The solution phase optimised geometries of the complexes were found without applying any geometry constraints. In order to verify all stationary points as the true minima in potential energy surface, frequency calculation was executed. The absence of any imaginary frequency (NImag = 0) indicates that all the obtained stationary points are indeed the true minima in potential energy surface. The X-Ray positional coordinates of complex **1a**, **2a** and **3a** were directly used as the initial input for geometry optimisation calculation. By using these ground state optimised geometries as well as excited state geometries, we performed subsequent Single Point Energy and TD-DFT[8-11]calculation. In TD-DFT calculation we employ conductor like continuum model (CPCM) [12-14] and dichloromethane (CH_2Cl_2) as solvent to simulate absorption spectra in dichloromethane solvent. The lowest 100 singlet-singlet transitions in absorption and emission processes for the complex **1a**, **2a** and **3a** were evaluated gradually. The experimental results and the results obtained from TD calculations were qualitatively comparable. Presently the approach of TD-DFT is documented as a rigorous formalism for the -of electronic excitation energies among the DFT framework for calculating spectral properties of many transition metal complexes[15-18]. In order to acquire the information and nature of absorption and emission processes natural transition orbital (NTO) analysis was executed. This method delivers the most accurate representation of the transition density between the ground and excited states in terms of an expansion into single-particle transitions (hole and

electron states for each given excitation). we refer to the unoccupied and occupied NTOs as "electron" and "hole" transition orbitals. The computed vertical transitions were calculated at the equilibrium geometry of the S_0 state and described in terms of one-electron excitations of molecular orbitals of the corresponding S_0 geometry. The calculated transitions with moderate intensities ($f \geq 0.02$) can be envisaged going from the lower to the higher energy region of the spectrum. The rhodium atom was described by a double-ζ basis set with the effective core potential of Hay and Wadt (LANL2DZ)[19,20], and the 6-311++G(d,p)[21,22] basis set was used for the other elements except hydrogen atom (6-31G) present in the complexes to optimize the ground state geometries. The calculated electronic density plots for frontier molecular orbitals were prepared by using the GaussView 6.0 software. GaussSum program, version 3.2[23], was used to calculate the molecular orbital contributions from groups or atoms.
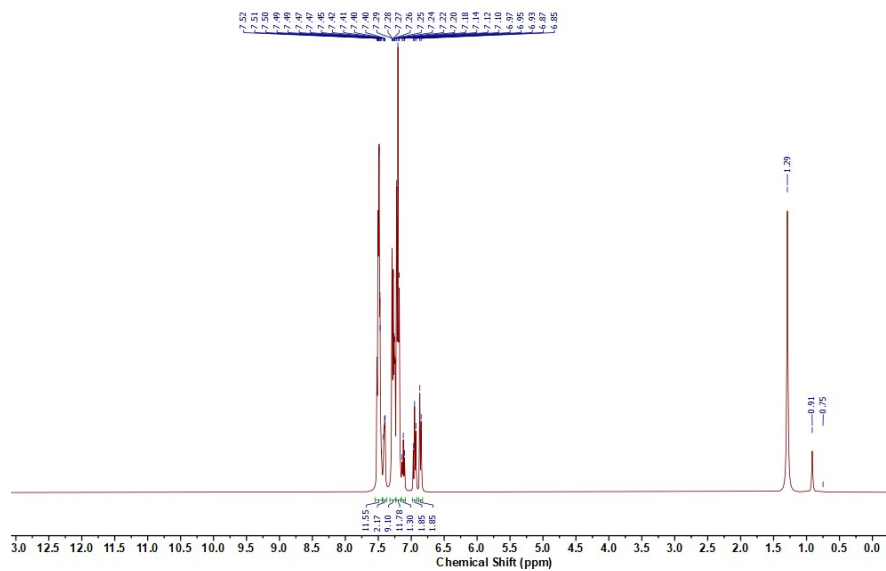
Figure S3: ^{1}H NMR spectrum of **1a**
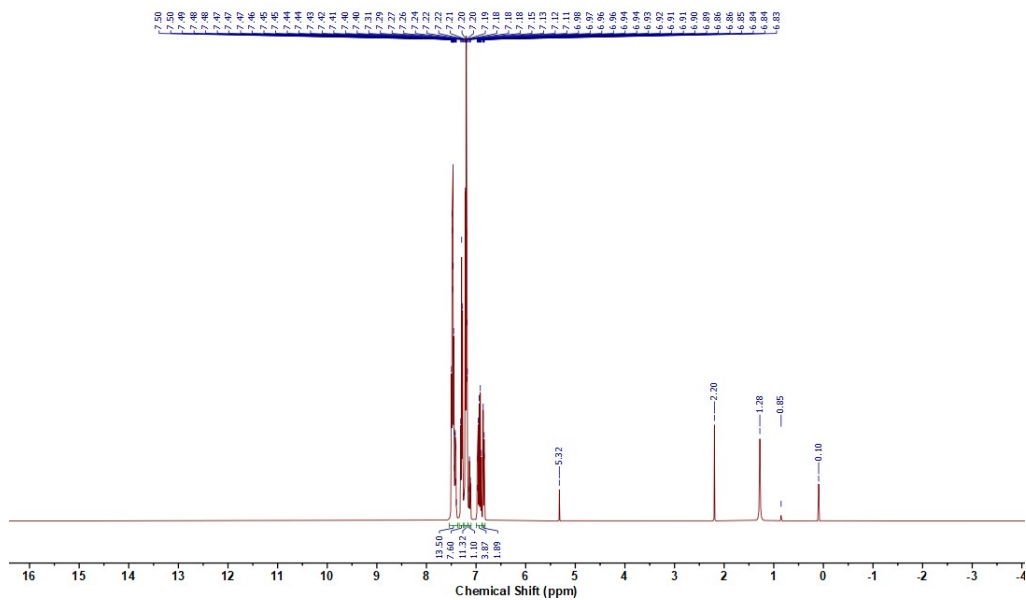
Figure S4: ^{1}H NMR spectrum of **2a**

S9
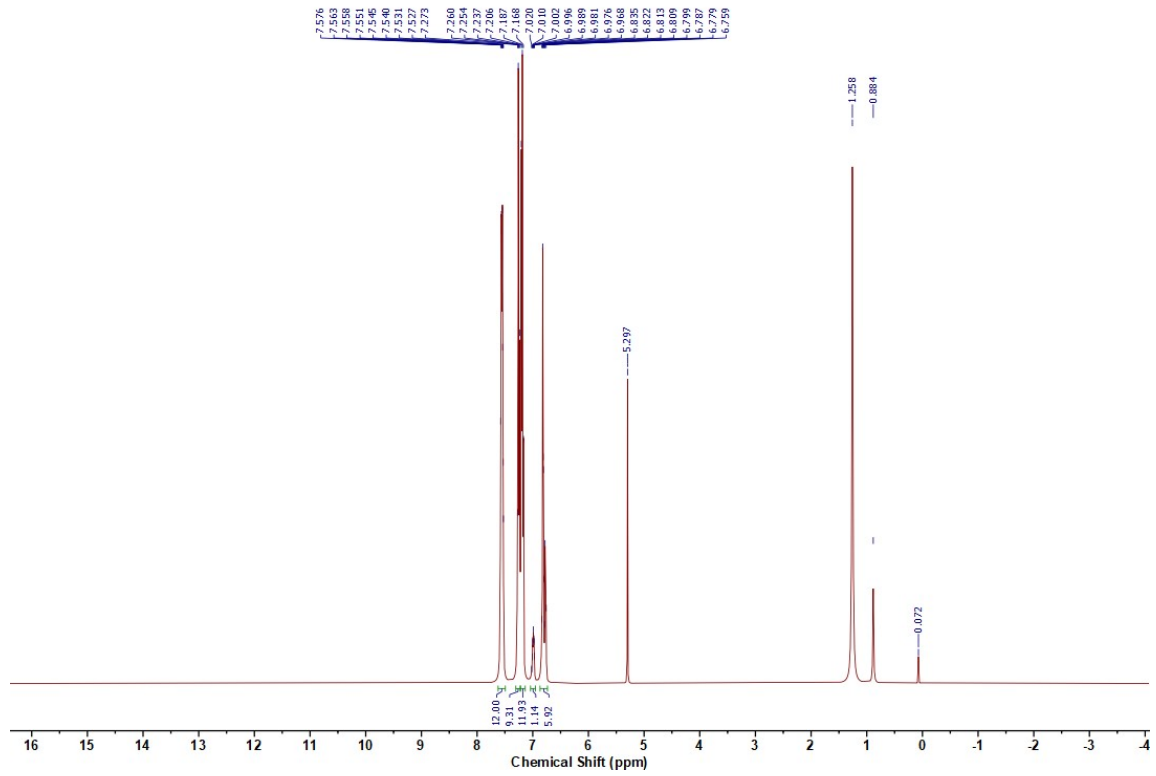
Figure S5: ^{1}H NMR spectrum of **3a**
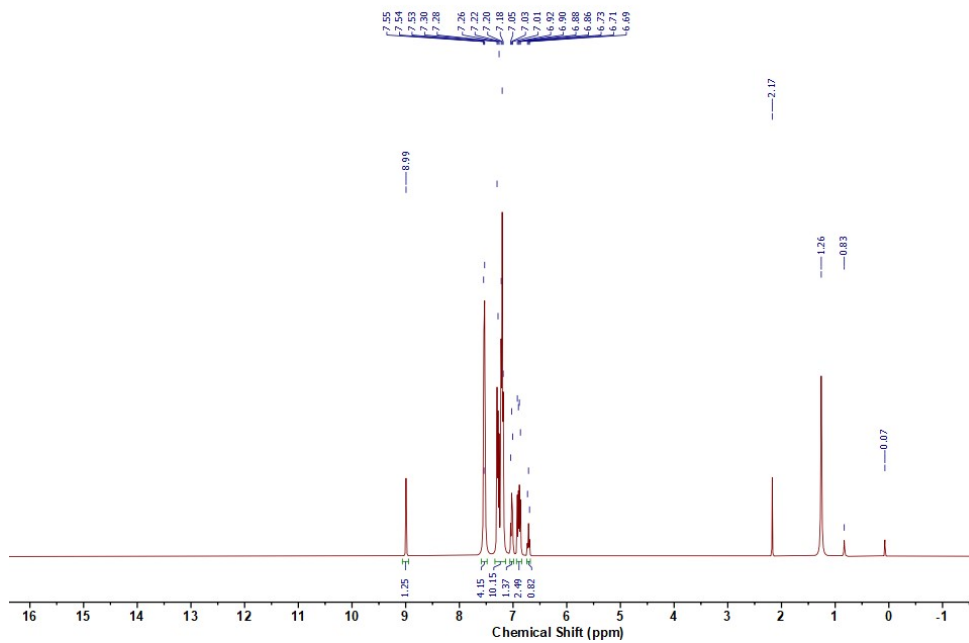
Figure S6: ^{1}H NMR spectrum of **4a**
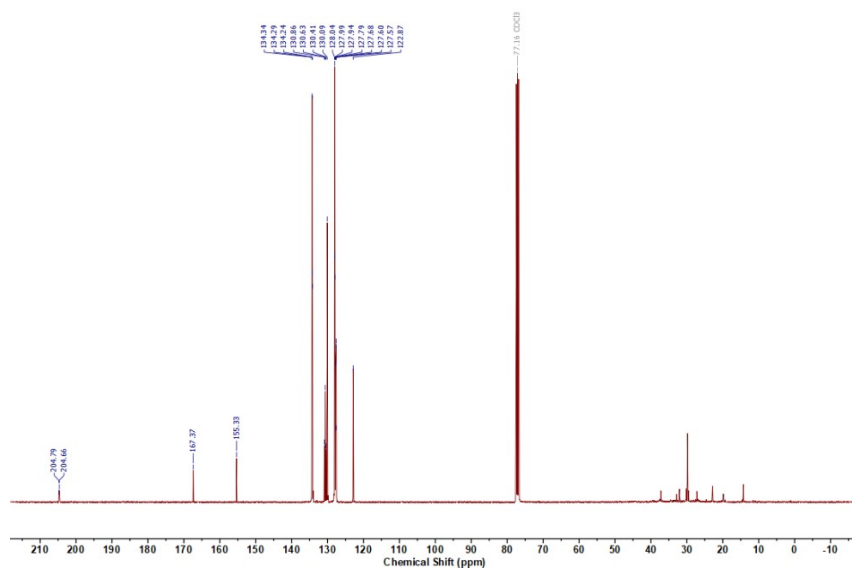
Figure S7: ^{13}C NMR spectrum of **1a**

S11
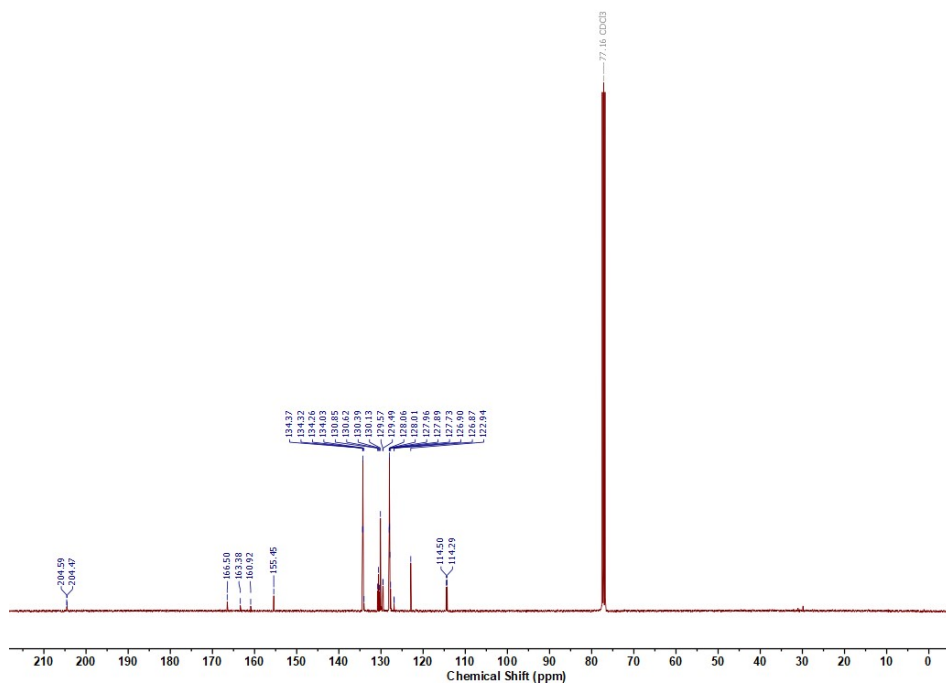
Figure S8: ^{13}C NMR spectrum of **2a**
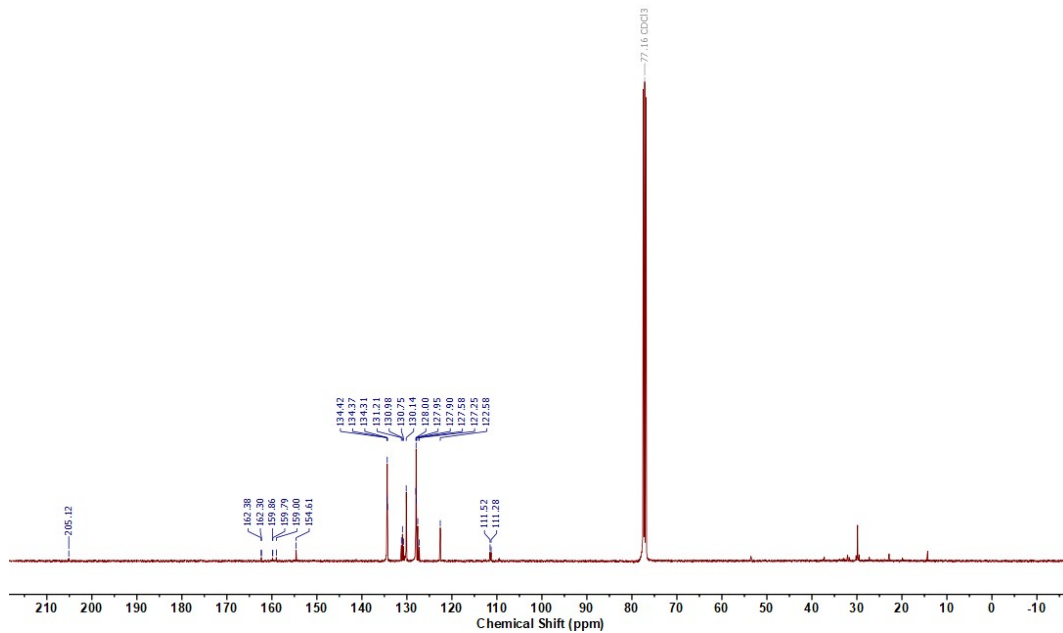
Figure S9: ^{13}C NMR spectrum of **3a**
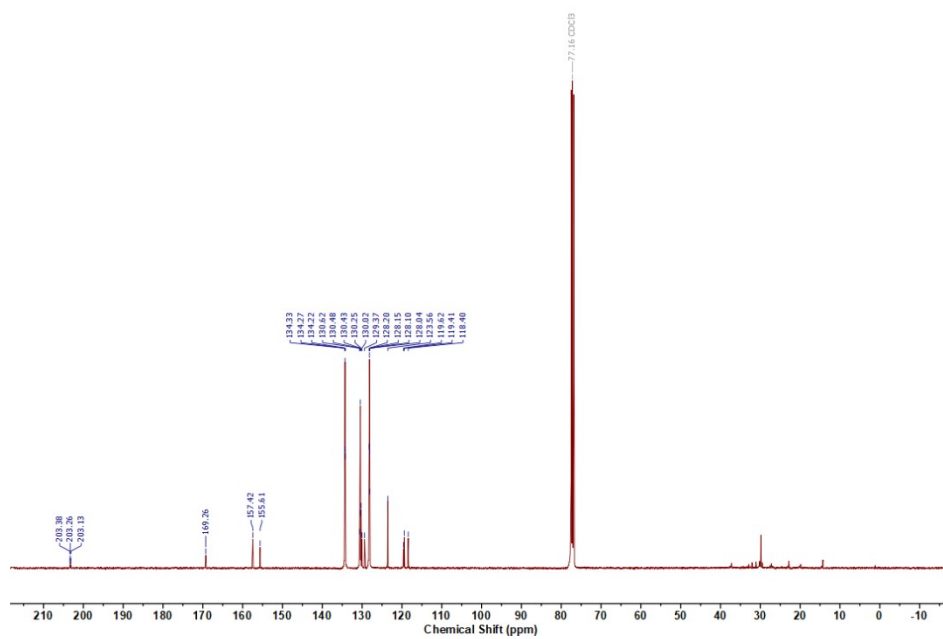
Figure S10: ^{13}C NMR spectrum of **4a**
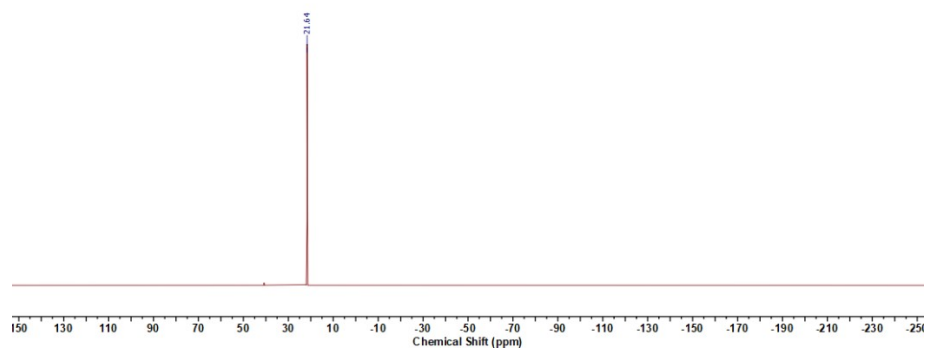
Figure S11: ^{31}P NMR spectrum of **1a**
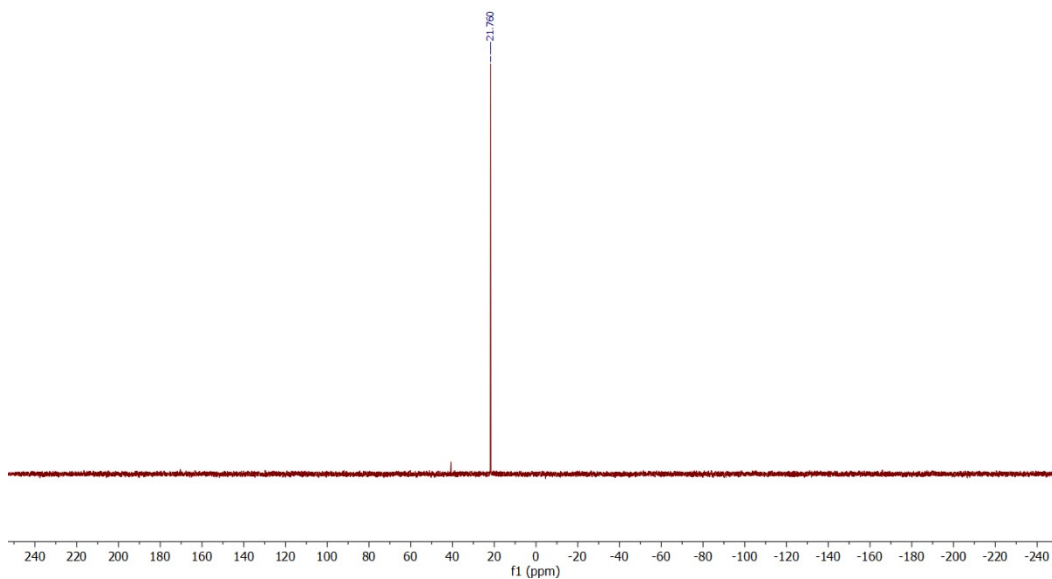
Figure S12: ^{31}P NMR spectrum of **2a**
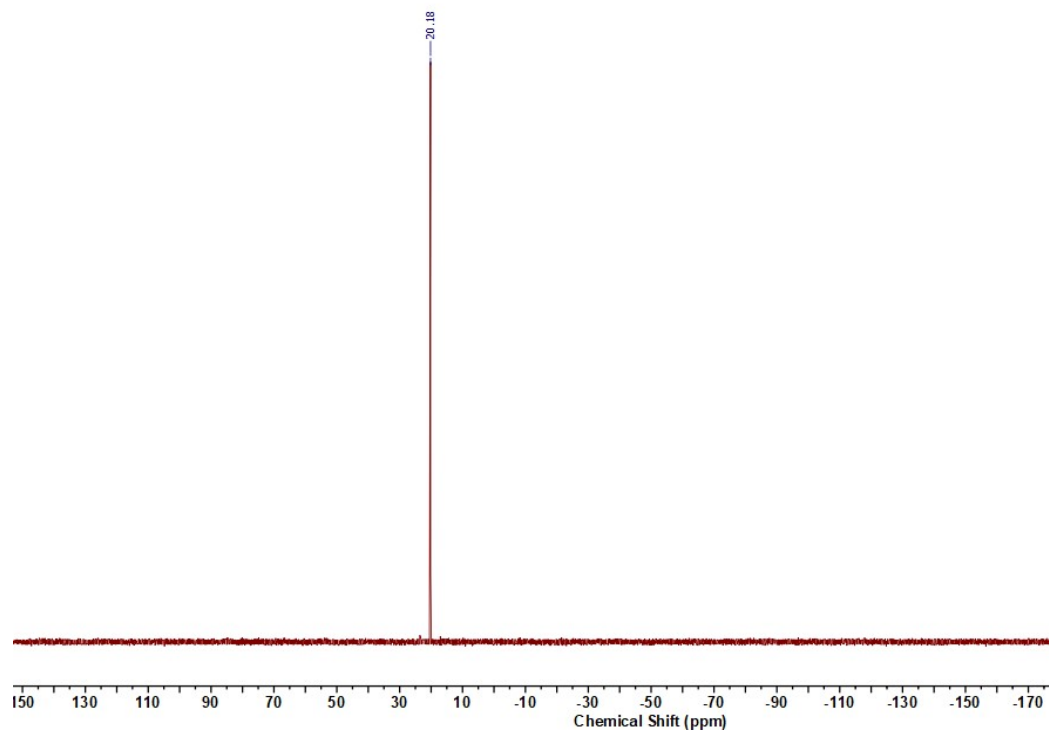
Figure S13: ^{31}P NMR spectrum of **3a**
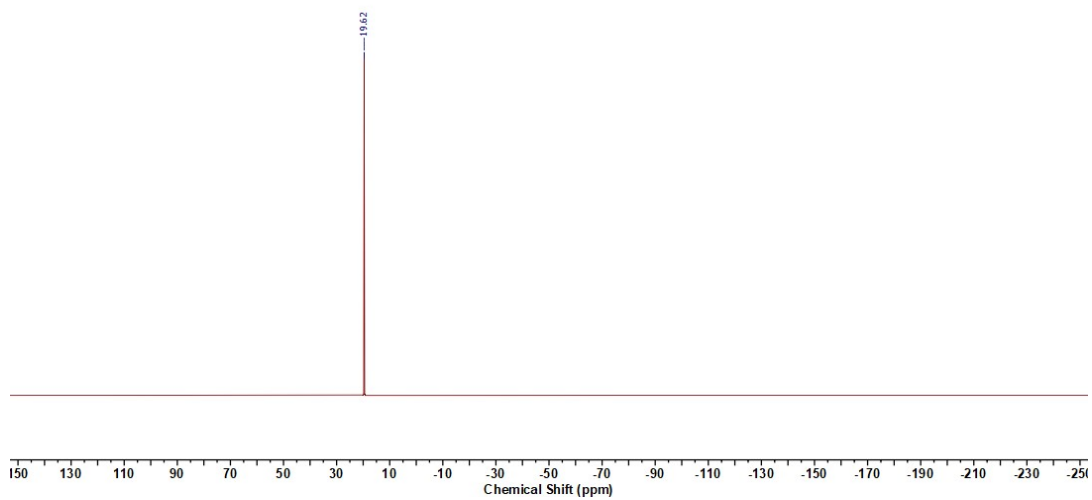
Figure S14: ^{31}P NMR spectrum of **4a**
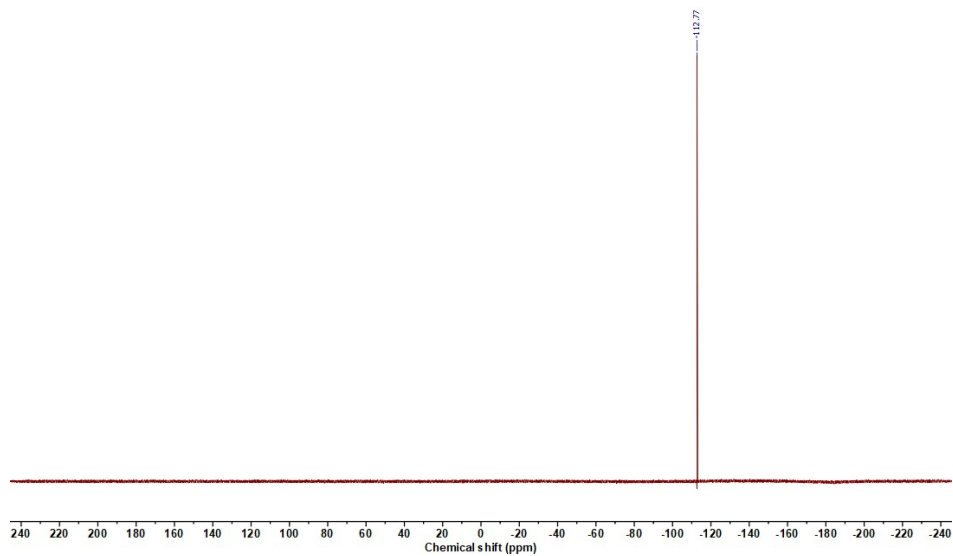
Figure S15: ^{19}F NMR spectrum of **2a**
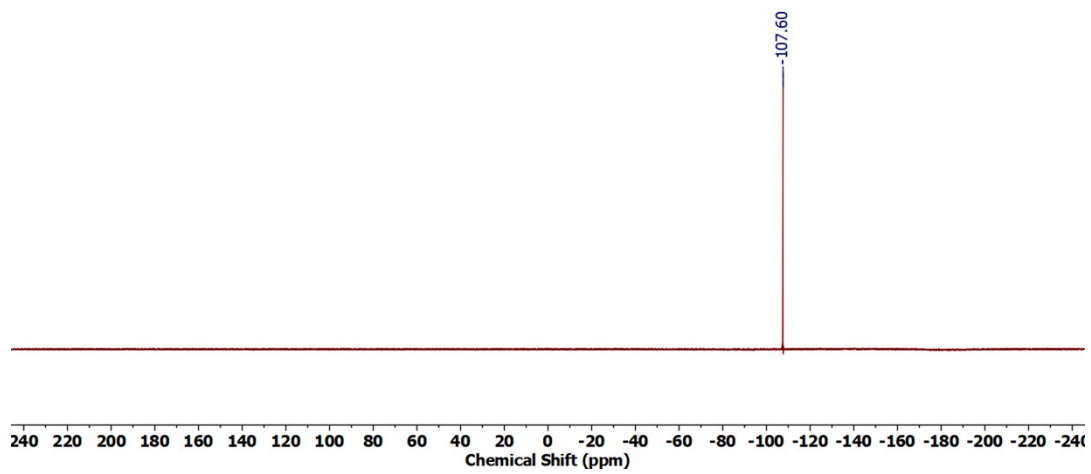
Figure S16: ^{19}F NMR spectrum of **3a**
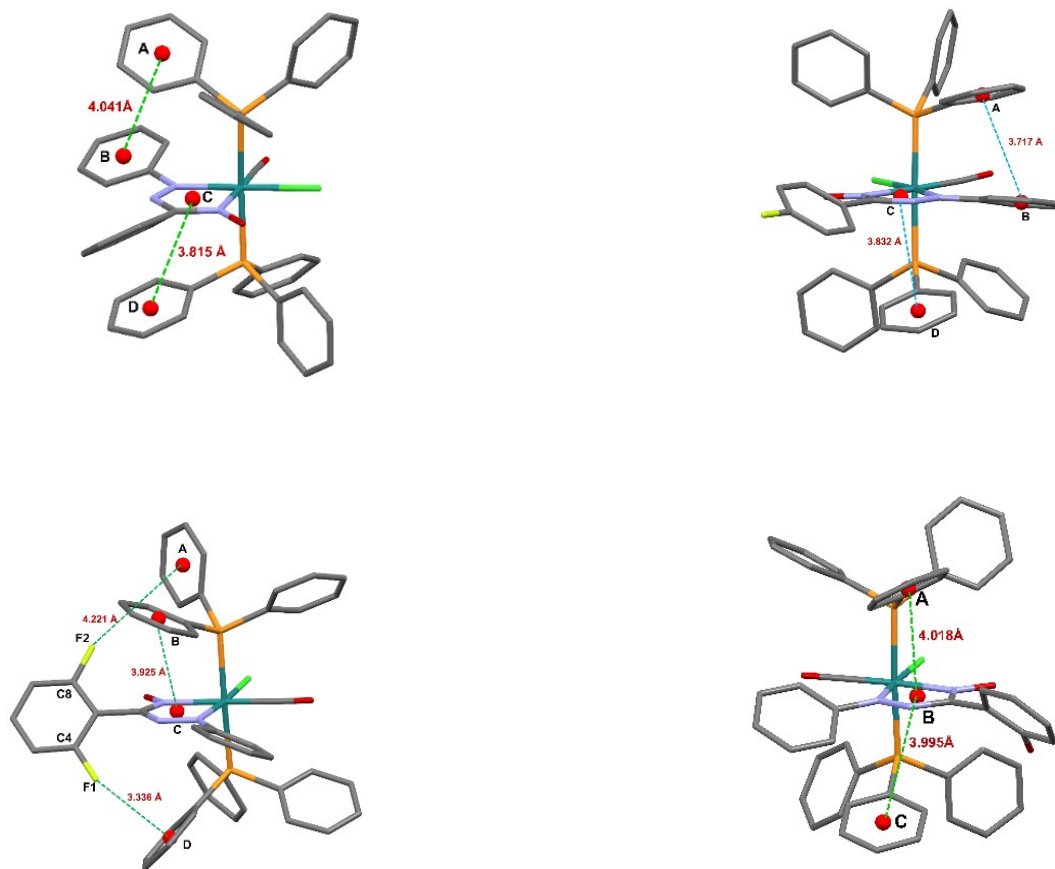
Figure S16: Intra-molecular π–π stacking and F–π interactions in the complex **1a, 2a, 3a** and **4a**

Table S4: Intra-molecular π-π stacking parameter* of **1a**

Stacking Parameters	Ring A–B	Ring C–D
d[$C_g(I) - C_g(J)$] Å/α°	4.041(3)/28.7(2)	3.815(2)/22.4(2)
d[$Cg(I) - R(J)$] Å/β°	3.575(2)/33.8	3.574(2)/40.6
d[$Cg(J) - R(I)$] Å/γ°	3.3597(17)/27.8	2.8973(14)/20.5

Table S5: Intra-molecular π-π stacking parameter* of **2a**

Stacking Parameters	Ring A–B	Ring C–D
d[$C_g(I) - C_g(J)$] Å/α°	3.717(3)/15.0(2)	3.832(2)/22.5
d[$Cg(I) - R(J)$] Å/β°	3.6640(19)/24.5	2.9612(13)/21.5

d[Cg(*J*) – R(*I*)] Å/γ˚	3.383(2)/9.7	3.566(2)/39.4

Table S6: Intramolecular π-π stacking parameter* of **3a**

Stacking Parameters	Ring B–C
d[C$_g$(*I*) – C$_g$(*J*)] Å/α˚	3.9251(19)/24.65(16)
d[Cg(*I*) – R(*J*)] Å/β˚	3.0073(10)/22.1
d[Cg(*J*) – R(*I*)] Å/γ˚	3.6371/40.0

Table S7: Intra-molecular π-π stacking parameter* of **4a**

Stacking Parameters	Ring A–B	Ring C–D
d[C$_g$(*I*) – C$_g$(*J*)] Å/α˚	4.0174(15)/23.29(12)	3.9945(15)/30.76(12)
d[Cg(*I*) – R(*J*)] Å/β˚	2.9498(8)/23.3	3.7882(12)/43.1
d[Cg(*J*) – R(*I*)] Å/γ˚	3.6899(12)/42.8	2.9184(8)/18.5

*C$_g$(*I*) = Centroid of ring *I*, C$_g$(*J*) = Centroid of ring *J*, d[C$_g$(*I*) – C$_g$(*J*)] = Separation between two ring centroids, d[Cg(*I*) – R(*J*)] = Perpendicular distance of Cg(*I*) on ring *J*, d[Cg(*J*) – R(*I*)] = Perpendicular distance of Cg(*J*) on ring *I*, α = Dihedral angle between Planes *I* of ring *I* and plane *J* of ring *J*, β and γ = Angle between the vector C$_g$(*I*) – C$_g$(*J*) and the normal to plane P(*I*) or P(*J*) from C$_g$(*I*) and C$_g$(*J*) respectively.

Table S8: Intramolecular F – π interaction parameter[a] of **3a**

Bond (X–Y)	d[(C$_g$(*I*) – Y]/Å	X–Y…C$_g$(*I*)/deg	d[X–C$_g$(*I*)]/ Å
C4–F1	3.336(3)	136.5(2)	4.405

[a]d[(Cg(*I*) – Y] = Distance between centroid of ring *I* (C$_g$) and Y, X–Y…C$_g$(*I*) = Angle between C$_g$-Y vector and ring *I* normal in degree, d[Y–C$_g$(*I*)] = Distance between centroid of ring *I* (C$_g$) and X
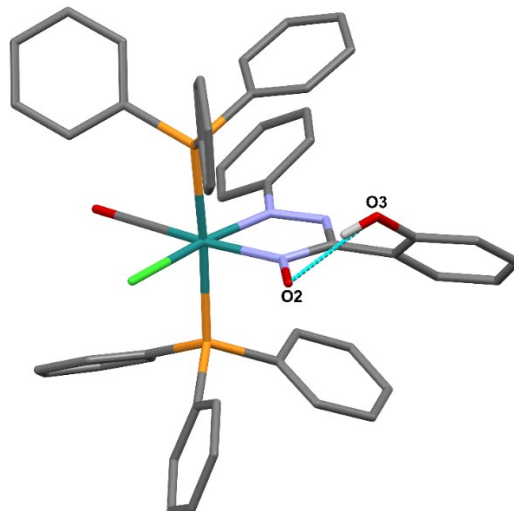
Figure S17: Intramolecular H-Bonding in **4a**

Table S9: Hydrogen bonding parameter of **4a**

Type of H-Bonding	Donor (D)	Acceptor (A)	D – A(Å)	D–H…..A(deg)
Intra-molecular	O3	O2	2.598(4)	155

Table S10: Frontier Molecular Orbital Composition (%) in the ground state for complex **1a**

Orbital	MO	Energy (eV)	Contribution (%)							Contribution
			Ru	Cl	CO	Azo	Oxime	Ph	PPh$_3$	
226	L+5	-0.92	4	1	2	0	2	9	83	π*(Oxime + PPh$_3$)
225	L+4	-0.98	1	0	1	1	1	4	91	π*(Ph + PPh$_3$)
224	L+3	-1.07	2	0	1	0	0	2	94	π*(PPh$_3$)
223	L+2	-1.09	3	0	3	0	4	11	79	π*(Ph + PPh$_3$)
222	L+1	-1.65	32	3	1	2	3	0	60	$d_{z^2} + \pi$*(PPh$_3$)
221	LUMO	-2.61	6	0	2	35	39	13	4	π*(Azo + Oxime + Ph)
220	HOMO	-5.51	14	5	0	11	38	30	3	$d_{xy} + \pi$ (Azo + Oxime + Ph)
219	H–1	-6.00	24	39	4	2	24	4	4	$d_{x^2-z^2} + \pi$ (Azo + Oxime + Ph)
218	H–2	-6.11	20	47	1	3	10	9	10	$d_{xz} + \pi$ (Cl + Azo + Oxime + Ph)
217	H–3	-6.34	9	31	5	3	48	3	2	$d_{xz} + \pi$ (Cl + Ph)
216	H–4	-6.51	13	1	0	3	1	7	76	$d_{xz} + \pi$ (Ph + PPh$_3$)
215	H–5	-6.80	0	2	0	2	1	89	6	π (Ph + PPh$_3$)

Table S11: Frontier Molecular Orbital Composition (%) in the ground state for complex **2a**

Orbital	MO	Energy (eV)	Contribution (%)							Contribution
			Ru	Cl	CO	Azo	Oxime	Ph	PPh$_3$	
230	L+5	-0.99	9	2	3	2	8	31	46	$d_{x^2-z^2} + \pi^*$(Oxime +Ph + PPh$_3$)
229	L+4	-1.01	2	0	2	0	1	2	93	π^*(PPh$_3$)
228	L+3	-1.13	2	0	2	2	0	4	95	π^*(PPh$_3$)
227	L+2	-1.25	0	0	2	1	1	0	96	π^*(PPh$_3$)
226	L+1	-1.71	32	3	2	3	1	0	60	$d_{z^2} + \pi^*$ (PPh$_3$)
225	LUMO	-2.69	6	0	2	35	38	15	4	π^*(Azo + Oxime + Ph)
224	HOMO	-5.58	14	5	0	10	38	30	3	$d_{xz} + \pi$ (Azo + Oxime + Ph)
223	H–1	-6.08	25	42	4	2	19	4	6	$d_{xy} + \pi$ (Azo + Oxime + Ph)
222	H–2	-6.14	20	44	2	3	15	7	10	$d_{yz} + \pi$ (Cl + Oxime + Ph + PPh$_3$)
221	H–3	-6.46	8	29	6	3	51	2	2	$d_{yz} + \pi$ (Cl + CO + Oxime + Ph)
220	H–4	-6.62	13	0	0	3	1	8	74	$d_{xy} + \pi$ (Ph + PPh$_3$)
219	H–5	-6.89	0	0	0	0	0	3	96	π (PPh$_3$)

Table S12: Frontier Molecular Orbital Composition (%) in the ground state for complex **3a**

Orbital	MO	Energy (eV)	Contribution (%)							Contribution
			Ru	Cl	CO	Azo	Oxime	Ph	PPh$_3$	
230	L+5	-0.90	1	1	2	0	4	8	84	π^*(PPh$_3$)
229	L+4	-0.95	3	0	1	1	6	31	60	π^*(Ph + PPh$_3$)
228	L+3	-1.04	4	0	3	1	2	25	64	$d_{x^2-z^2} + \pi^*$(Ph + PPh$_3$)
227	L+2	-1.09	0	0	2	1	1	4	92	π^*(PPh$_3$)
226	L+1	-1.63	35	4	1	3	2	0	57	$d_{z^2} + \pi^*$(PPh$_3$)
225	LUMO	-2.62	6	0	2	34	39	14	4	$d_{xz} + \pi^*$(Azo + Oxime + Ph)
224	HOMO	-5.68	23	12	0	11	34	16	3	$d_{xz} + \pi$ (Cl + Azo + Oxime + Ph)
223	H–1	-6.10	27	43	5	1	20	0	3	$d_{xz} + \pi$ (Cl + CO + Oxime)
222	H–2	-6.17	10	43	0	4	11	13	19	$d_{yz} + \pi$ (Cl + Azo + Oxime + Ph)
221	H–3	-6.43	6	21	5	4	59	1	4	$d_{xz} + \pi$ (Cl + Oxime)
220	H–4	-6.50	14	2	0	3	2	6	73	$d_{xz} + \pi$ (PPh$_3$)
219	H–5	-6.78	1	0	0	0	1	2	96	π (PPh$_3$)

Table S13: Frontier Molecular Orbital Composition (**α-MO**) (%) in the ground state for complex [**3a**]$^{\cdot-}$

Orbital	MO	Energy (eV)	Contribution (%)							Contribution
			Ru	Cl	CO	Azo	Oxime	Ph	PPh$_3$	
235	L+5	1.55	2	0	0	2	1	26	69	π*(Ph + PPh$_3$)
234	L+4	1.46	4	0	0	0	1	0	97	π*(PPh$_3$)
233	L+3	1.44	1	0	0	0	3	0	98	π*(PPh$_3$)
232	L+2	1.34	2	0	1	0	1	1	95	π*(PPh$_3$)
231	L+1	1.20	0	0	0	0	0	1	99	π*(PPh$_3$)
230	LUMO	1.04	24	2	1	1	1	0	72	d_{z^2} + π*(PPh$_3$)
229	HOMO	-1.01	6	0	1	35	34	21	3	d_{xz} + π (Azo + Oxime + Ph)
228	H–1	-2.63	13	3	1	13	41	26	3	d_{yz} + π (Azo + Oxime + Ph)
227	H–2	-2.94	7	3	5	2	80	1	1	d_{yz} + π (CO + Oxime)
226	H–3	-3.30	33	45	2	2	3	11	4	d_{xz} + π (Cl + Oxime + Ph)
225	H–4	-3.36	38	47	6	2	4	1	1	d_{xz} + π (Cl + CO)
224	H–5	-3.99	15	5	0	2	1	13	66	d_{xy} + π (Cl + Ph + PPh$_3$)

Table S14: Frontier Molecular Orbital Composition (**β-MO**) (%) in the ground state for complex [**3a**]$^{\cdot-}$

Orbital	MO	Energy (eV)	Contribution (%)							Contribution
			Ru	Cl	CO	Azo	Oxime	Ph	PPh$_3$	
234	L+5	1.47	5	1	0	0	2	1	92	π*(PPh$_3$)
233	L+4	1.44	1	0	0	0	3	0	98	π*(PPh$_3$)
232	L+3	1.36	2	0	1	1	4	2	91	π*(PPh$_3$)
231	L+2	1.22	2	0	1	8	9	7	73	π*(Oxime + PPh$_3$)
230	L+1	1.16	6	1	3	11	16	7	56	π*(Azo + Oxime + PPh$_3$)
229	LUMO	1.00	18	1	1	8	9	5	58	d_{z^2} + π*(Azo + Oxime + PPh$_3$)
228	HOMO	-2.03	8	1	0	22	34	33	2	d_{xz} + π (Azo + Oxime + Ph)
227	H–1	-2.71	6	2	6	2	82	0	1	d_{yz} + π (Oxime)
226	H–2	-3.35	41	43	1	2	3	5	5	d_{yz} + π (Cl)
225	H–3	-3.93	40	49	7	2	2	0	1	d_{xz} + π (Cl + CO)
224	H–4	-3.95	0	10	2	47	16	16	15	d_{yz} + π (Cl + Azo + Oxime + Ph)
223	H–5	-3.93	8	6	1	14	1	25	44	d_{xy} + π (Cl + Azo + Ph + PPh$_3$)
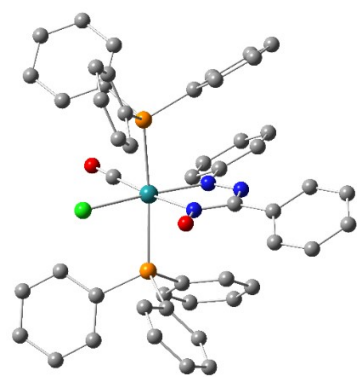
1a
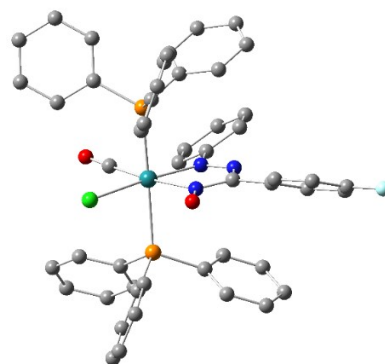
2a
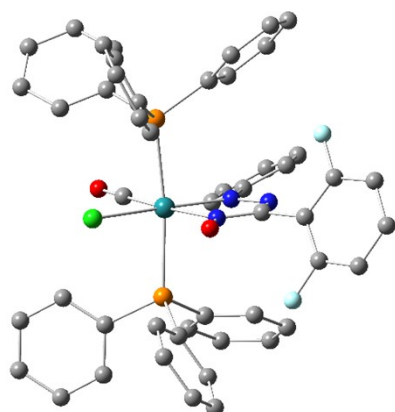
3a
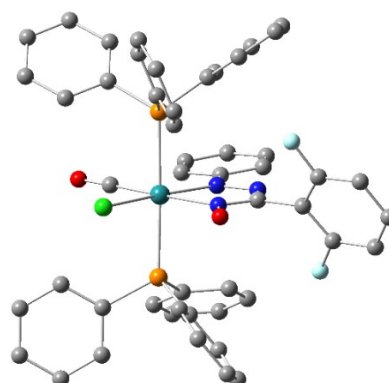
[3a]·⁻

Figure S18: Optimized geometry of **1a**, **2a**, **3a** and [**3a**]·⁻ calculated at B3LYP/6-311+G(d,p) level of theory.
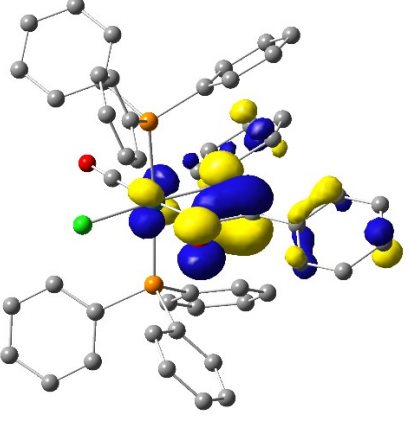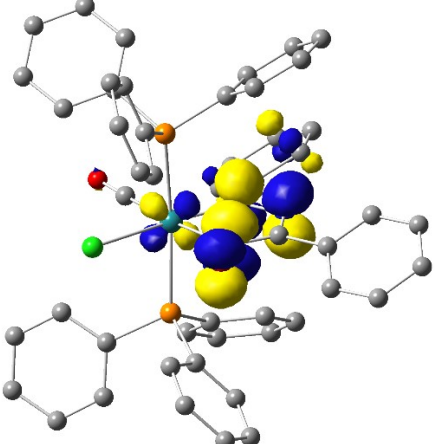
Table S15. Main Optical Transition at the TD-DFT/B3LYP/6-311+G(d,p) Level for the complex **1a** with composition in terms of Molecular Orbital Contribution of the Transition, Computed Vertical Excitation Energies, and Oscillator Strength in Dichloromethane.

Transition	CI	Composition	E (eV)	Oscillator strength (f)	λ_{theo} (nm)
$S_0 \rightarrow S_2$	0.63328	HOMO → LUMO (80%)	2.4871	0.0766	498.50

$S_0 \rightarrow S_5$	0.63410	H—2 → LUMO (80%)	2.9774	0.1186	416.41
$S_0 \rightarrow S_{27}$	0.49547	H—3 → L+1 (49%)	4.0853	0.3764	303.48
$S_0 \rightarrow S_{83}$	0.32198	H—4 → L+4 (21%)	5.0059	0.0743	247.67

Table S16. Main Optical Transition at the TD-DFT/B3LYP/6-311+G(d,p) Level for the complex **2a** with composition in terms of Molecular Orbital Contribution of the Transition, Computed Vertical Excitation Energies, and Oscillator Strength in Dichloromethane.

Transition	CI	Composition	E (eV)	Oscillator strength (f)	λ_{theo} (nm)
$S_0 \rightarrow S_2$	0.62095	HOMO → LUMO (77%)	2.4822	0.0634	499
$S_0 \rightarrow S_4$	0.53343	H—4 → LUMO (57%)	2.8956	0.0221	428
$S_0 \rightarrow S_6$	0.67492	H—3 → LUMO (91%)	3.1515	0.0294	393
$S_0 \rightarrow S_{27}$	0.39175	H—3 → L+1 (31%)	4.1194	0.2933	300
$S_0 \rightarrow S_{82}$	0.41354	H—3 → L+4 (34%)	5.0202	0.0454	246

Table S17. Main Optical Transition at the TD-DFT/B3LYP/6-311+G(d,p) Level for the complex **3a** with composition in terms of Molecular Orbital Contribution of the Transition, Computed Vertical Excitation Energies, and Oscillator Strength in Dichloromethane.

Transition	CI	Composition	E (eV)	Oscillator strength (f)	λ_{theo} (nm)
$S_0 \to S_2$	0.62256	HOMO → LUMO (78%)	2.5432	0.0612	487.51
$S_0 \to S_5$	0.62859	H—2 → LUMO (79%)	3.0510	0.1255	406.37
$S_0 \to S_{24}$	0.34323	H—2 → L+1 (24%)	4.0279	0.3605	307.81
	0.40551	H—3 → L+1 (33%)			
$S_0 \to S_{73}$	0.32840	H—4 → L+2 (22%)	4.9841	0.0193	248.75

Table S18. Natural transition orbitals (NTOs) for complex **1a** illustrating the nature of singlet excited states in the absorption bands in the range 200–700 nm. For each state, the respective number of the state, transition energy (eV), and the oscillator strength (in parentheses) are listed. Shown are only occupied (holes) and unoccupied (electrons) NTO pairs that contribute more than 15% to each excited state.

		Hole	Electron
534 nm	S_2 w = 0.8020 2.4871 (0.0766) 498.50 nm ILCT & d-d π (Azo + Oxime) → π^* (Azo + Oxime) & $d_{xz} \to d_{yz}$		
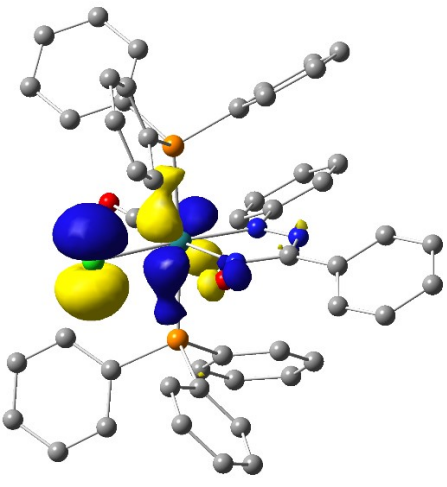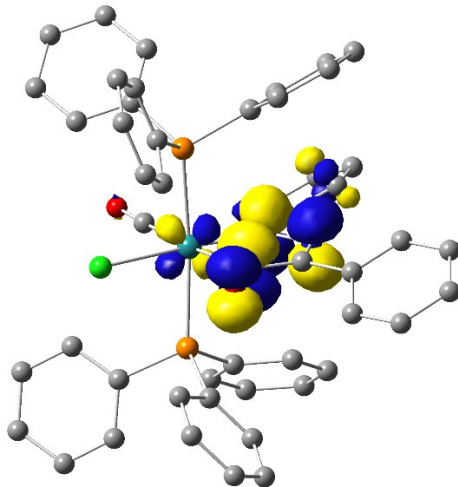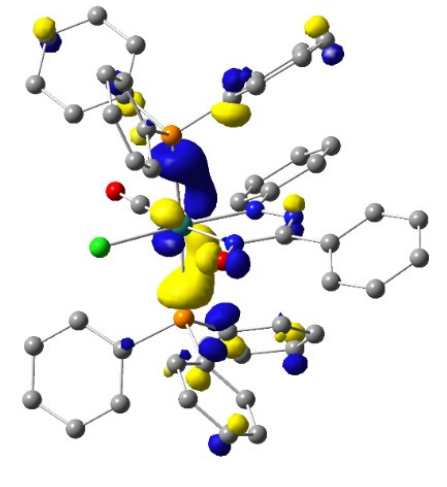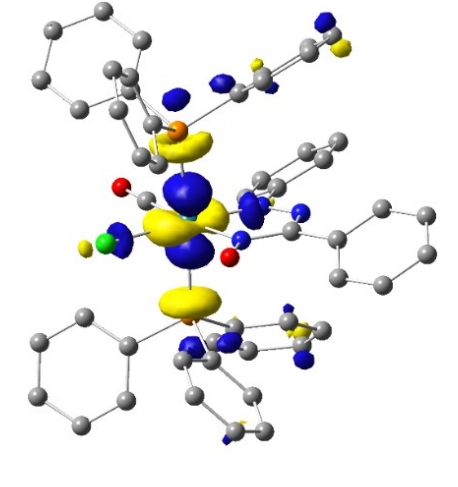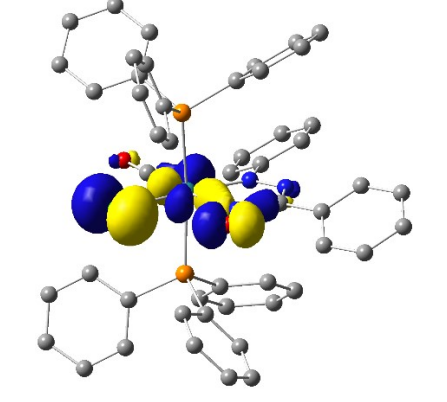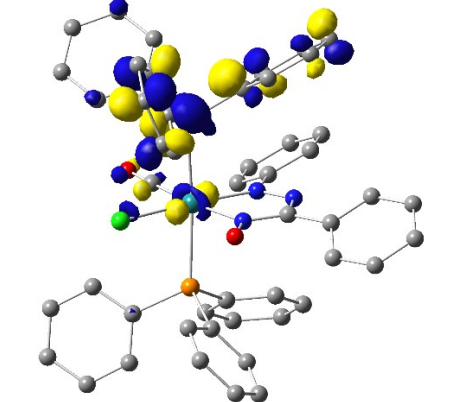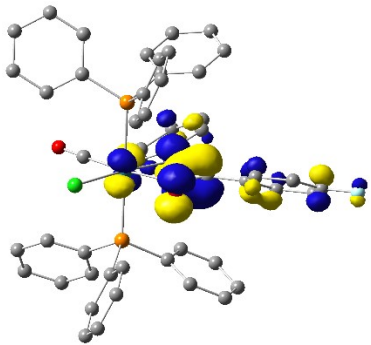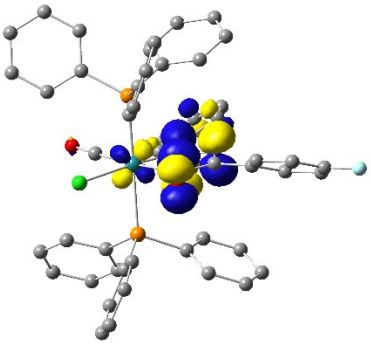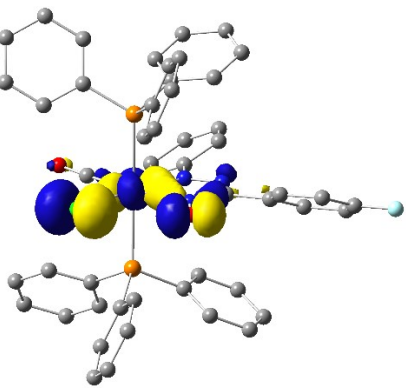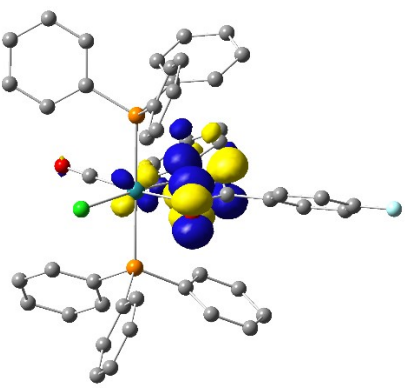
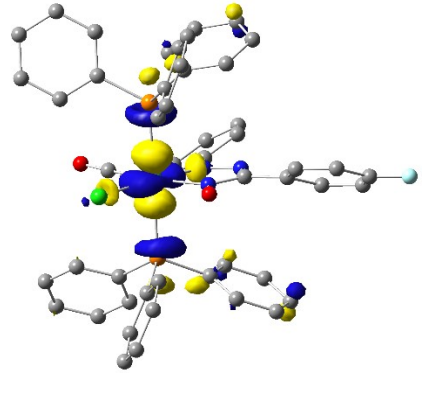|			
419 nm	S_5 w = 0.8041 2.9774 (0.1186) 416.41 nm LLCT & d-d π (Cl) $\rightarrow$ π^* (Azo + Oxime) & $d_{xz} \rightarrow d_{yz}$		
277 nm	S_{27} w = 0.4909 4.0853 (0.3764) 303.48 nm ILCT, LLCT & d-d π (PPh$_3$) $\rightarrow$ π^* (Cl+ PPh$_3$) & $d_{yz} \rightarrow d_z^2$		
232 nm	S_{83} w = 0.2073 5.0059 (0.0743) 247.67 nm LLCT & d-d π (Cl + Oxime) $\rightarrow$ π^* (PPh$_3$) & $d_{x^2-z^2} \rightarrow d_{xz}$		

Table S19. Natural transition orbitals (NTOs) for complex **2a** illustrating the nature of singlet excited states in the absorption bands in the range 200–700 nm. For each state, the respective number of the state, transition energy (eV), and the oscillator strength (in parentheses) are listed. Shown are only occupied (holes) and unoccupied (electrons) NTO pairs that contribute more than 15% to each excited state.

		Hole	Electron
528 nm	S_2 w = 0.7711 2.4822 (0.0634) 499.49 nm ILCT & d-d π (Azo + Oxime + Ph) → π* (Azo + Oxime) & d_{xz} → d_{yz}		
420 nm	S_4 w = 0.5689 2.8956 (0.0221) 428.18 nm ILCT & d-d π (Cl + Oxime) → π* (Azo + Oxime + Ph) & $d_{x^2-y^2}$ → d_{yz}		
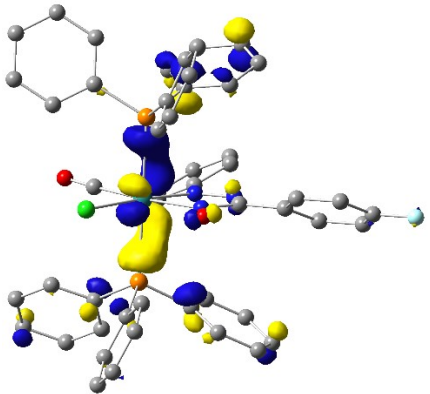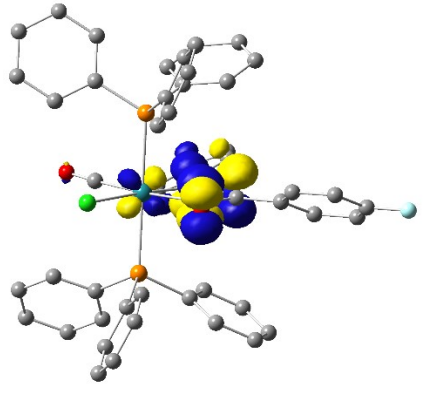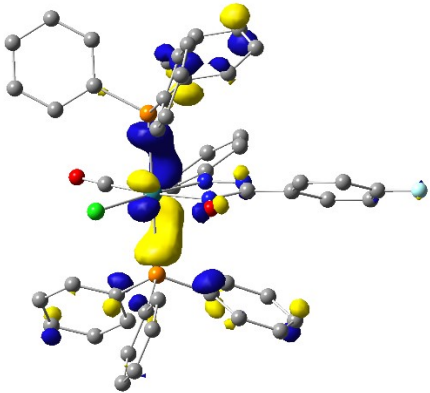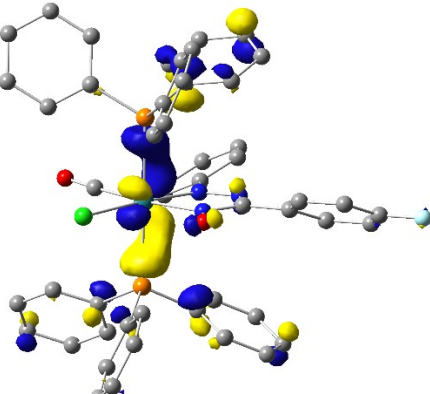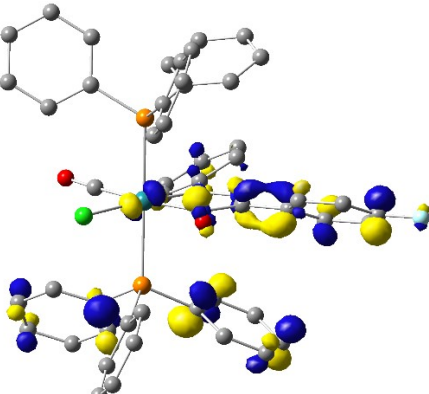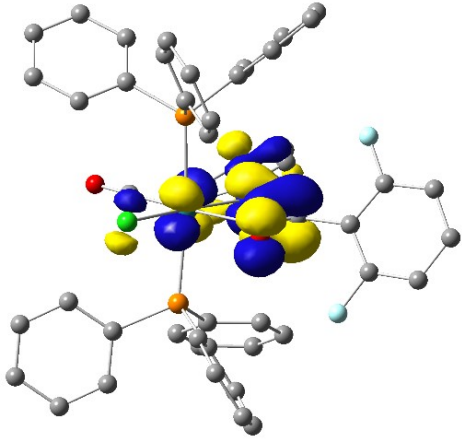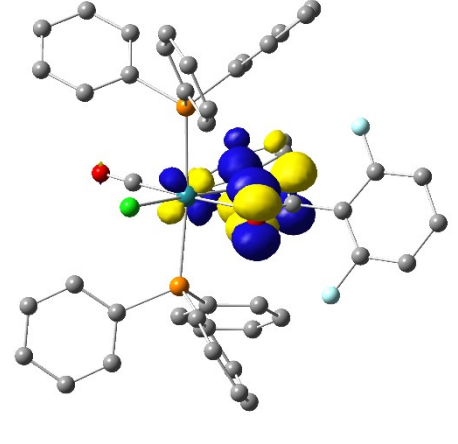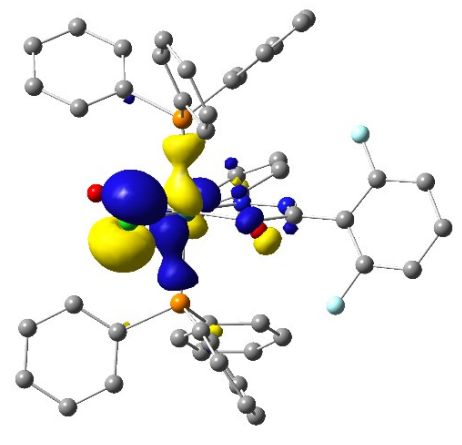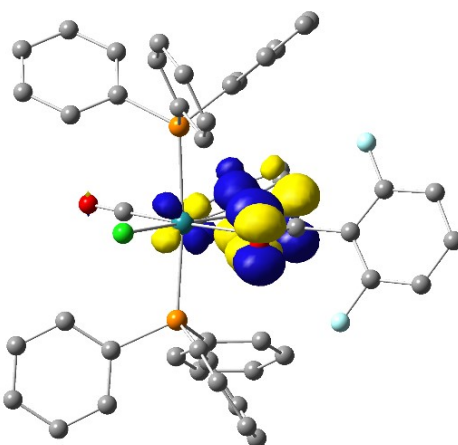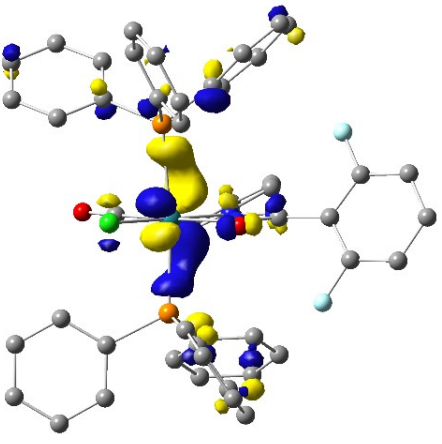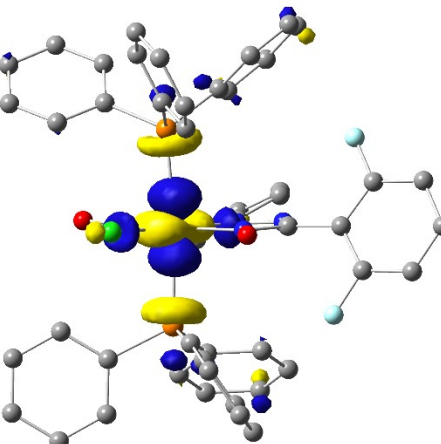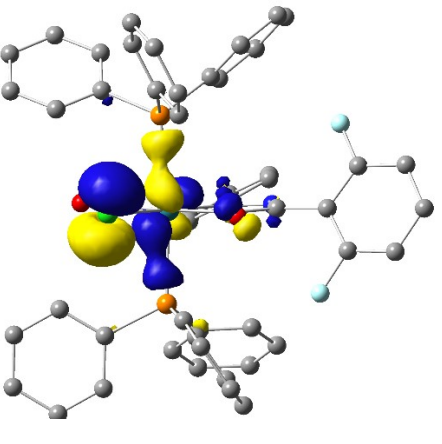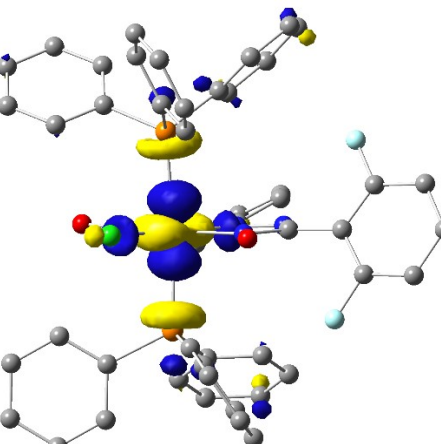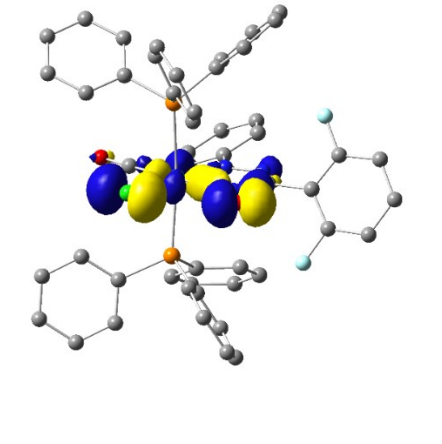
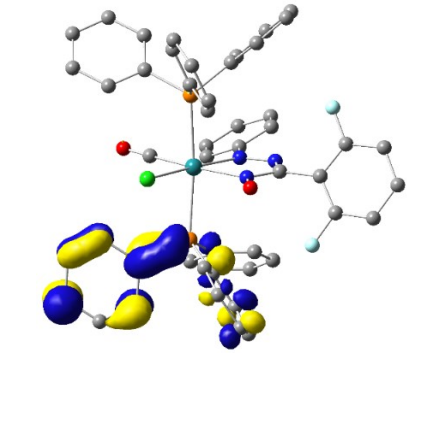| 358 nm	S_6 w = 0.9110 3.1515 (0.0294) 393.41 nm LLCT & d-d π (PPh$_3$) $\rightarrow$ π* (Azo + Oxime + Ph) & $d_{xz} \rightarrow d_{yz}$		
279 nm	S_{27} w = 0.3069 4.1194 (0.2933) 300.97 nm ILCT & d-d π (PPh$_3$) $\rightarrow$ π* (PPh$_3$) & $d_{yz} \rightarrow d_{z^2}$		
232 nm	S_{82} w = 0.3420 5.0202 (0.0454) 246.97 nm LLCT & d-d π (PPh$_3$) $\rightarrow$ π* (Ph + PPh$_3$) & $d_{yz} \rightarrow d_{x^2-y^2}$		

Table S20. Natural transition orbitals (NTOs) for complex **3a** illustrating the nature of singlet excited states in the absorption bands in the range 200–700 nm. For each state, the respective number of the state, transition energy (eV), and the oscillator strength (in parentheses) are listed. Shown are only occupied (holes) and unoccupied (electrons) NTO pairs that contribute more than 15% to each excited state.

		Hole	Electron
543 nm	S_2 w = 0.7751 2.5432 (0.0612) 487.51 nm ILCT, LLCT & d-d π (Cl + Azo + Oxime + Ph) → π^* (Azo + Oxime + Ph) & d_{xz} → d_{yz}		
399 nm	S_5 w = 0.7902 3.0510 (0.1255) 406.37 nm ILCT, LLCT & d-d π (Cl + Oxime) → π^* (Azo + Oxime + Ph) & d_{xz} → d_{yz}		

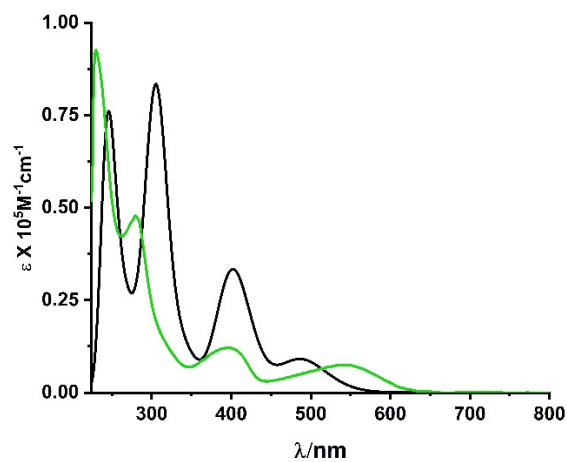|			
279 nm	S_{24} w = 0.3288 4.0279 (0.3605) 307.81 nm ILCT & d-d π (Cl + Oxime + Ph + PPh$_3$) → π* (Cl + Azo + Oxime + PPh$_3$) & d$_{xz}$ → d$_{yz}$		
	S_{24} w = 0.2343 4.0279 (0.3605) 307.81 nm ILCT & d-d π (Cl + Oxime) → π* (Cl + PPh$_3$) & d$_{xz}$ → d$_z^2$		
230 nm	S_{73} w = 0.2156 4.9841 (0.0193) 248.75 nm LLCT & MLCT π (Cl + Oxime) → π* (PPh$_3$)		
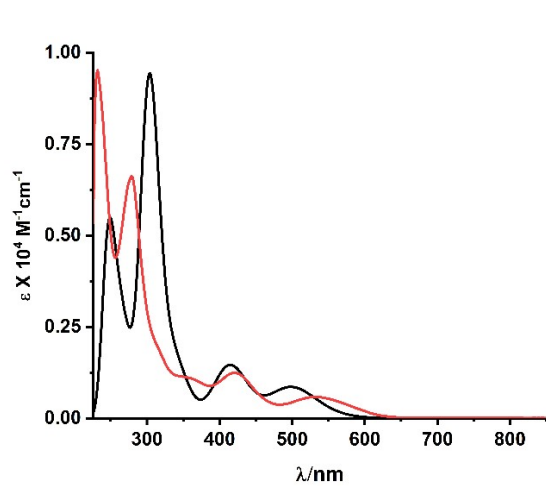
1a
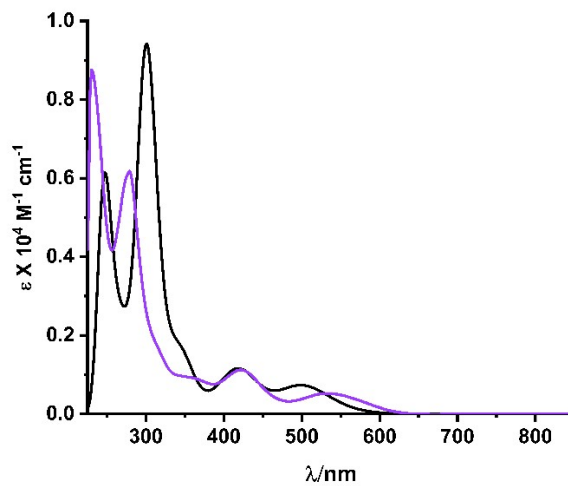
2a

3a
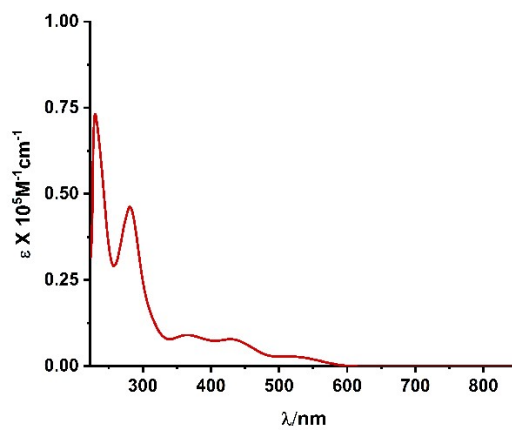
4a
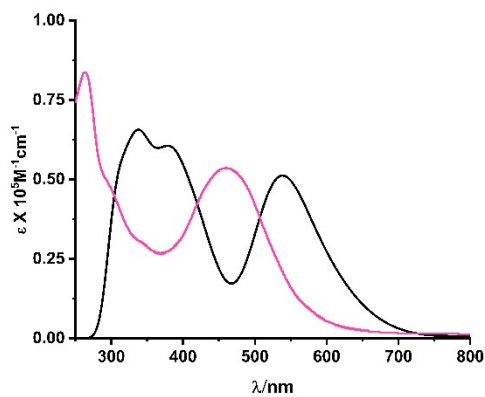
[3a]•−

Figure S19: Experimental (red, violet, green, maroon and pink) and Calculated (black) absorption spectrum of **1a, 2a, 3a, 4a** and **[3a]**•−

The UV-VIS absorption spectra of **1a, 2a** and **3a** were taken in dichloromethane solution at room temperature. All the spectra were plotted together with their respective theoretically calculated spectra (See Figure S20). All complexes exhibit multiple transition and can be assigned as charge transfer (CT) transition within azo-oxime moiety with significant contribution from metal d-orbitals. Time-dependent density functional theory (TD-DFT) in dichloromethane was performed using the CPCM model to realize the absorption spectra. The major transitions along with their corresponding energies, characteristics and oscillator strengths (f) of all the complexes have been given in the ESI† (Tables S13, S14, S15†). Natural Transition Orbital (NTO) analysis was utilised to make out the basis of transitions and are represented in ESI† (Table S18, S19, S20†). A compact diagram of transition density amongst the ground and excited states in terms of expansion into single-particle transitions (hole and electron states for each given excitation) is given by this method. The occupied and unoccupied NTO's are epitomized as 'electron' and 'hole'.

In **1a**, the transition at 534 nm is computed to be near λ_{theo} = 498 nm (2.4871 eV, f = 0.0766) and ascribed as mainly [π(azo + oxime) $\rightarrow$ π*(azo + oxime) + d_{xz} $\rightarrow$ d_{yz}] ILCT with little d-d transition. The next band at 419 nm is quantified at near about λ_{theo} = 416 nm (2.9774 eV, f = 0.1186) and assigned as [π(Cl) $\rightarrow$ π*(azo + oxime)] LLCT transition along with some amount d-d transition. The band near UV region is observed at 277 nm which is calculated at λ_{theo} = 303 nm (4.0853 eV, f = 0.3764), having [π(PPh$_3$) $\rightarrow$ π*(Cl + PPh$_3$) + d_{yz} $\rightarrow$ d_z^2] ILCT combined with LLCT and d-d transition. The band at very near to UV region is detected at 232 nm which is evaluated at λ_{theo} = 247 nm (5.0059 eV, f = 0.0743), having [π(Cl + Oxime) $\rightarrow$ π*(PPh$_3$) + $d_{x^2-y^2}$ $\rightarrow$ d_{xz}] LLCT with slight contribution from d-d transition.

In **2a**, the lowest energy band at 528 nm is computed to be near λ_{theo} = 499 nm (2.4822 eV, f = 0.0634) and assigned as primarily [π(Azo + Oxime + Ph) $\rightarrow$ π*(Azo + oxime) + d_{xz} $\rightarrow$ d_{yz}] ILCT with small amount of d-d transition. The next following band at 420 nm is determined at close to λ_{theo} = 428 nm (2.8956 eV, f = 0.0221) and assigned as [π(Cl + Oxime) $\rightarrow$ π*(Azo + Oxime + Ph) + $d_{x^2-y^2}$ $\rightarrow$ d_{yz}] ILCT transition with some contribution from d-d transition. The band near UV region is observed at 358 nm which is calculated at λ_{theo} = 393 nm (3.1515 eV, f = 0.0294), having [π(PPh$_3$) $\rightarrow$ π*(Azo + Oxime + Ph) + d_{xz} $\rightarrow$ d_{yz}] LLCT combined with LLCT and d-d transition. The band at near to UV region is detected at 279 nm which is evaluated at λ_{theo} = 300 nm (4.1194 eV, f = 0.2933), having [π(PPh$_3$) $\rightarrow$ π*(PPh$_3$) + d_{yz} $\rightarrow$ d_z^2] ILCT with little contribution from d-d transition. Another band at near about UV region is computed at 232 nm and quantified

at λ_{theo} = 246 nm (5.0202 eV, f = 0.0454), having [π(PPh$_3$) → π*(Ph + PPh$_3$) + d$_{yz}$ → d$_{x^2-y^2}$] LLCT together with d-d transition.

For **3a**, the band with lowest energy is observed at 543 nm which is enumerated at λ_{theo} = 487 nm (2.5432 eV, f = 0.0612) and can be ascribed as mostly [π (Cl +Azo + Oxime + Ph) → π*(Azo + Oxime + Ph) + d$_{xz}$ → d$_{yz}$] ILCT, LLCT as well as small amount of d-d transition. The next band appeared at 399 nm which is calculated at λ_{theo} = 406 nm (3.0510 eV, f = 0.1255) and can be ascribed as typically [π (Cl + Oxime) → π*(Azo + Oxime + Ph) + d$_{xz}$ → d$_{yz}$] ILCT, LLCT along with minute amount of d-d transition. The band at 279 nm which composed with two transitions computed at λ_{theo} = 307 nm (4.0279 eV, f = 0.3605). The first transition can be assessed as mostly [π (Cl + Oxime + Ph + PPh$_3$) → π*(Cl + Azo + Oxime + PPh$_3$) + d$_{xz}$ → d$_{yz}$] ILCT and d-d transition while the another one may be designated as [π (Cl + Oxime) → π*(Cl + PPh$_3$) + d$_{xz}$ → d$_{z^2}$] ILCT and d-d transition. The last band at 230 nm is determined at λ_{theo} = 248 nm (4.9841 eV, f = 0.0193) and can be attributed as [π (Cl + Oxime) → π*(PPh$_3$)] ILCT, LLCT and MLCT.
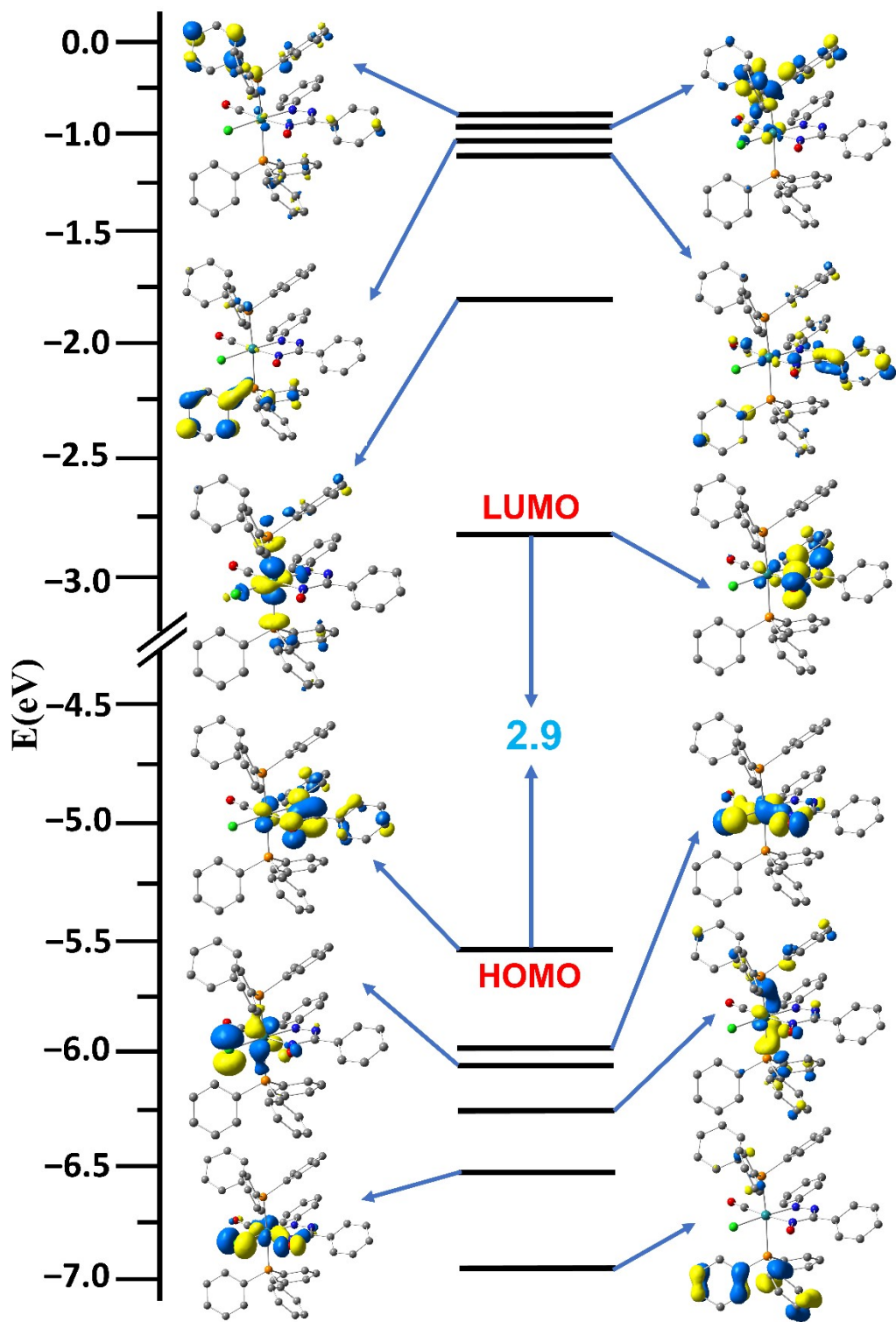
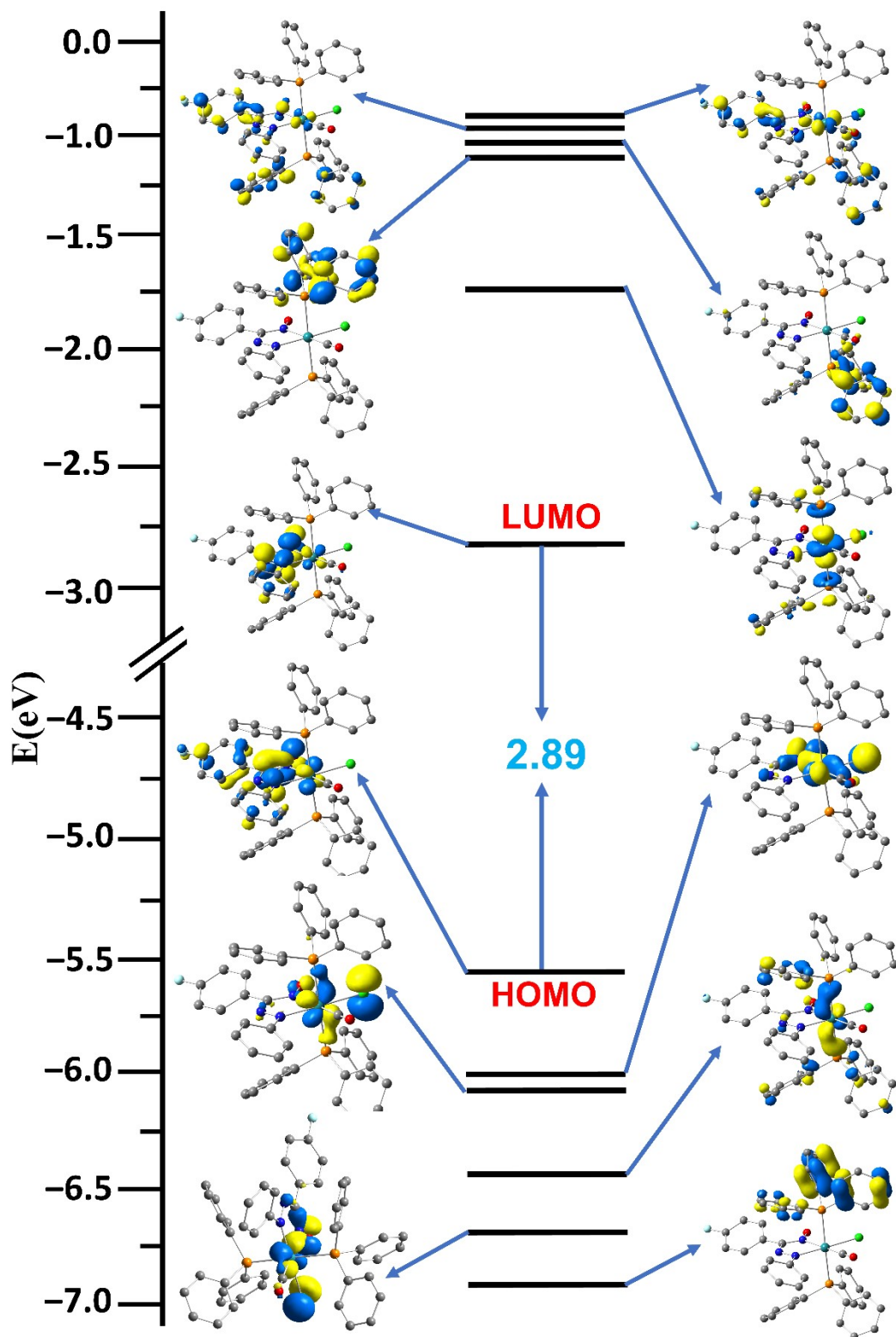**Figure S20:** Partial MO diagram of **1a**

Figure S21: Partial MO diagram of **2a**
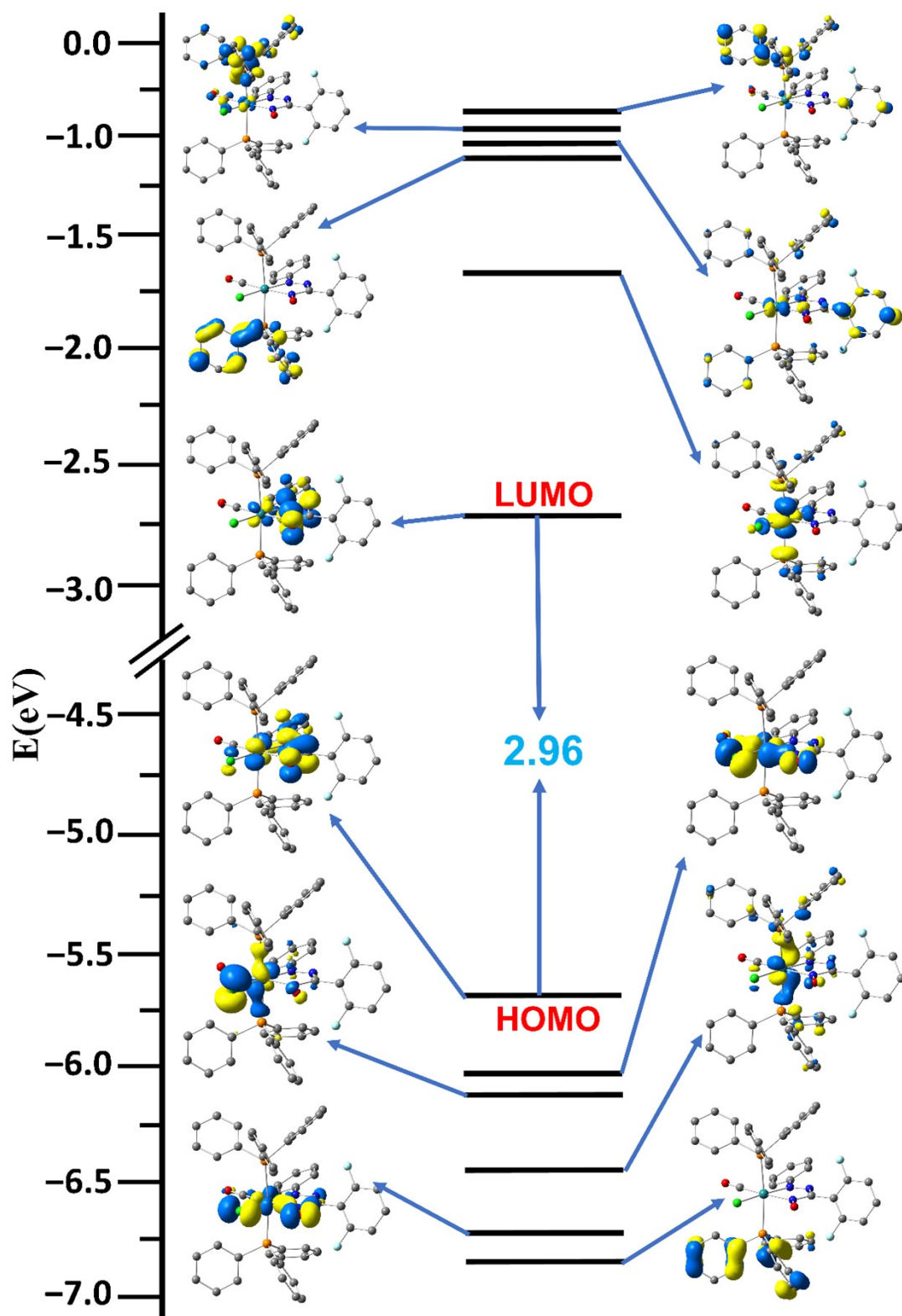
Figure S22: Partial MO diagram of **3a**

Table S21: Coordinates of optimised geometry of **1a**

Tag	Symbol	X	Y	Z
1	Ru	2.73207	8.442736	8.280366
2	Cl	3.593433	10.78072	7.906925
3	P	1.148992	9.43763	9.943558
4	P	4.510473	7.719389	6.64821
5	C	1.532679	8.684291	6.826334
6	N	2.908002	5.9483	9.746109
7	O	4.905643	8.698599	10.40762
8	C	1.945629	9.911648	11.54835
9	O	0.826555	8.817667	5.930992
10	N	2.219521	6.486554	8.804211
11	C	6.145994	8.593397	6.670395
12	C	0.291819	11.02184	9.502611
13	C	-0.25416	8.328162	10.41267
14	N	4.040375	7.952141	9.890313
15	C	5.00197	5.944379	6.793739
16	C	-0.00666	7.138048	11.11389
17	H	1.003047	6.872616	11.41324
18	C	4.021213	7.955529	4.874942
19	C	3.016558	10.81642	11.49454
20	H	3.389256	11.15947	10.53394
21	C	6.62407	9.227701	7.82117
22	H	6.012559	9.278602	8.714963
23	C	4.095037	4.92811	6.461694
24	H	3.098013	5.172879	6.106658
25	C	3.868259	6.683578	10.3457
26	C	6.954705	8.561046	5.523839
27	H	6.604449	8.078972	4.61543
28	C	0.196856	11.48567	8.187964

29	H	0.687907	10.95868	7.38099
30	C	4.458773	3.588159	6.574124
31	H	3.745572	2.814504	6.298973
32	C	-1.05123	6.279947	11.44709
33	H	-0.83959	5.36766	12.0005
34	C	-0.50636	12.65561	7.896513
35	H	-0.56485	13.00227	6.867152
36	C	6.268925	5.585179	7.274115
37	H	6.98984	6.349928	7.546449
38	C	7.892085	9.811515	7.825443
39	H	8.250494	10.30278	8.727748
40	C	6.624425	4.242916	7.401243
41	H	7.61235	3.984102	7.775973
42	C	-0.32475	11.76113	10.52462
43	H	-0.26075	11.42881	11.55726
44	C	-2.3588	6.585199	11.06975
45	H	-3.17389	5.913115	11.32883
46	C	8.691138	9.774996	6.685039
47	H	9.677219	10.23464	6.691361
48	C	3.36937	8.50413	2.199099
49	H	3.115557	8.715976	1.162776
50	C	8.217788	9.147871	5.532063
51	H	8.83116	9.115255	4.634111
52	C	3.605499	11.28177	12.66732
53	H	4.432609	11.98618	12.6082
54	C	1.485502	9.479878	12.79829
55	H	0.64617	8.79664	12.87538
56	C	4.066286	6.94288	3.910643
57	H	4.372559	5.936731	4.177305
58	C	3.736487	7.216597	2.581749

59	H	3.775976	6.416576	1.845603
60	C	5.724788	3.240726	7.043778
61	H	6.006477	2.193907	7.133704
62	C	1.221032	5.604151	8.269754
63	C	-1.02506	12.92844	10.23345
64	H	-1.49562	13.48777	11.03911
65	C	3.145939	10.84305	13.90913
66	H	3.609674	11.20571	14.82406
67	C	-1.11937	13.37908	8.916122
68	H	-1.66433	14.29255	8.688347
69	C	3.655371	9.25152	4.47977
70	H	3.624974	10.0557	5.211707
71	C	4.639058	6.045859	11.43482
72	C	3.335244	9.52246	3.152733
73	H	3.055904	10.53338	2.863662
74	C	-1.56991	8.621129	10.03054
75	H	-1.79266	9.529627	9.4792
76	C	4.810077	4.649863	11.41789
77	H	4.397787	4.073001	10.59521
78	C	-2.61303	7.753835	10.35578
79	H	-3.62794	7.999624	10.0508
80	C	2.086615	9.940494	13.97064
81	H	1.714608	9.596112	14.93329
82	C	5.499719	4.001005	12.4371
83	H	5.623882	2.920704	12.39824
84	C	1.391288	4.211848	8.338031
85	H	2.292005	3.807098	8.783999
86	C	-0.73715	3.875658	7.237568
87	H	-1.49261	3.206724	6.831982
88	C	5.864038	6.113806	13.53259

89	H	6.269091	6.692969	14.35996
90	C	5.180091	6.770386	12.51048
91	H	5.062251	7.846167	12.55058
92	C	0.05478	6.114864	7.695339
93	H	-0.13016	7.17987	7.689004
94	C	6.031637	4.730338	13.50155
95	H	6.571932	4.224045	14.29862
96	C	-0.91561	5.255922	7.183489
97	H	-1.82056	5.675176	6.74965
98	C	0.42157	3.360495	7.822678
99	H	0.576683	2.284788	7.871908

Table S22: Coordinates of optimised geometry of **2a**

Tag	Symbol	X	Y	Z
1	Ru	4.934585	14.22016	13.75228
2	Cl	5.782196	15.87138	15.46867
3	P	4.043372	12.90804	15.70453
4	P	6.013005	15.56428	11.92507
5	F	10.17352	7.80574	11.71093
6	O	2.482443	16.00944	13.46206
7	O	7.680209	13.03878	14.40713
8	N	6.629841	12.92265	13.72635
9	N	5.305402	11.80652	12.2028
10	N	4.421682	12.71015	12.41646
11	C	3.389762	15.31931	13.59031
12	C	6.484199	11.8887	12.85983
13	C	7.481785	10.83091	12.59816
14	C	7.038452	9.582364	12.12501
15	H	5.975497	9.40901	11.99081

16	C	7.93484	8.562538	11.8259
17	H	7.590831	7.596343	11.46655
18	C	9.289228	8.800187	12.00024
19	C	9.771271	10.01366	12.45956
20	H	10.8407	10.16539	12.57913
21	C	8.86402	11.02709	12.76205
22	H	9.237106	11.97632	13.12442
23	C	3.226343	12.52093	11.64562
24	C	1.996539	12.98834	12.11816
25	H	1.929225	13.48217	13.07917
26	C	0.831794	12.77708	11.38346
27	H	-0.11645	13.13908	11.77404
28	C	0.879128	12.10047	10.16641
29	H	-0.02965	11.94129	9.590711
30	C	2.10572	11.62964	9.693977
31	H	2.158543	11.10602	8.741866
32	C	3.270667	11.83409	10.42324
33	H	4.22259	11.47928	10.0457
34	C	7.860019	15.73211	11.97986
35	C	8.602284	15.98209	10.81441
36	H	8.120881	15.99284	9.84127
37	C	9.972815	16.21713	10.88583
38	H	10.53316	16.40488	9.972395
39	C	10.62188	16.21515	12.12128
40	H	11.69243	16.40106	12.17592
41	C	9.890377	15.97734	13.28203
42	H	10.38652	15.97595	14.25036
43	C	8.517322	15.73606	13.21516
44	H	7.959679	15.55611	14.1265
45	C	5.516171	17.34594	11.73668

46	C	5.737914	18.01857	10.52445
47	H	6.132567	17.48923	9.662396
48	C	5.448663	19.37494	10.40289
49	H	5.621798	19.87731	9.453614
50	C	4.941548	20.0854	11.49168
51	H	4.715651	21.14515	11.39557
52	C	4.732518	19.42973	12.70202
53	H	4.345913	19.97479	13.56047
54	C	5.018781	18.06927	12.82576
55	H	4.879501	17.58319	13.78508
56	C	5.668692	14.83898	10.26262
57	C	4.535338	15.22868	9.535171
58	H	3.863765	15.98753	9.928011
59	C	4.266094	14.66696	8.289088
60	H	3.389854	14.99239	7.732704
61	C	5.113926	13.69638	7.757967
62	H	4.906707	13.26366	6.781704
63	C	6.223745	13.27674	8.489211
64	H	6.886119	12.51174	8.089806
65	C	6.497413	13.83964	9.73469
66	H	7.373638	13.50466	10.28271
67	C	3.969937	11.08054	15.41056
68	C	3.04805	10.5352	14.50499
69	H	2.33911	11.17252	13.98686
70	C	3.015027	9.164408	14.26009
71	H	2.283101	8.762295	13.56292
72	C	3.914981	8.314506	14.9018
73	H	3.89096	7.244386	14.70811
74	C	4.845393	8.846427	15.7917
75	H	5.555082	8.194829	16.29684

76	C	4.872192	10.21706	16.04769
77	H	5.59987	10.60541	16.75333
78	C	4.963917	13.01214	17.30864
79	C	6.356311	13.1553	17.3274
80	H	6.907355	13.28165	16.40139
81	C	7.046983	13.14095	18.53905
82	H	8.129269	13.25303	18.53893
83	C	6.35955	12.99274	19.7424
84	H	6.901372	12.98705	20.68583
85	C	4.972206	12.85312	19.73049
86	H	4.424531	12.73753	20.66335
87	C	4.277777	12.86109	18.52196
88	H	3.197664	12.74881	18.53535
89	C	2.339914	13.41518	16.21904
90	C	1.277735	12.52266	16.40104
91	H	1.408299	11.46154	16.21532
92	C	0.03635	12.98361	16.84304
93	H	-0.77986	12.27701	16.97668
94	C	-0.154	14.33505	17.12058
95	H	-1.12138	14.69131	17.4676
96	C	0.905782	15.22863	16.95905
97	H	0.770628	16.28443	17.18317
98	C	2.141911	14.77403	16.5092
99	H	2.962635	15.47979	16.4009

Table S23: Coordinates of optimised geometry of **3a**

Tag	Symbol	X	Y	Z
1	Ru	2.801451	8.405738	8.358971
2	Cl	3.791517	10.69027	8.004597
3	P	1.211477	9.463201	9.983424
4	P	4.522016	7.655204	6.651279
5	C	1.605024	8.686883	6.911
6	N	2.900067	5.897672	9.826301
7	O	4.960432	8.5812	10.5524
8	C	1.936295	10.10549	11.56469
9	O	0.897342	8.848198	6.022405
10	N	2.227014	6.450918	8.879824
11	C	6.201581	8.43308	6.712513
12	C	0.267657	10.96047	9.422207
13	C	-0.11728	8.299404	10.52246
14	N	4.083038	7.884675	9.991599
15	C	4.909623	5.848491	6.610821
16	C	0.195968	7.240582	11.38822
17	H	1.201895	7.131968	11.78479
18	C	4.008994	8.056764	4.911126
19	C	3.090021	10.89858	11.49441
20	H	3.590348	11.04608	10.54308
21	C	6.741676	8.900422	7.914589
22	H	6.153206	8.889508	8.824795
23	C	3.896618	4.923046	6.321096
24	H	2.880051	5.25776	6.136449
25	C	3.862311	6.619775	10.42202
26	C	6.980764	8.490974	5.547164
27	H	6.583543	8.134369	4.601064
28	C	0.417526	11.51495	8.148852

29	H	1.12856	11.09603	7.449265
30	C	4.17886	3.561243	6.2469
31	H	3.381076	2.860848	6.010951
32	C	-0.7806	6.323616	11.76788
33	H	-0.52141	5.514318	12.44699
34	C	-0.31056	12.64725	7.777136
35	H	-0.17621	13.06622	6.782311
36	C	6.205212	5.373148	6.852614
37	H	7.00817	6.063587	7.089573
38	C	8.040092	9.410416	7.95046
39	H	8.445686	9.77372	8.892451
40	C	6.483087	4.008515	6.786904
41	H	7.495518	3.659179	6.977694
42	C	-0.61487	11.57549	10.32583
43	H	-0.7405	11.17746	11.32915
44	C	-2.08287	6.44221	11.28171
45	H	-2.84504	5.725754	11.58003
46	C	8.8093	9.465279	6.790146
47	H	9.819775	9.8673	6.820871
48	C	3.297071	8.817347	2.301948
49	H	3.020474	9.111315	1.291789
50	C	8.275318	9.003761	5.586803
51	H	8.86587	9.042738	4.673957
52	C	3.60006	11.50332	12.6415
53	H	4.497072	12.11496	12.56985
54	C	1.3079	9.931757	12.80516
55	H	0.408492	9.330647	12.89283
56	C	3.88469	7.098241	3.899798
57	H	4.077241	6.049982	4.102133
58	C	3.526402	7.477857	2.604582

59	H	3.434086	6.717889	1.831595
60	C	5.474185	3.099333	6.477756
61	H	5.693728	2.035453	6.420304
62	C	1.219393	5.582292	8.340955
63	C	-1.34181	12.70171	9.95377
64	H	-2.02291	13.1614	10.66662
65	C	2.970874	11.32442	13.87274
66	H	3.371354	11.7975	14.7669
67	C	-1.1938	13.24036	8.674217
68	H	-1.75973	14.12287	8.384044
69	C	3.780174	9.40543	4.596372
70	H	3.877855	10.1669	5.366232
71	C	4.631578	6.00719	11.53102
72	C	3.430083	9.780841	3.302753
73	H	3.258935	10.83126	3.076876
74	C	-1.42444	8.403432	10.03075
75	H	-1.69359	9.20685	9.351308
76	C	5.509729	4.941576	11.3281
77	C	-2.39983	7.481544	10.41004
78	H	-3.41086	7.58096	10.02098
79	C	1.823729	10.53708	13.9504
80	H	1.321924	10.3917	14.90477
81	C	6.236328	4.343459	12.34513
82	H	6.904452	3.518572	12.116
83	C	1.357819	4.187158	8.436664
84	C	-0.75048	3.878007	7.290582
85	H	-1.51044	3.218383	6.878176
86	C	5.223516	5.890379	13.90613
87	H	5.085803	6.279854	14.91045
88	C	4.518975	6.445576	12.85147

89	C	0.081082	6.10736	7.725862
90	C	6.088835	4.830524	13.64162
91	H	6.6504	4.377963	14.4543
92	C	-0.89542	5.260137	7.205054
93	H	-1.77843	5.691098	6.738729
94	C	0.381842	3.348434	7.91405
95	H	0.512127	2.270707	7.985484
96	H	2.2409	3.770965	8.907413
97	H	-0.07789	7.175494	7.687888
98	F	5.666149	4.473598	10.06751
99	F	3.653462	7.452057	13.11447

Table S24: Coordinates of optimised geometry of [**3a**]$^{\bullet-}$

Tag	Symbol	X X	Y Y	Z Z
1	Ru	2.792605	8.49803	8.288729
2	Cl	3.788218	10.82054	7.913481
3	P	1.206994	9.445231	9.936822
4	P	4.467677	7.646867	6.617634
5	C	1.578423	8.838112	6.888037
6	N	3.00194	5.993873	9.8632
7	O	5.049619	8.774333	10.44471
8	C	1.919521	9.908409	11.58659
9	O	0.854342	9.094783	6.024535
10	N	2.249065	6.502963	8.867735
11	C	6.178445	8.367245	6.617679
12	C	0.334792	11.04083	9.530459
13	C	-0.20933	8.324939	10.33531
14	N	4.144241	8.032669	9.887643
15	C	4.80475	5.827672	6.651146
16	C	0.011328	7.167851	11.09523

17	H	1.005237	6.93558	11.46603
18	C	3.970917	7.98683	4.857319
19	C	3.063662	10.71865	11.58149
20	H	3.550479	10.95904	10.64157
21	C	6.731402	8.893697	7.789349
22	H	6.147193	8.936714	8.70472
23	C	3.769742	4.923125	6.374911
24	H	2.772482	5.283676	6.1408
25	C	3.941091	6.772653	10.36348
26	C	6.956345	8.339651	5.449742
27	H	6.548287	7.937431	4.526381
28	C	0.448923	11.66099	8.283822
29	H	1.096608	11.24332	7.524584
30	C	4.000455	3.549802	6.399913
31	H	3.185707	2.865218	6.174745
32	C	-1.03774	6.297154	11.38014
33	H	-0.84864	5.408097	11.97814
34	C	-0.23398	12.84977	8.014573
35	H	-0.12714	13.31847	7.038431
36	C	6.068009	5.320784	6.982303
37	H	6.884383	5.996414	7.216193
38	C	8.04147	9.378003	7.789632
39	H	8.459001	9.786504	8.708187
40	C	6.29417	3.944779	7.020481
41	H	7.282189	3.571343	7.282375
42	C	-0.47076	11.64623	10.50914
43	H	-0.57072	11.1935	11.49228
44	C	-2.31916	6.55442	10.8931
45	H	-3.13668	5.871276	11.11432
46	C	8.808799	9.349035	6.627287

47	H	9.827551	9.731825	6.631907
48	C	3.285652	8.681912	2.220022
49	H	3.019074	8.950338	1.19988
50	C	8.261457	8.82684	5.454425
51	H	8.849824	8.799062	4.539334
52	C	3.58558	11.20834	12.77695
53	H	4.473587	11.83715	12.7562
54	C	1.32018	9.590099	12.81179
55	H	0.428851	8.971354	12.84694
56	C	3.863631	7.005263	3.866334
57	H	4.057986	5.962847	4.097744
58	C	3.518261	7.351151	2.557812
59	H	3.438266	6.572339	1.80202
60	C	5.264043	3.055046	6.722748
61	H	5.442039	1.981892	6.747052
62	C	1.277238	5.608911	8.4156
63	C	-1.15256	12.82938	10.24099
64	H	-1.77297	13.28014	11.01294
65	C	2.985219	10.88547	13.99374
66	H	3.397698	11.26546	14.92635
67	C	-1.03783	13.43538	8.988225
68	H	-1.56837	14.36172	8.777779
69	C	3.736173	9.32558	4.506626
70	H	3.817356	10.10463	5.261729
71	C	4.758078	6.234503	11.48509
72	C	3.400691	9.669181	3.200035
73	H	3.224387	10.71295	2.947599
74	C	-1.49605	8.567275	9.837152
75	H	-1.69371	9.447038	9.231568
76	C	6.129947	5.997467	11.37522

77	C	-2.54287	7.687577	10.11377
78	H	-3.5356	7.893849	9.718662
79	C	1.853501	10.07198	14.00781
80	H	1.375967	9.812985	14.95079
81	C	6.911497	5.489295	12.40036
82	H	7.973202	5.327816	12.23687
83	C	1.199242	4.275708	8.900686
84	C	-0.6903	3.768944	7.458162
85	H	-1.43747	3.068557	7.091002
86	C	4.937106	5.398917	13.78868
87	H	4.436783	5.177098	14.72699
88	C	4.208591	5.916038	12.72788
89	C	0.321653	5.977148	7.445664
90	C	6.302719	5.187901	13.61727
91	H	6.895412	4.785461	14.43445
92	C	-0.63372	5.07846	6.978983
93	H	-1.34928	5.416767	6.230323
94	C	0.240926	3.387913	8.429033
95	H	0.224648	2.37372	8.827854
96	H	1.91113	3.950688	9.649454
97	H	0.309285	6.984838	7.059111
98	F	6.733617	6.252062	10.18898
99	F	2.882073	6.136188	12.92792
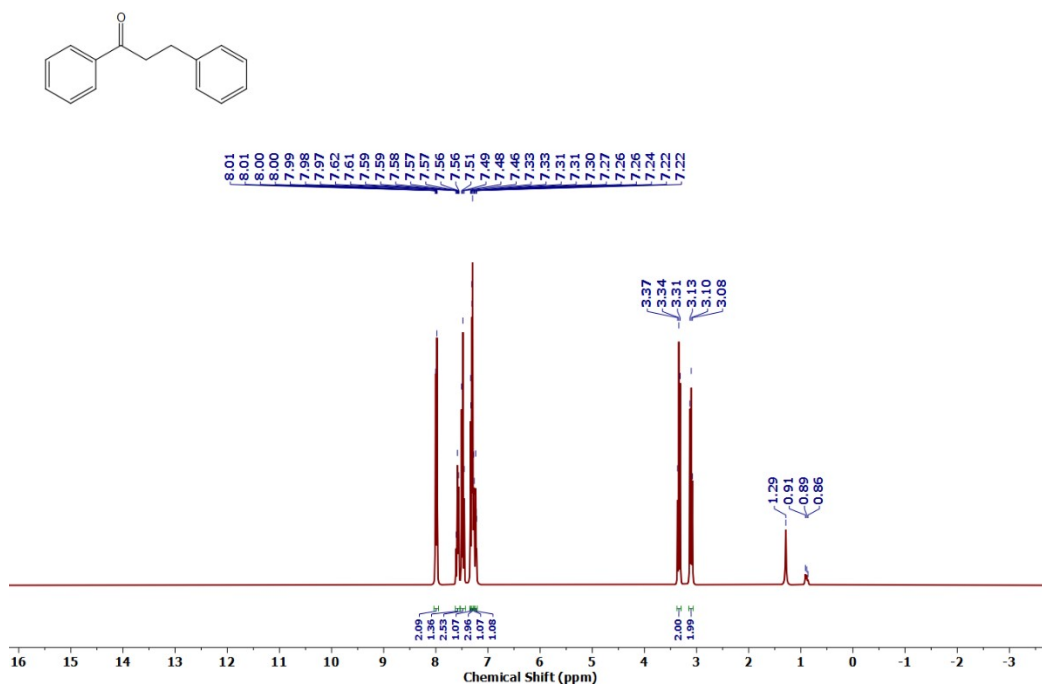
Figure S23: ^{1}H NMR spectrum of **7a**
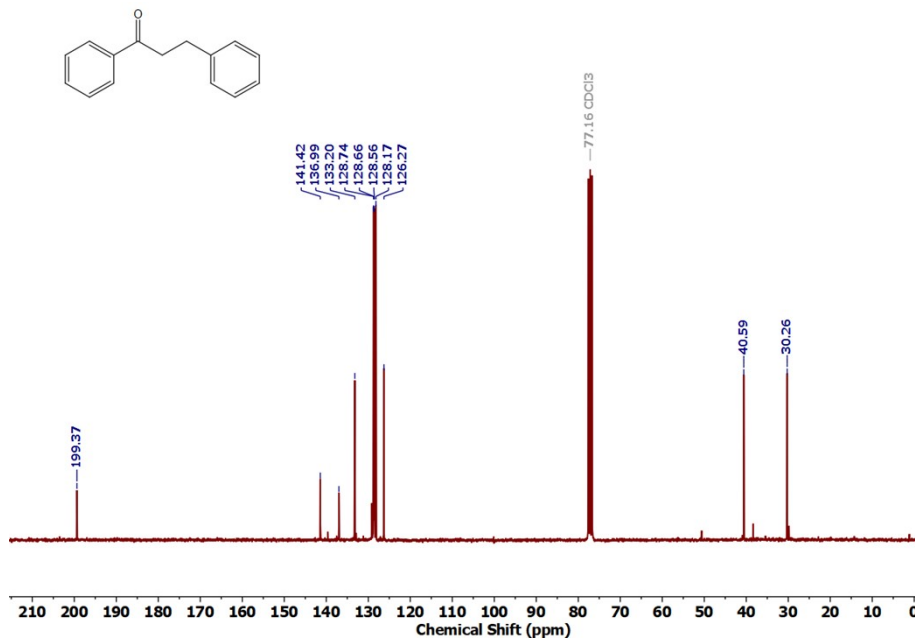
Figure S24: ^{13}C NMR spectrum of **7a**
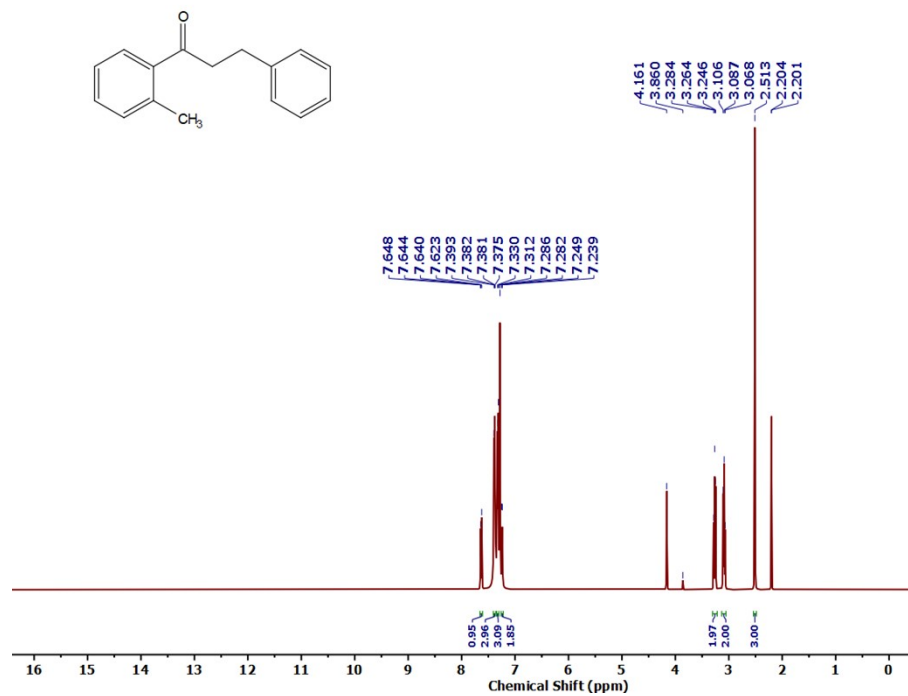
Figure S25: ^{1}H NMR spectrum of **7b**
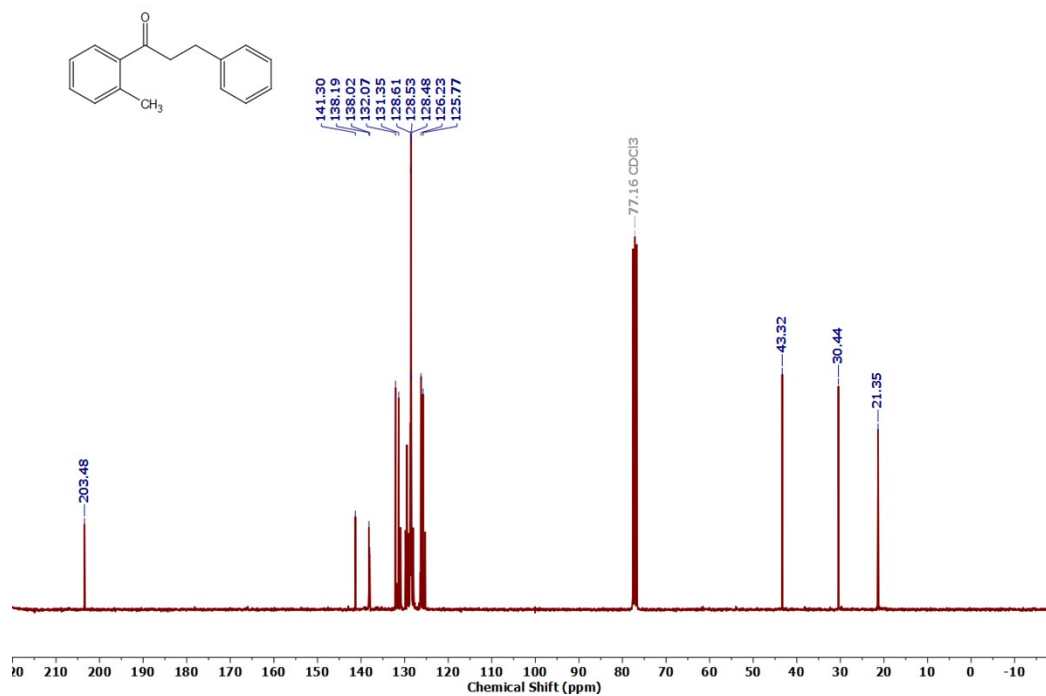
Figure S26: ^{13}C NMR spectrum of **7b**
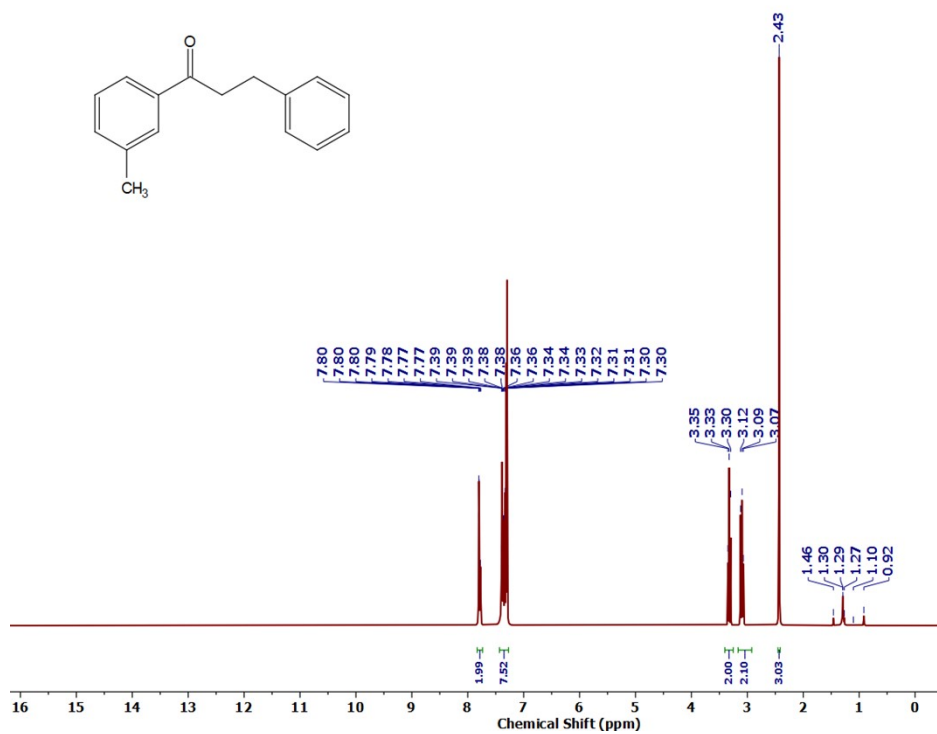
Figure S27: ^{1}H NMR spectrum of **7c**
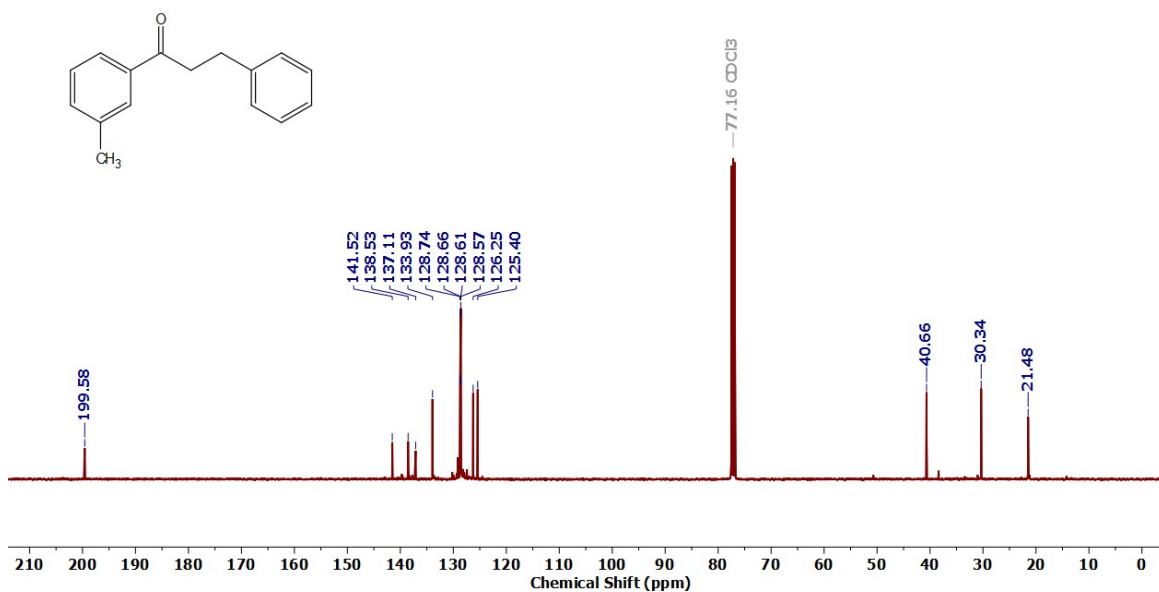
Figure S28: ^{13}C NMR spectrum of **7c**
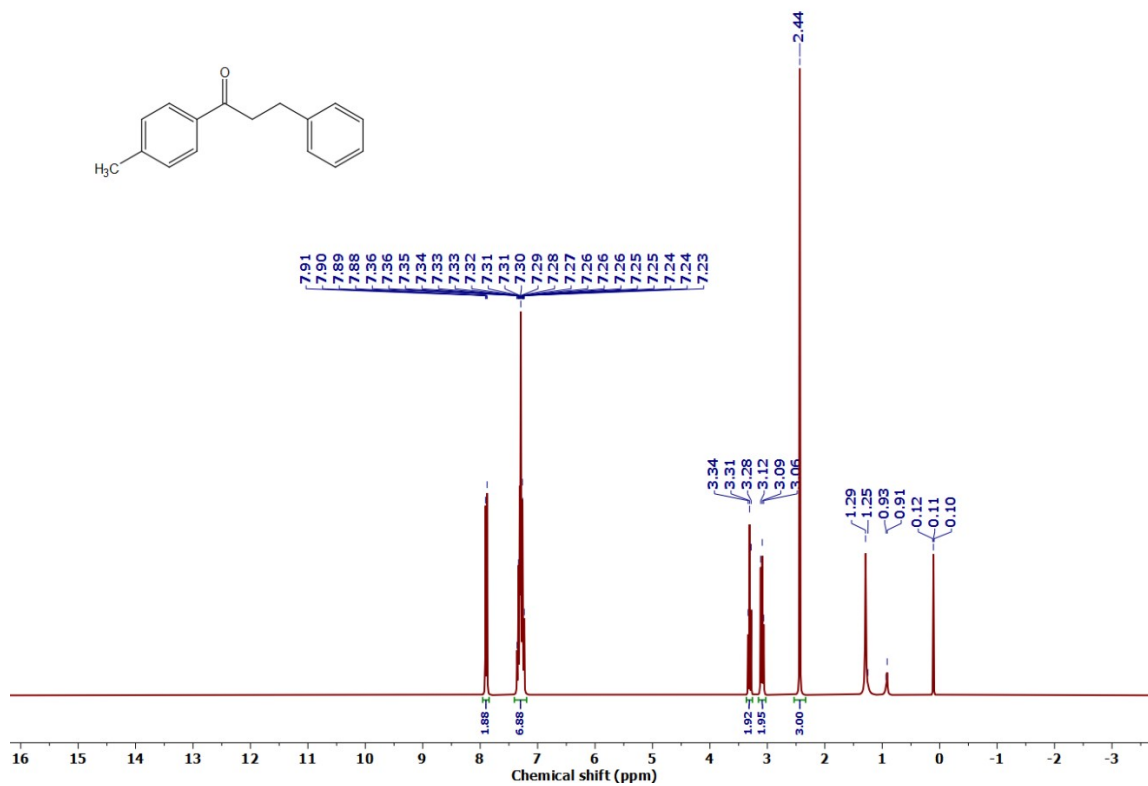
Figure S29: ^{1}H NMR spectrum of **7d**
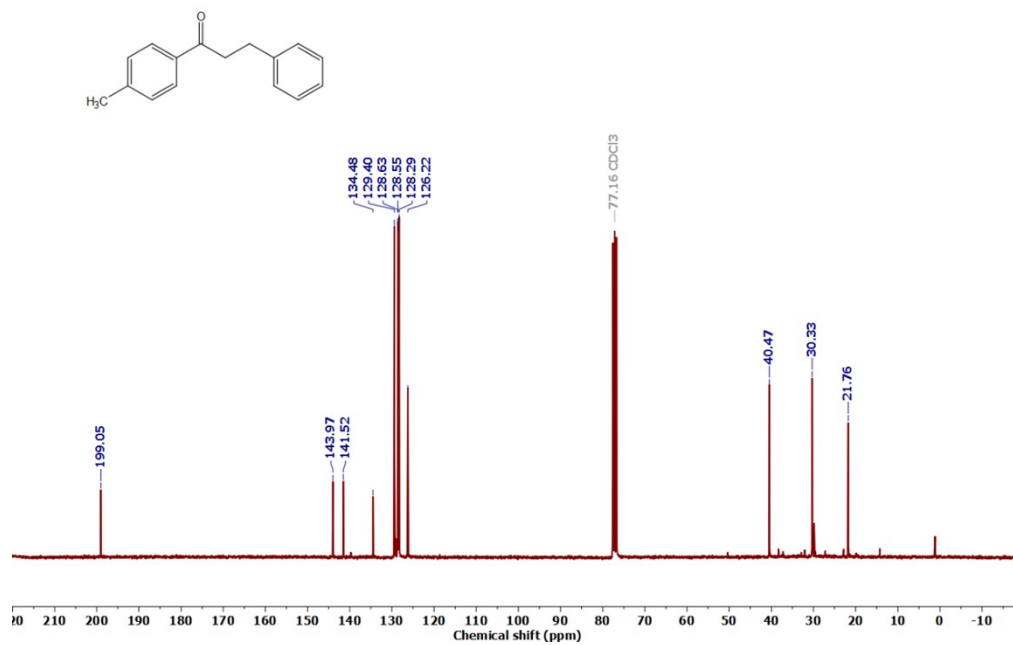
Figure S30: ^{13}C NMR spectrum of **7d**
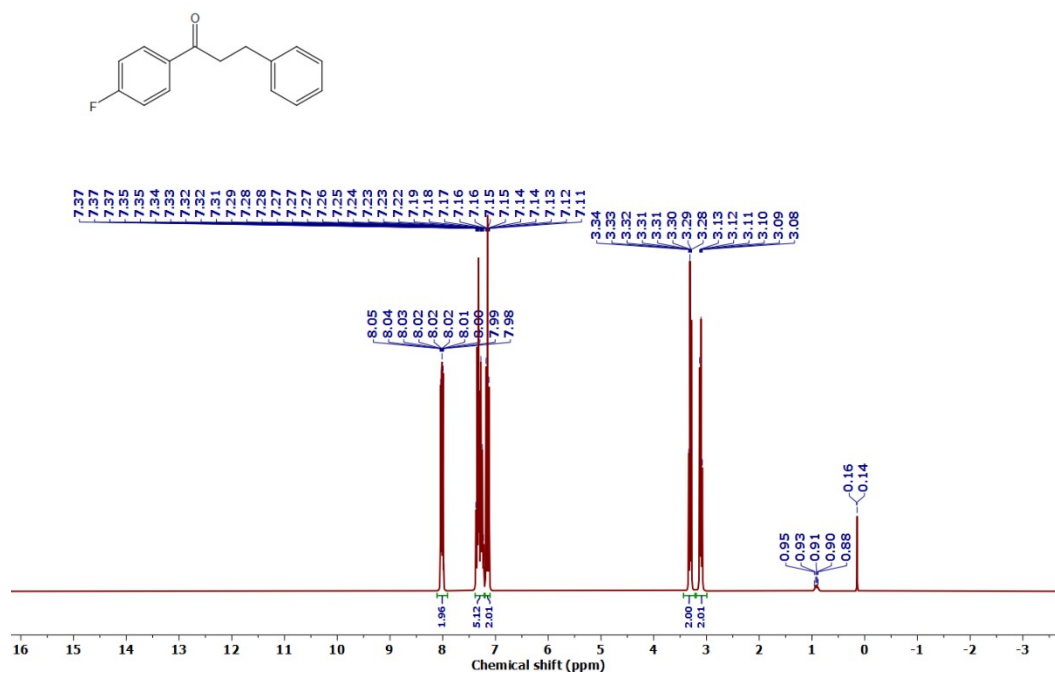
Figure S31: ^{1}H NMR spectrum of **7e**
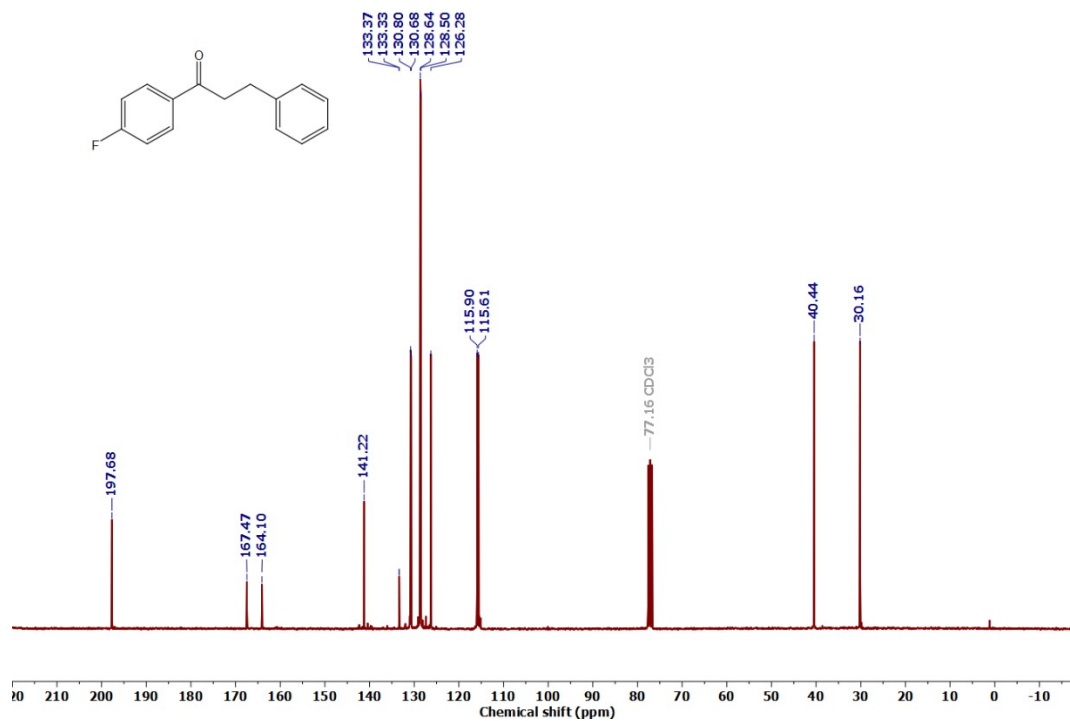
Figure S32: ^{13}C NMR spectrum of **7e**

S53
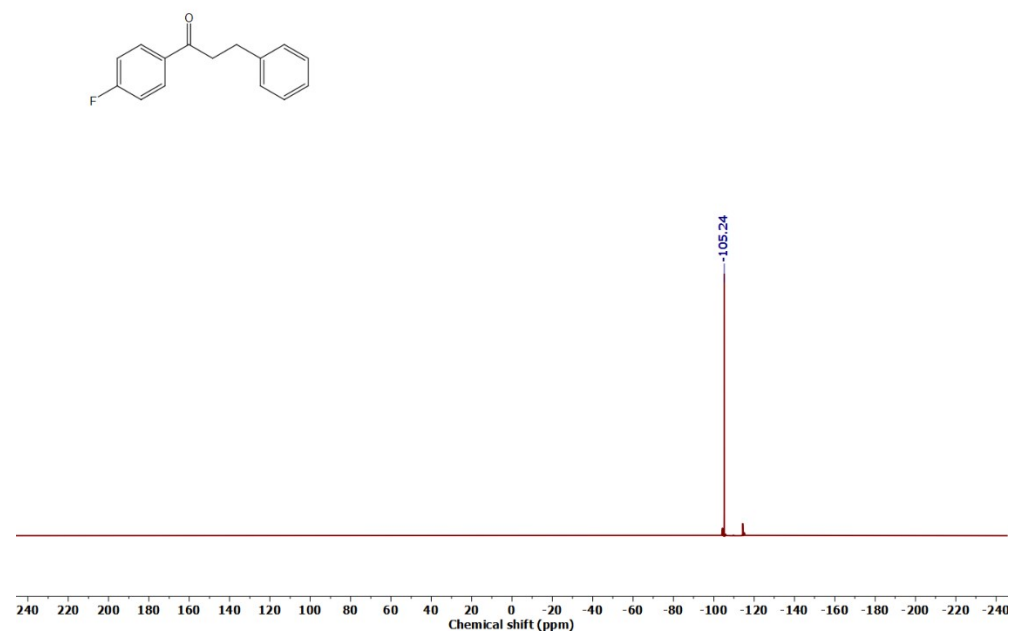
Figure S33: ^{19}F NMR spectrum of **7e**
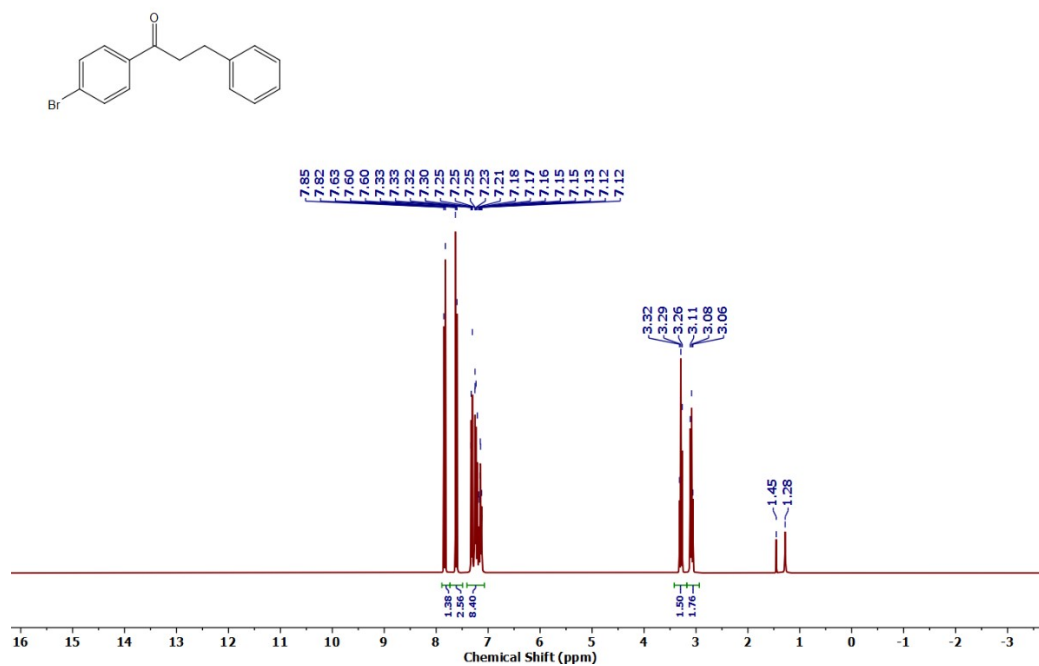
Figure S34: ^{1}H NMR spectrum of **7f**
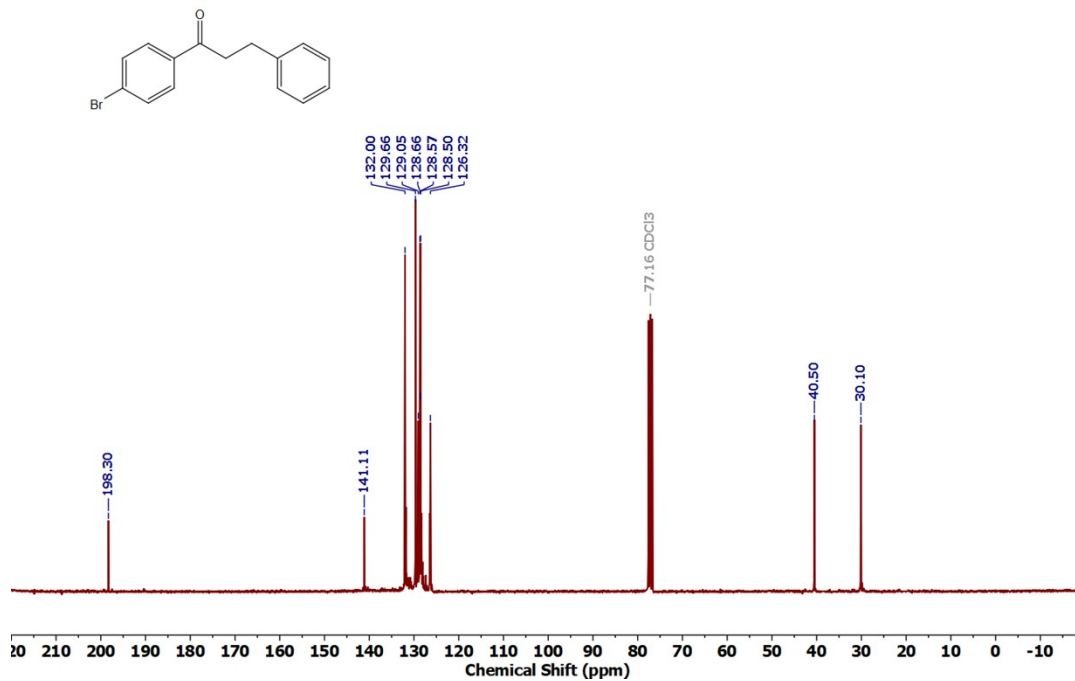
Figure S35: ^{13}C NMR spectrum of **7f**
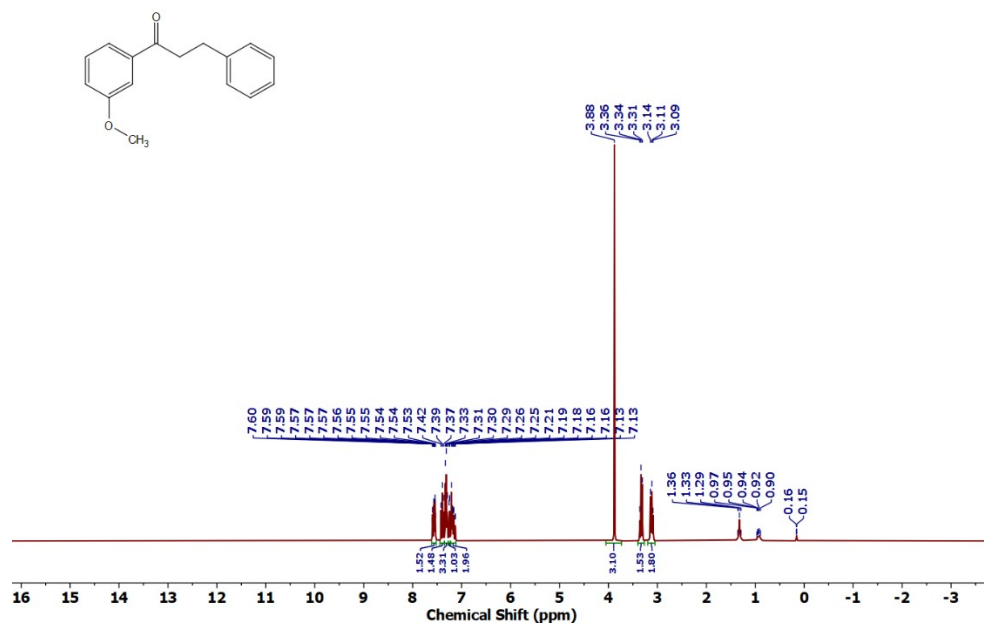
Figure S36: ^1H NMR spectrum of **7g**
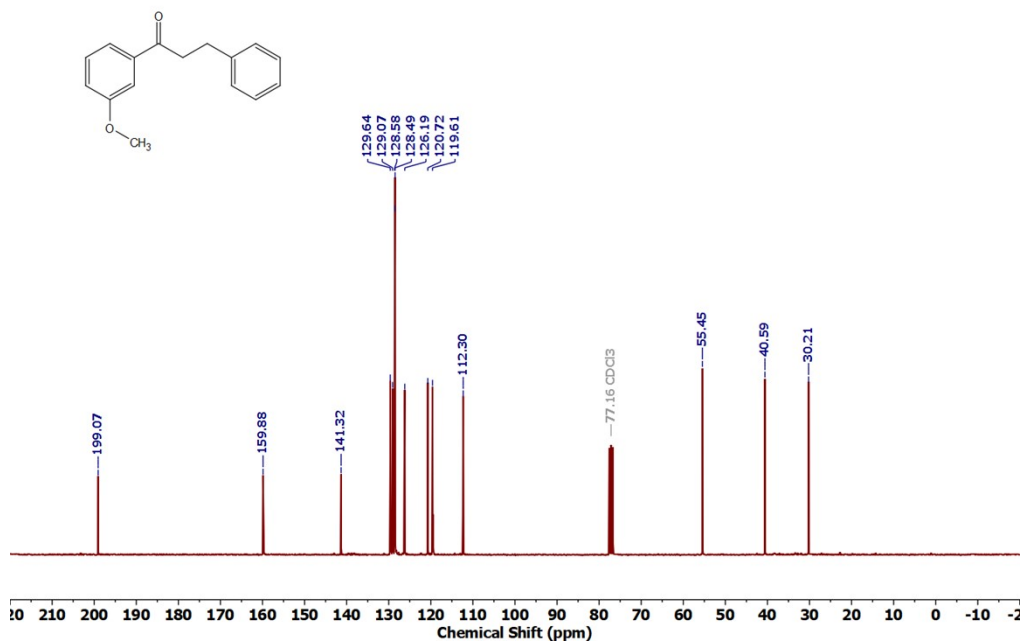
Figure S37: ^{13}C NMR spectrum of **7g**
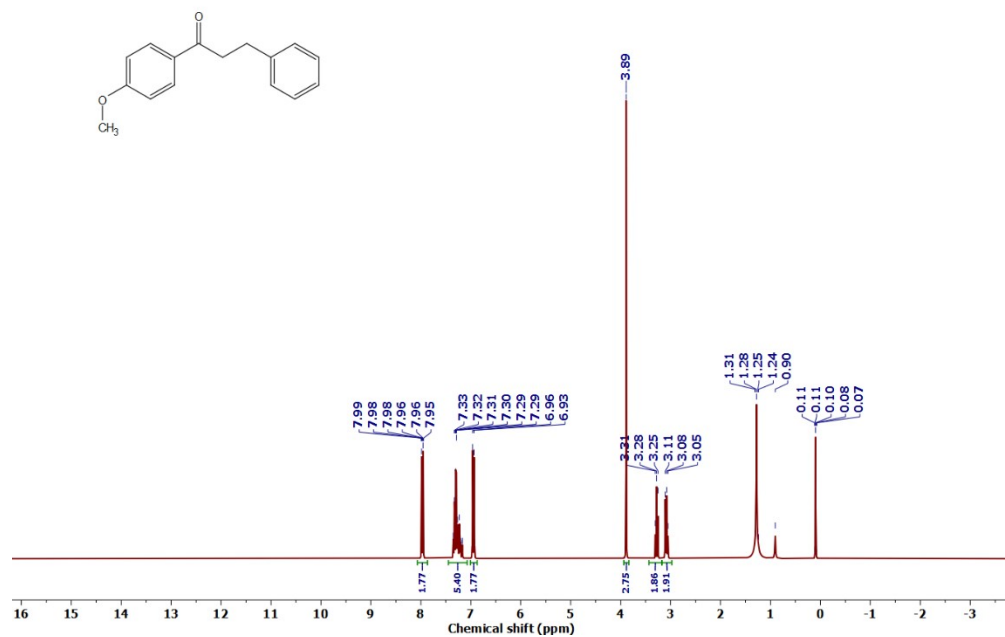
Figure S38: ^{1}H NMR spectrum of **7h**
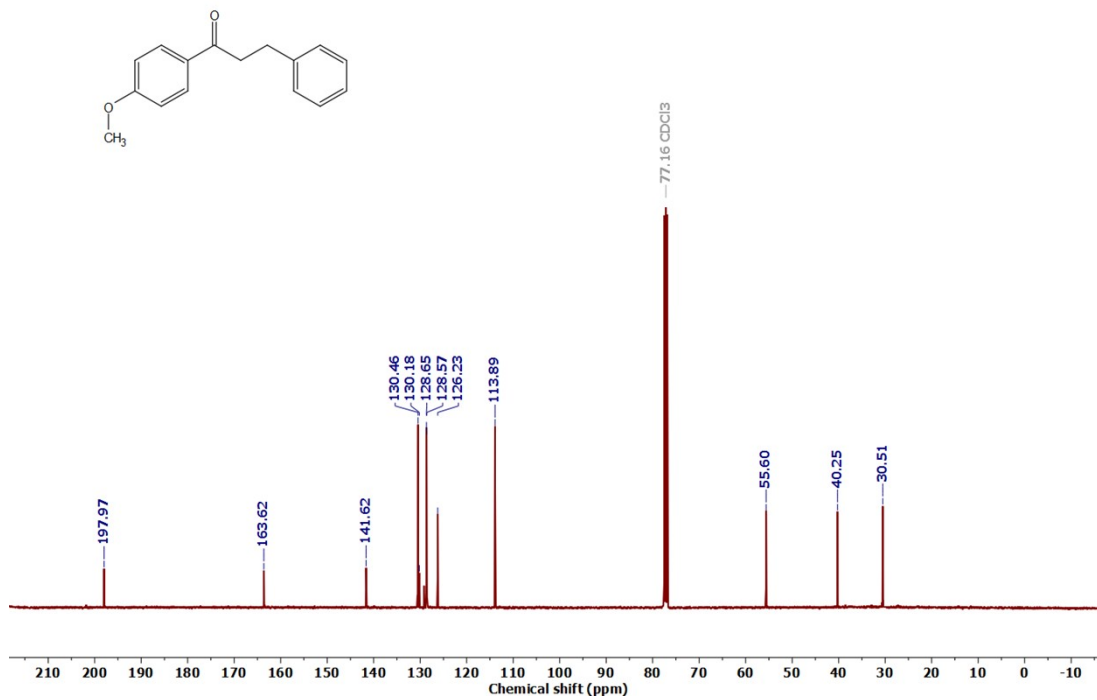
Figure S39: ^{13}C NMR spectrum of **7h**
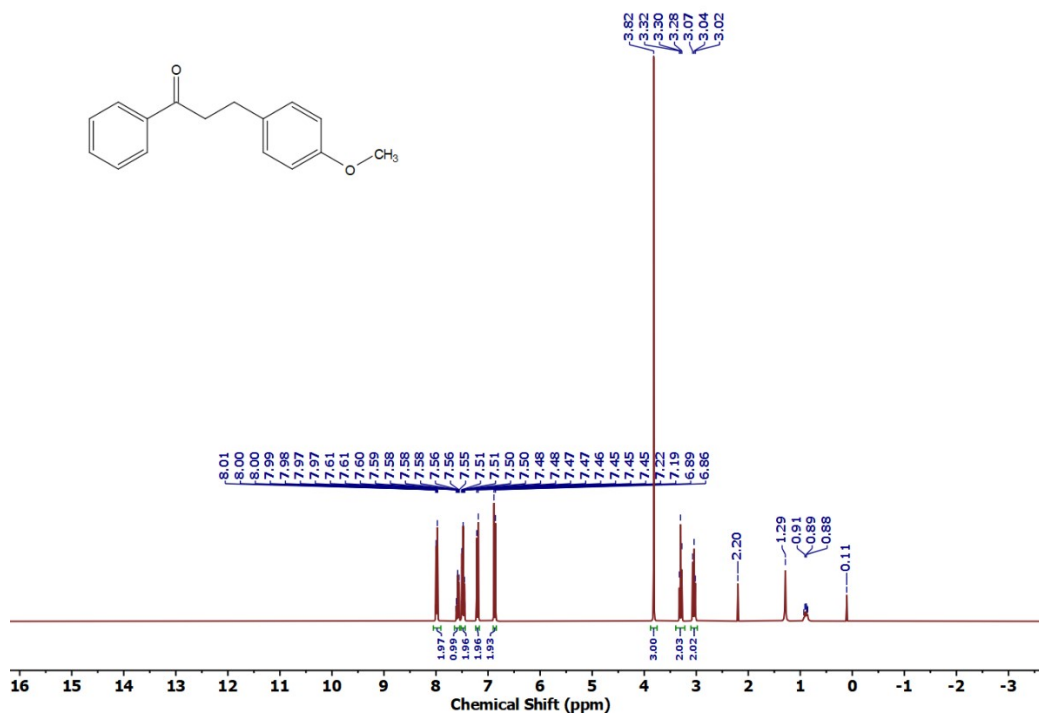
Figure S40: ^1H NMR spectrum of **7i**
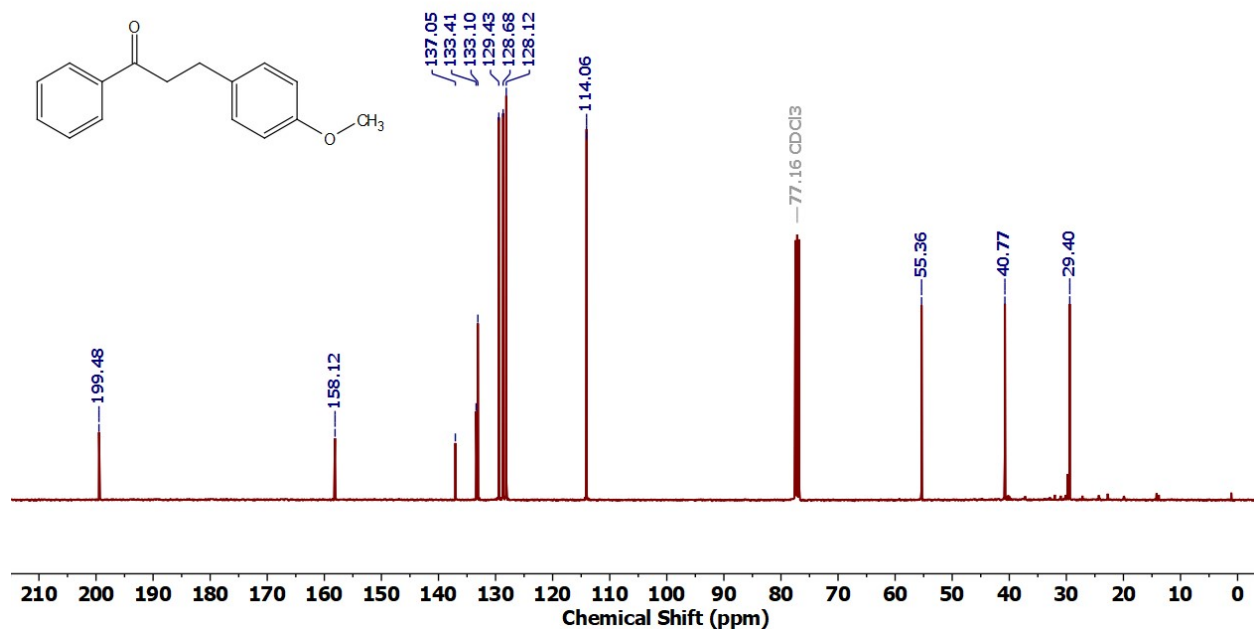
Figure S41: ^{13}C NMR spectrum of **7i**
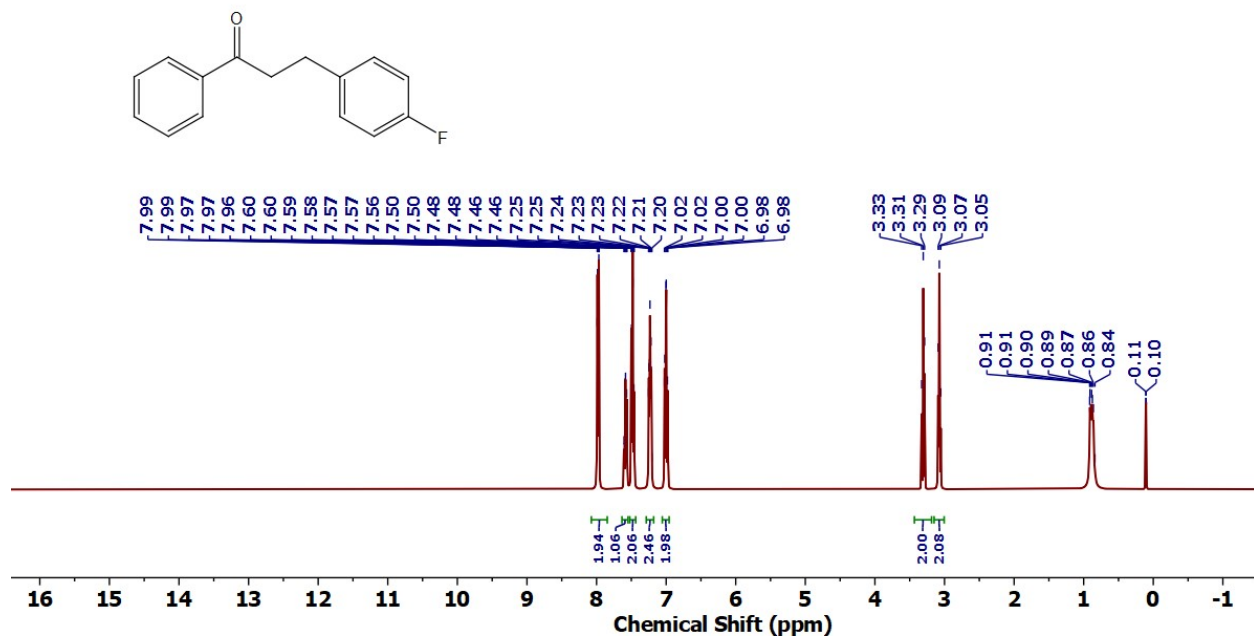
Figure S42: ^{1}H NMR spectrum of **7j**
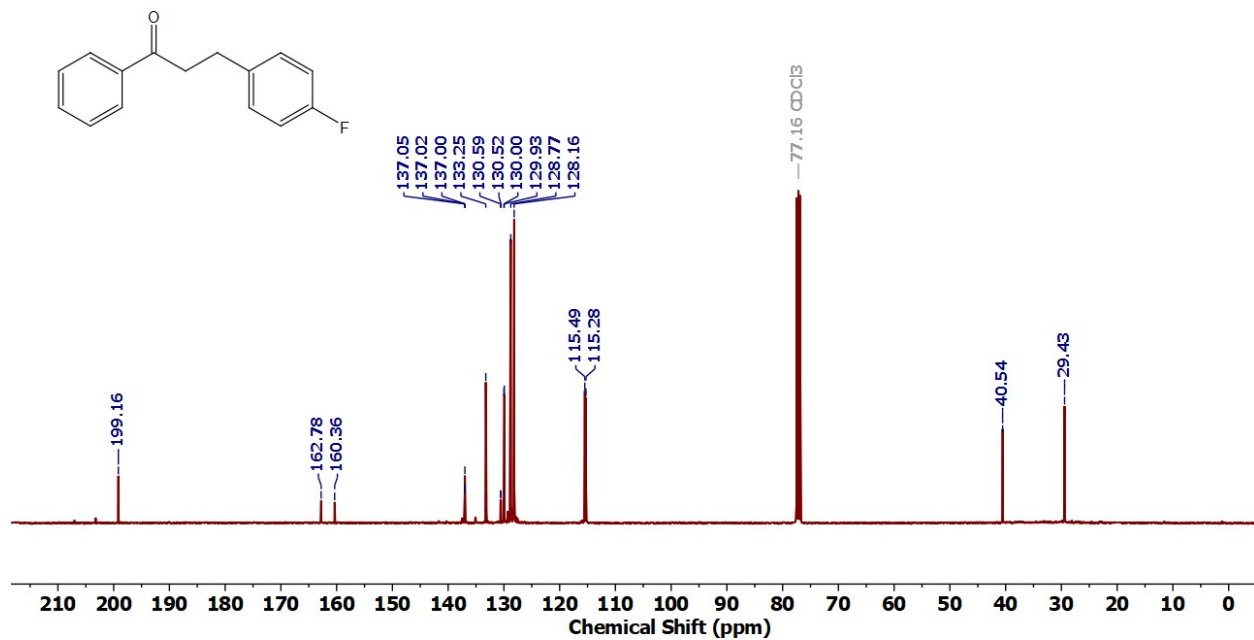
Figure S43: ^{13}C NMR spectrum of **7j**
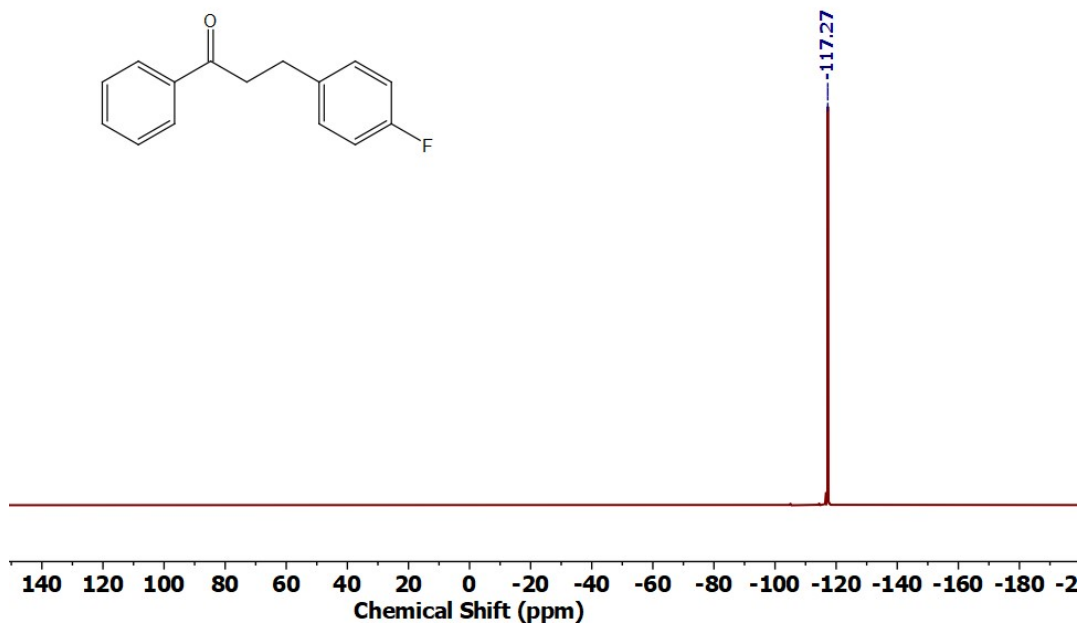
Figure S44: ^{19}F NMR spectrum of **7j**
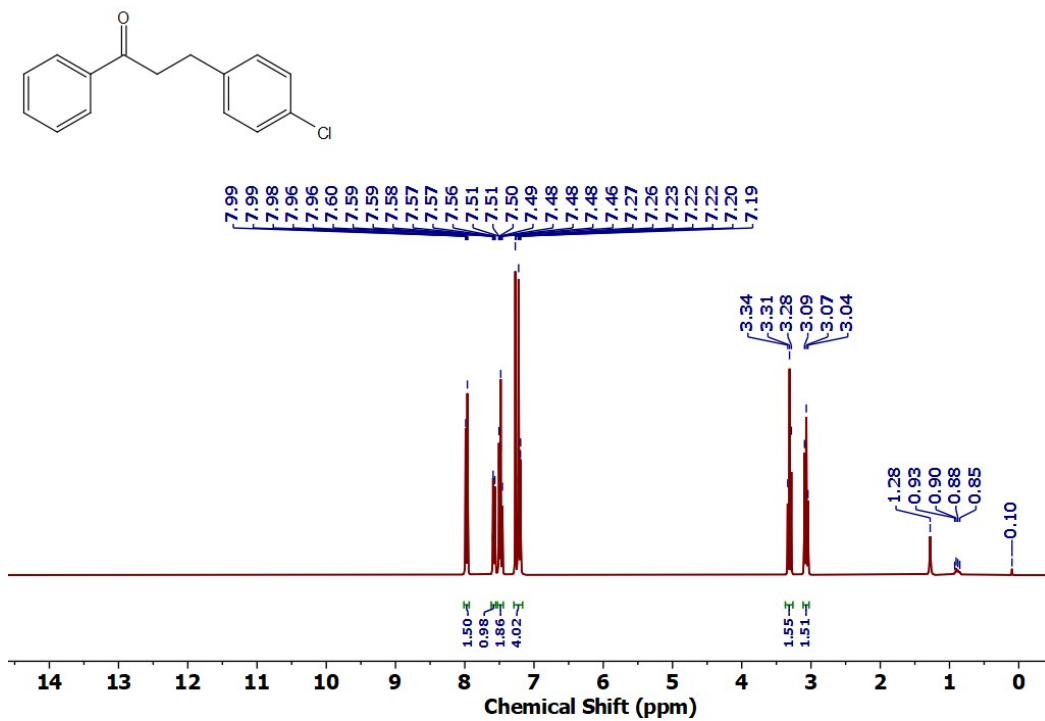
Figure S45: ¹H NMR spectrum of **7k**
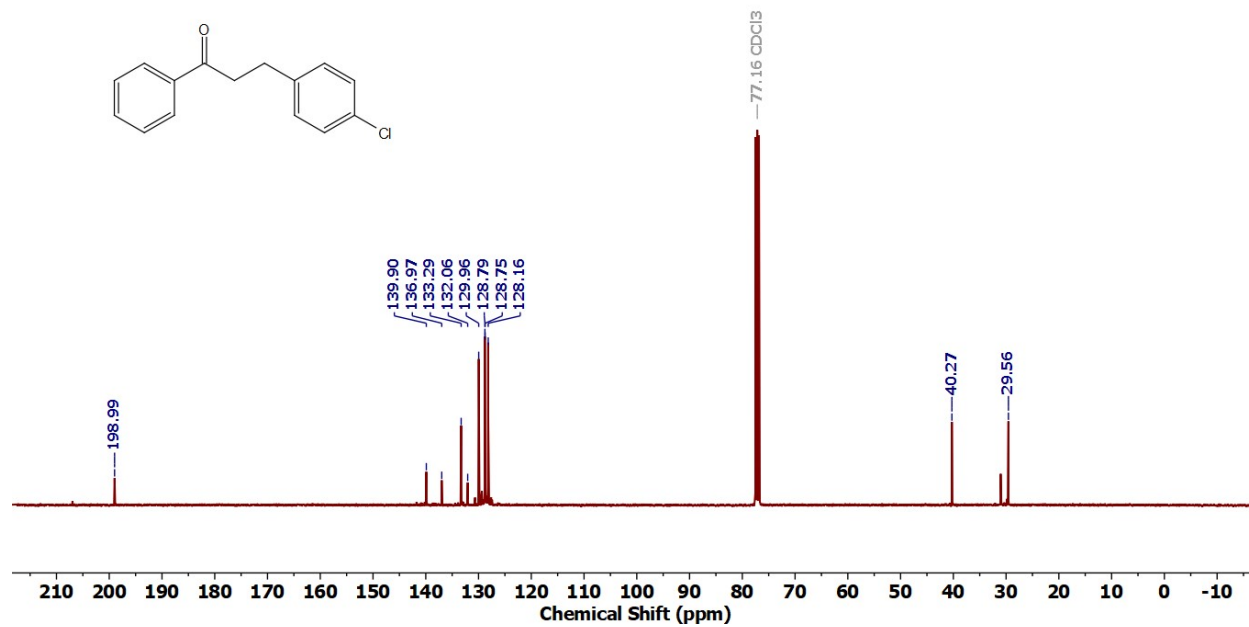
Figure S46: ¹³C NMR spectrum of **7k**
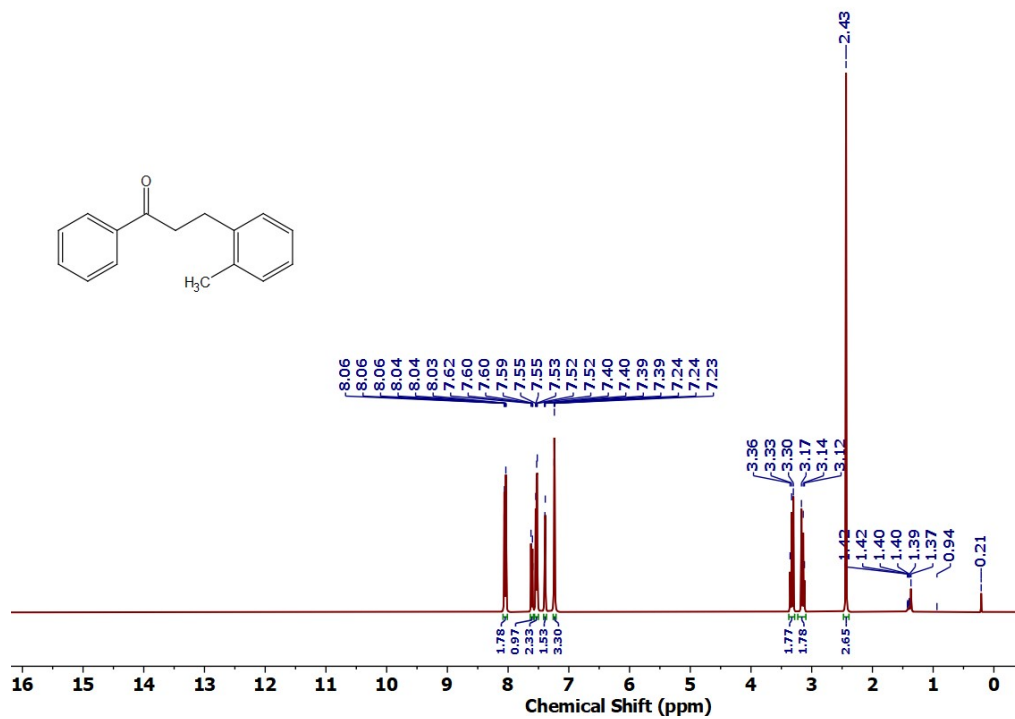
Figure S47: ^{1}H NMR spectrum of **7l**
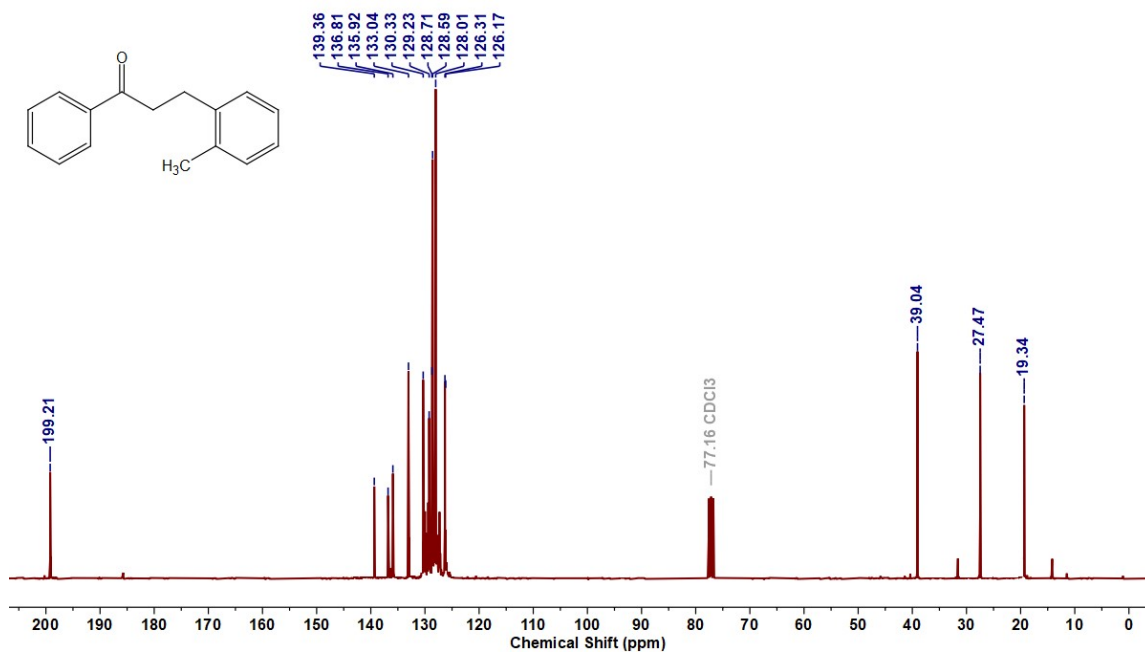
Figure S48: ^{13}C NMR spectrum of **7l**
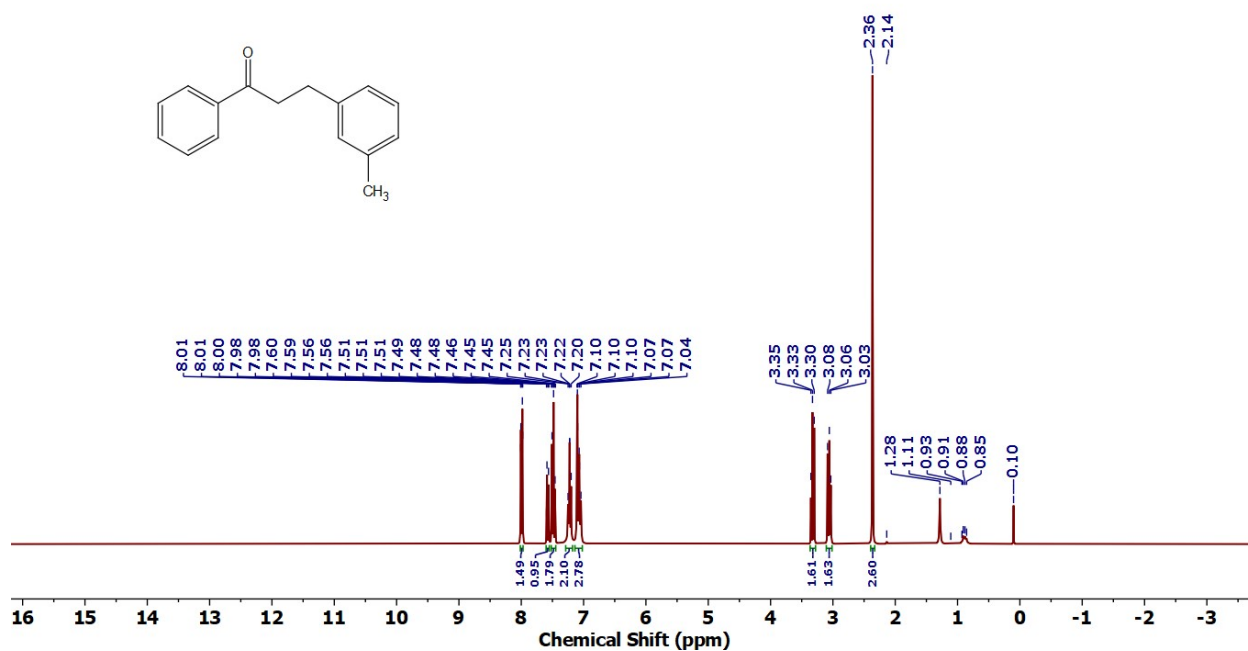
Figure S49: ^{1}H NMR spectrum of **7m**
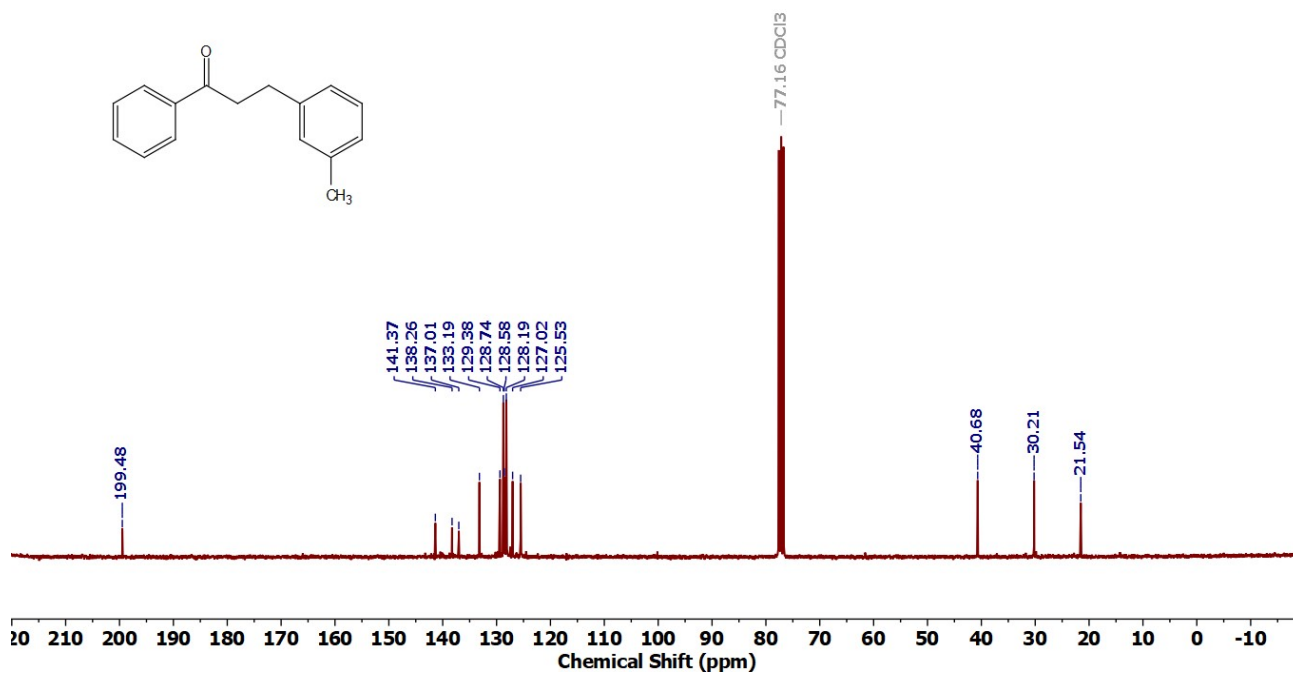
Figure S50: ^{13}C NMR spectrum of **7m**

S62
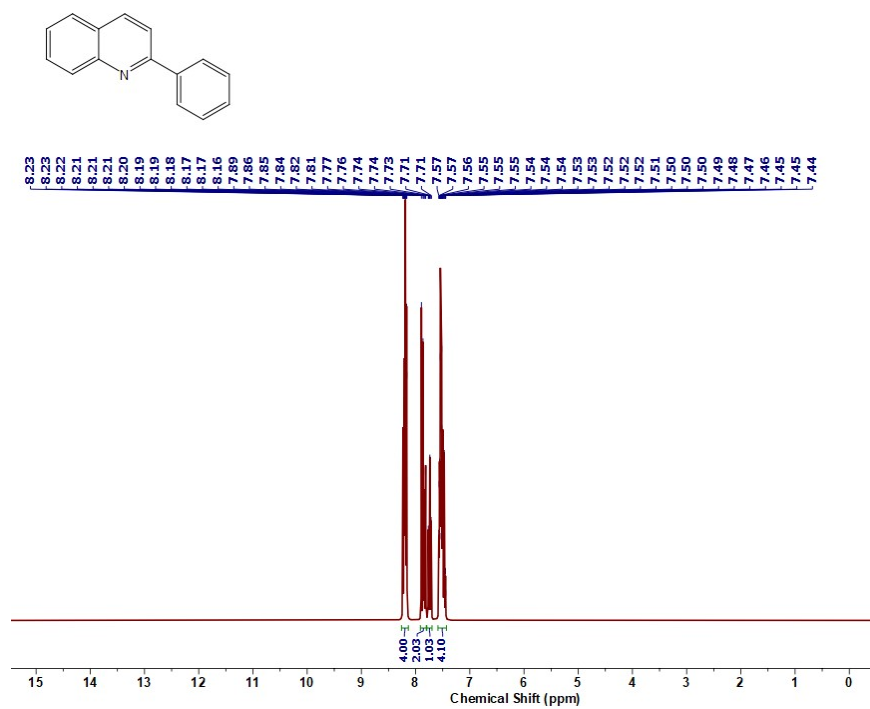
Figure S51: ^{1}H NMR spectrum of 10**a**
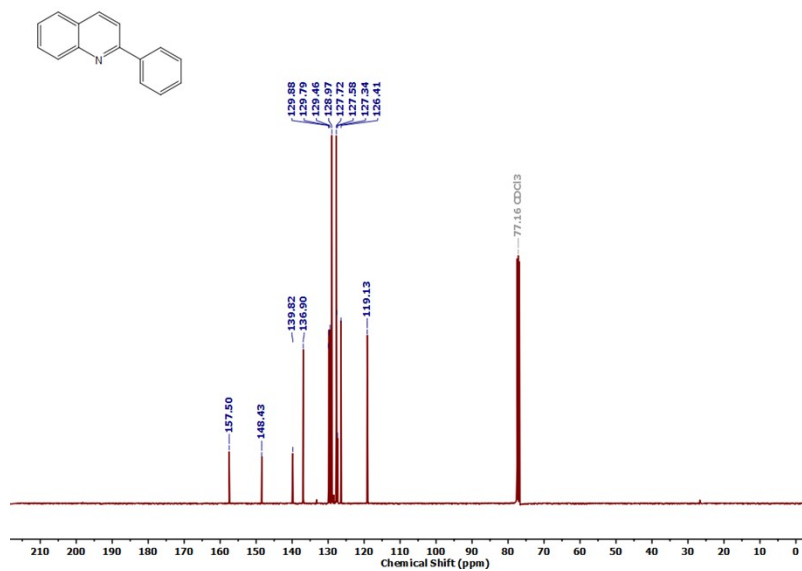
Figure S52: ^{13}C NMR spectrum of 10**a**
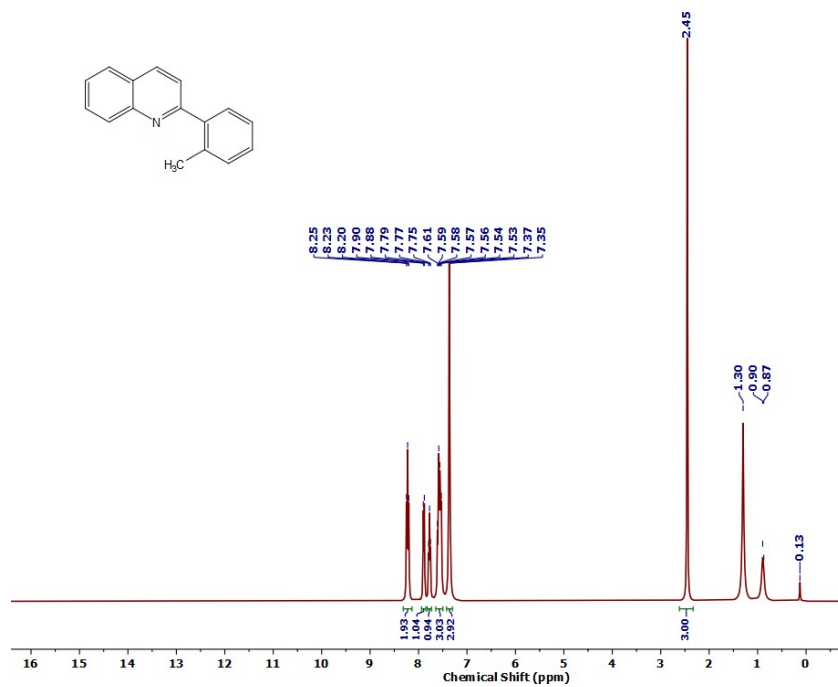
Figure S53: ^{1}H NMR spectrum of **10b**
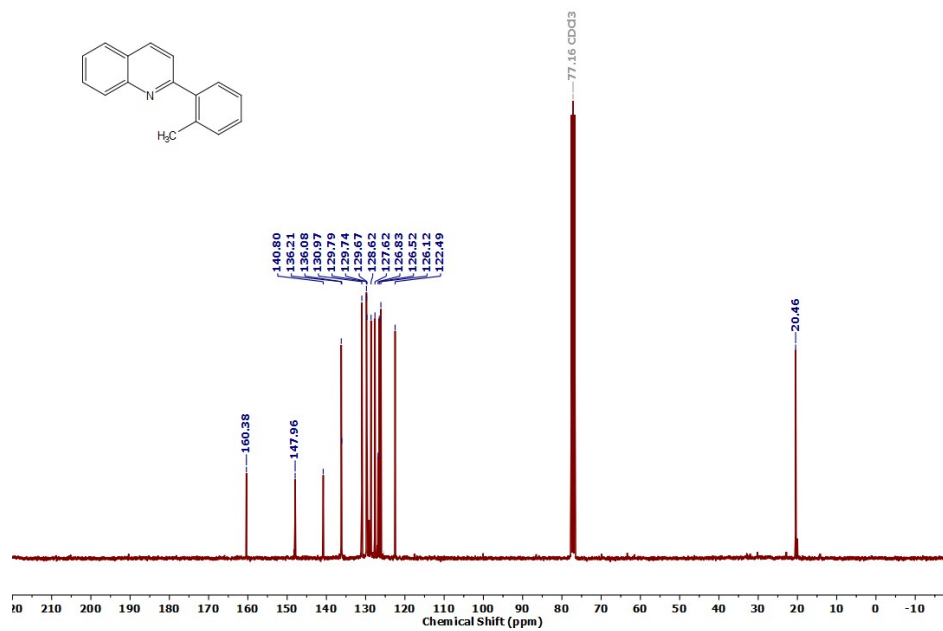
Figure S54: ^{13}C NMR spectrum of **10b**
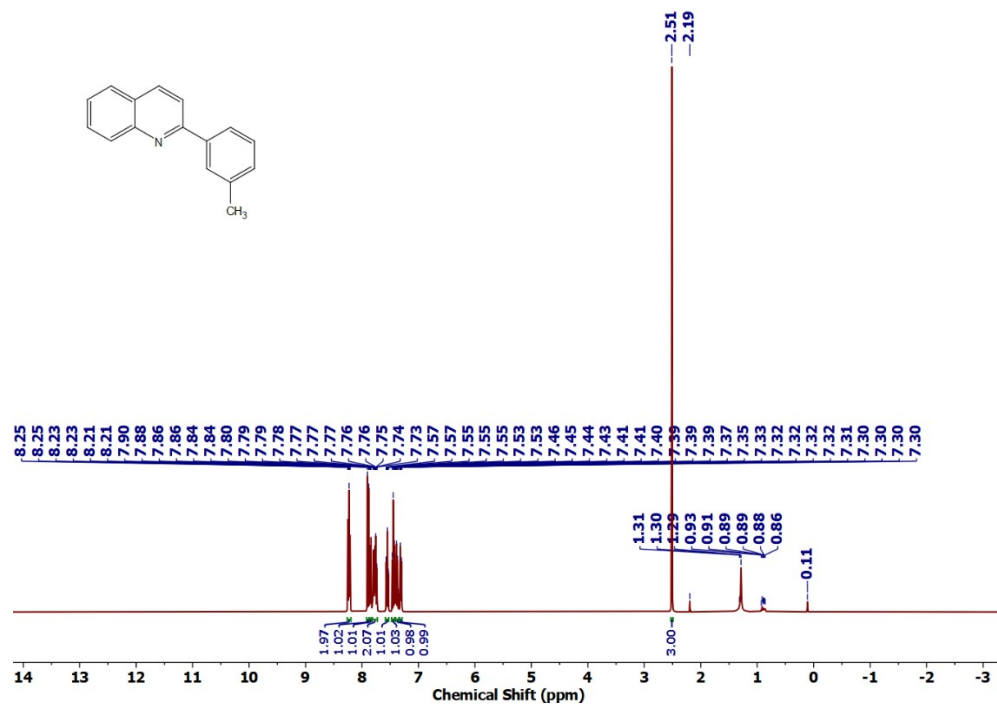
Figure S55: ^{1}H NMR spectrum of **10c**
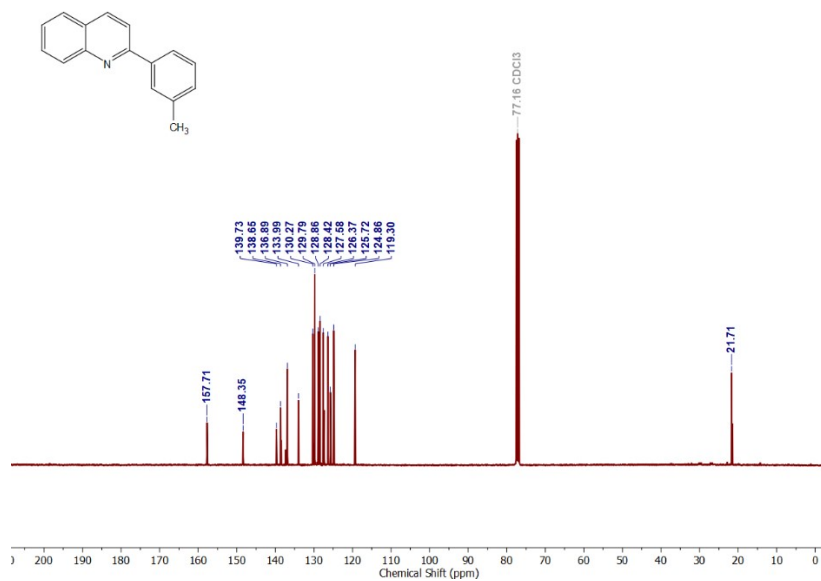
Figure S56: ^{13}C NMR spectrum of **10c**
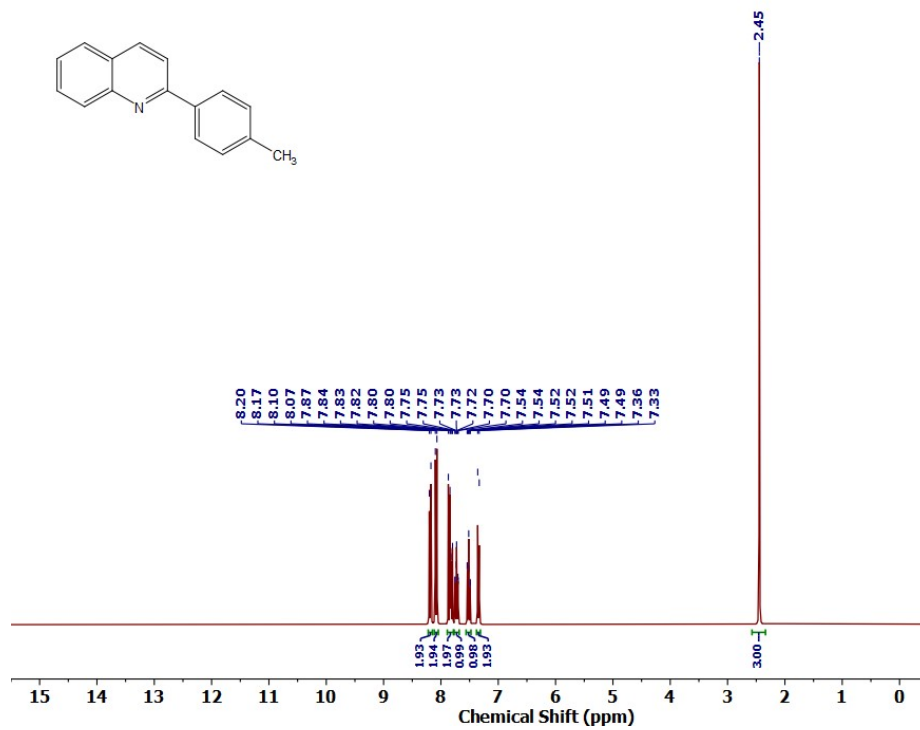
Figure S57: ^{1}H NMR spectrum of **10d**
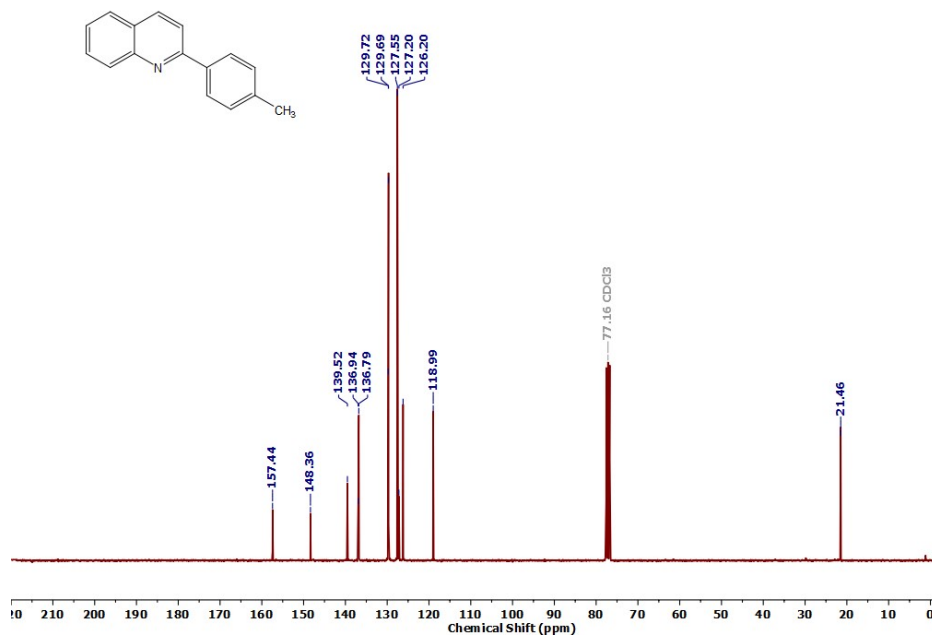
Figure S58: ^{13}C NMR spectrum of **10d**
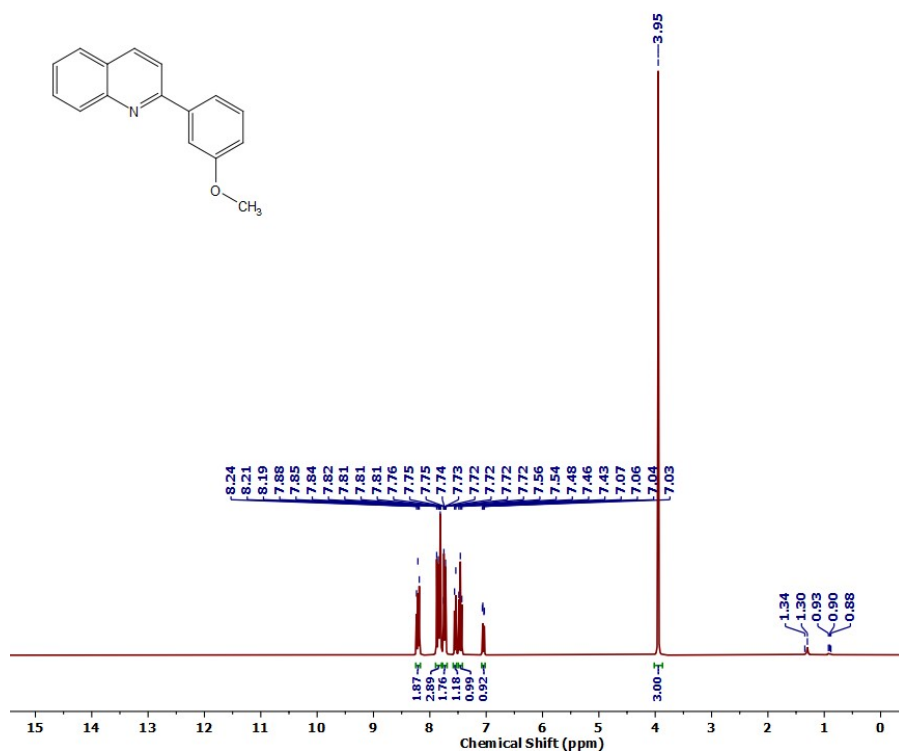
Figure S59: ^{1}H NMR spectrum of **10e**
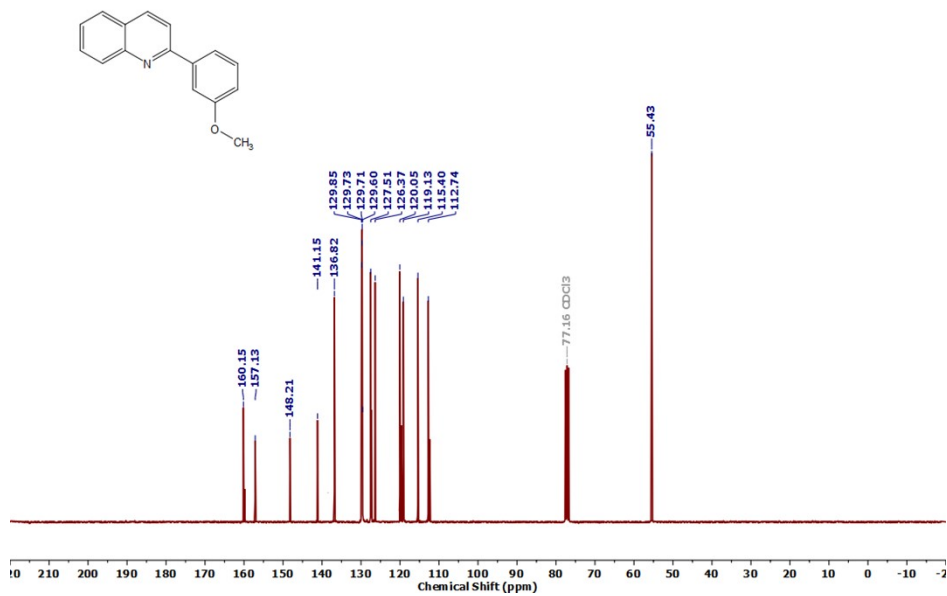
Figure S60: ^{13}C NMR spectrum of **10e**
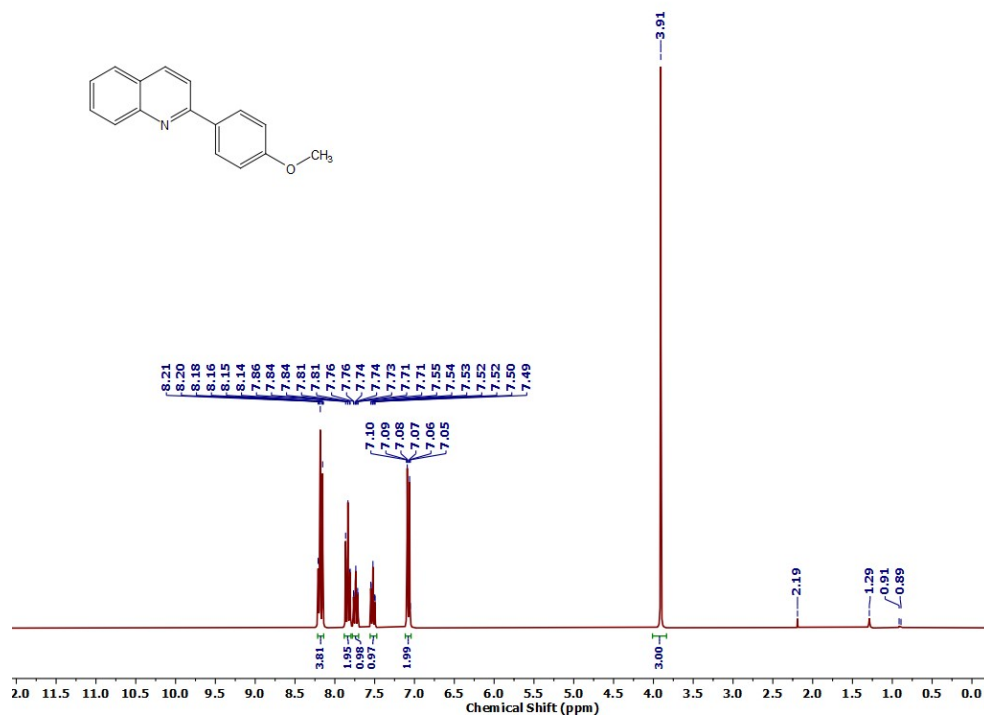
Figure S61: ^{1}H NMR spectrum of **10f**
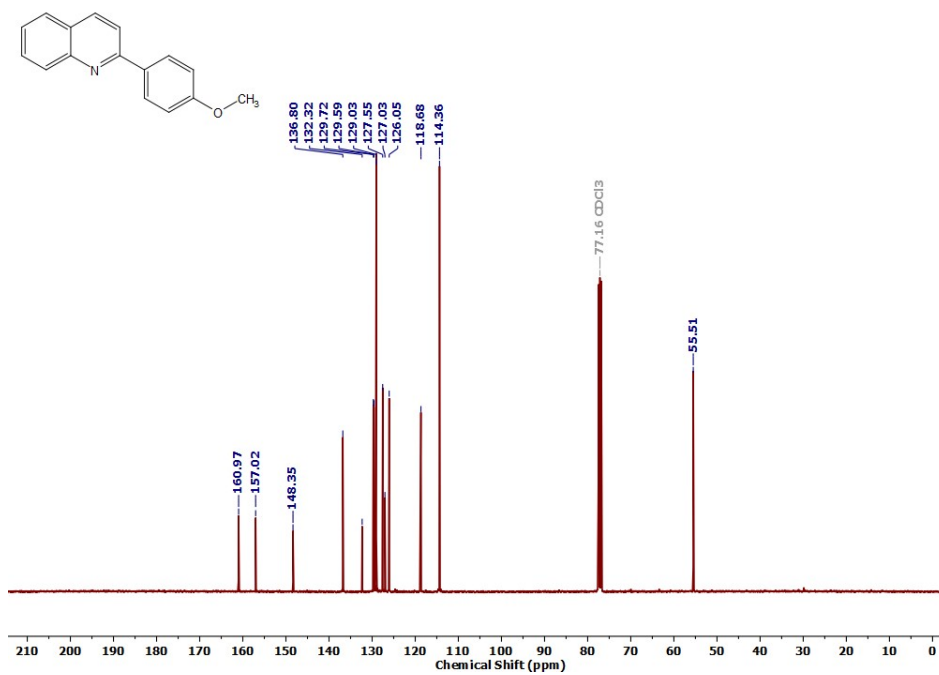
Figure S62: ^{13}C NMR spectrum of **10f**
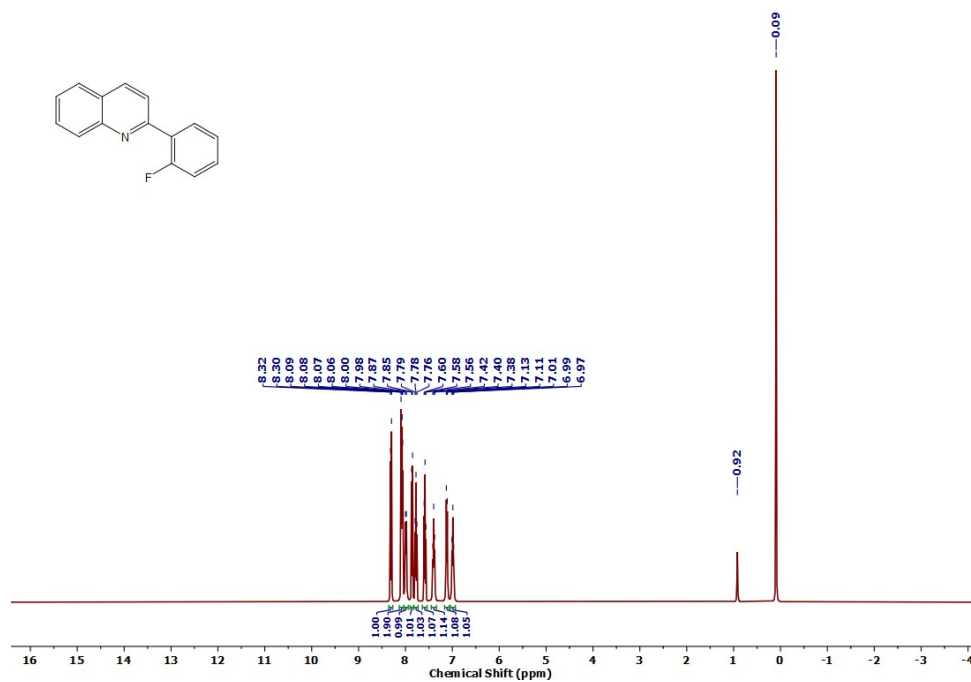
Figure S63: ^{1}H NMR spectrum of **10g**
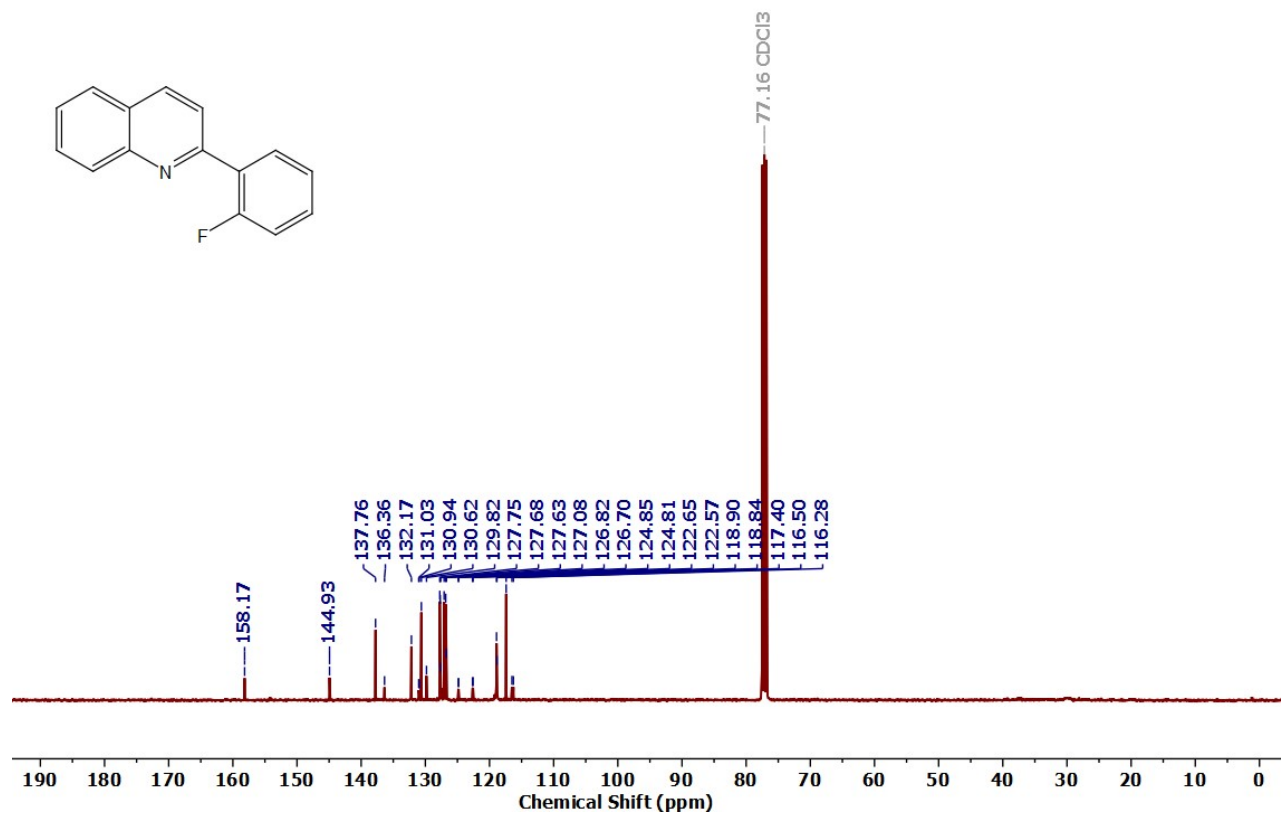
Figure S64: ^{13}C NMR spectrum of **10g**
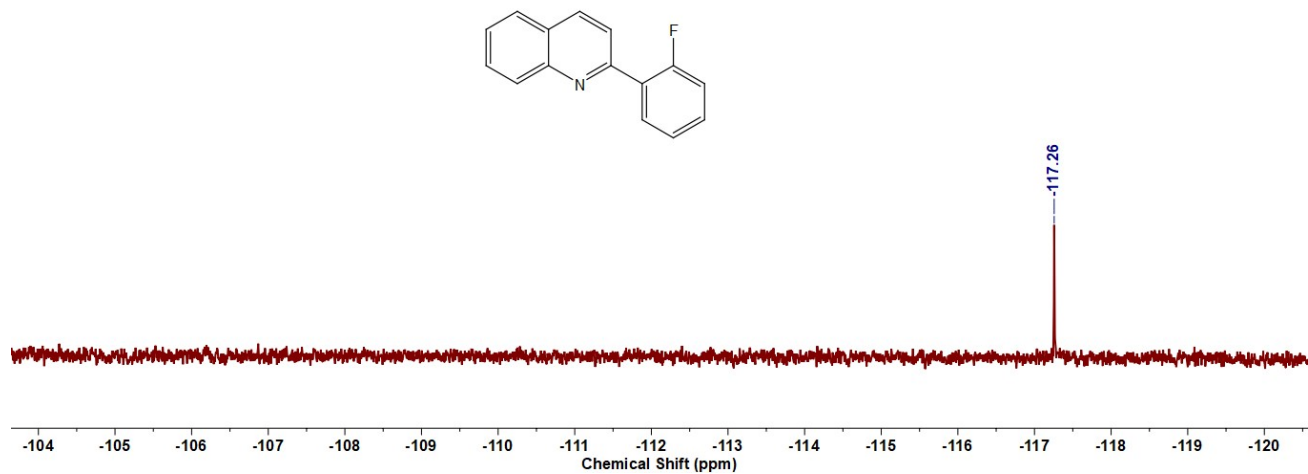
Figure S65: ^{19}F NMR spectrum of **10g**
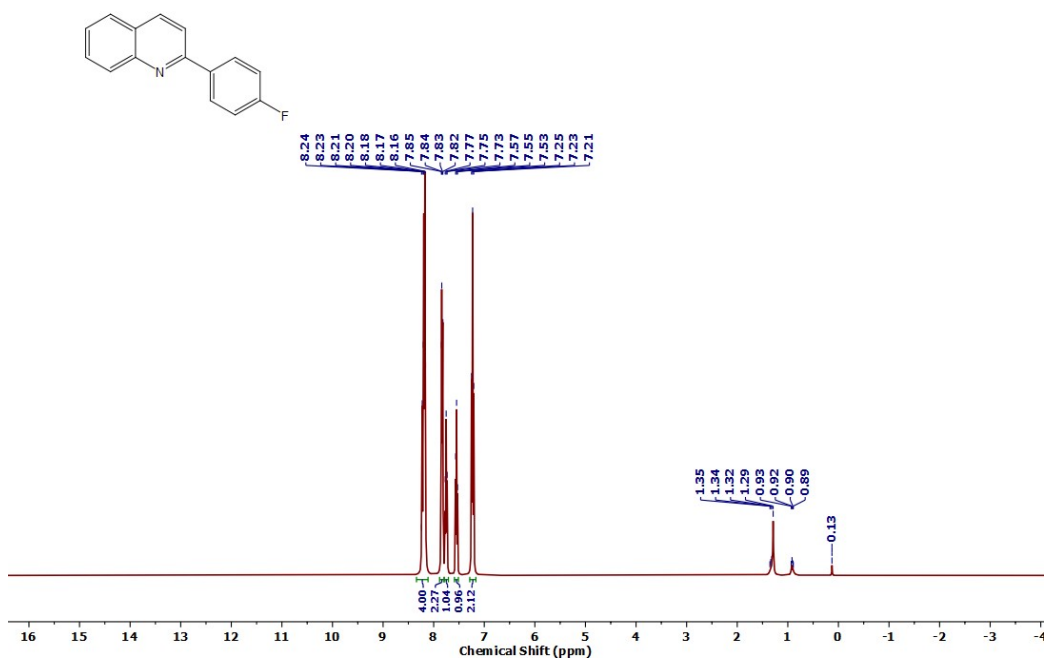
Figure S66: ^{1}H NMR spectrum of **10h**
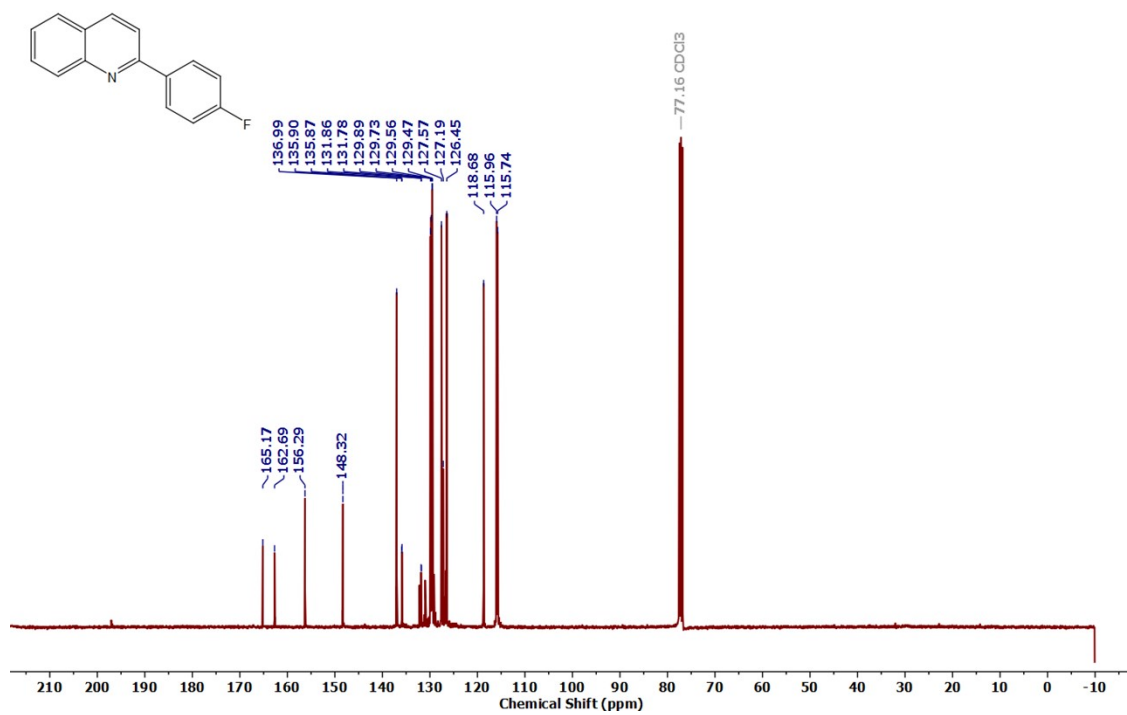
Figure S67: ^{13}C NMR spectrum of **10h**
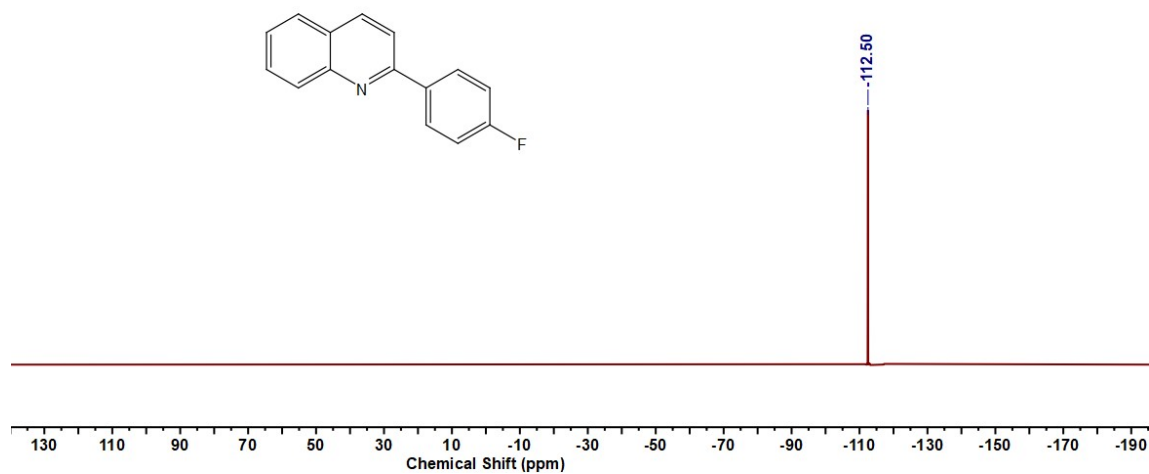
Figure S68: ^{19}F NMR spectrum of **10h**
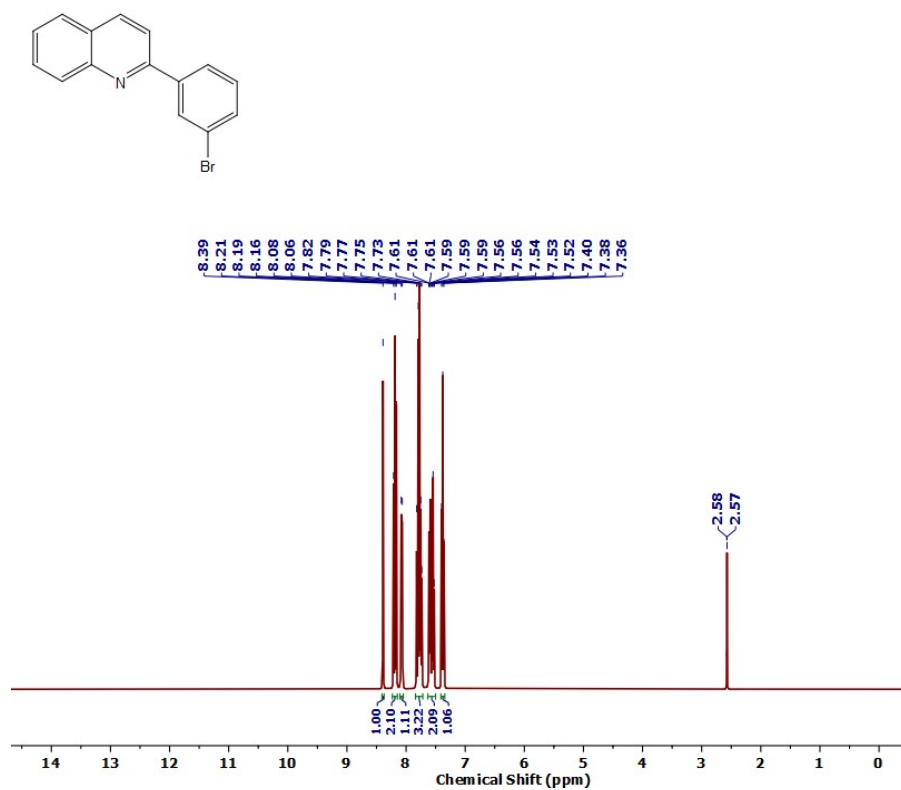
Figure S69: ^{1}H NMR spectrum of **10i**
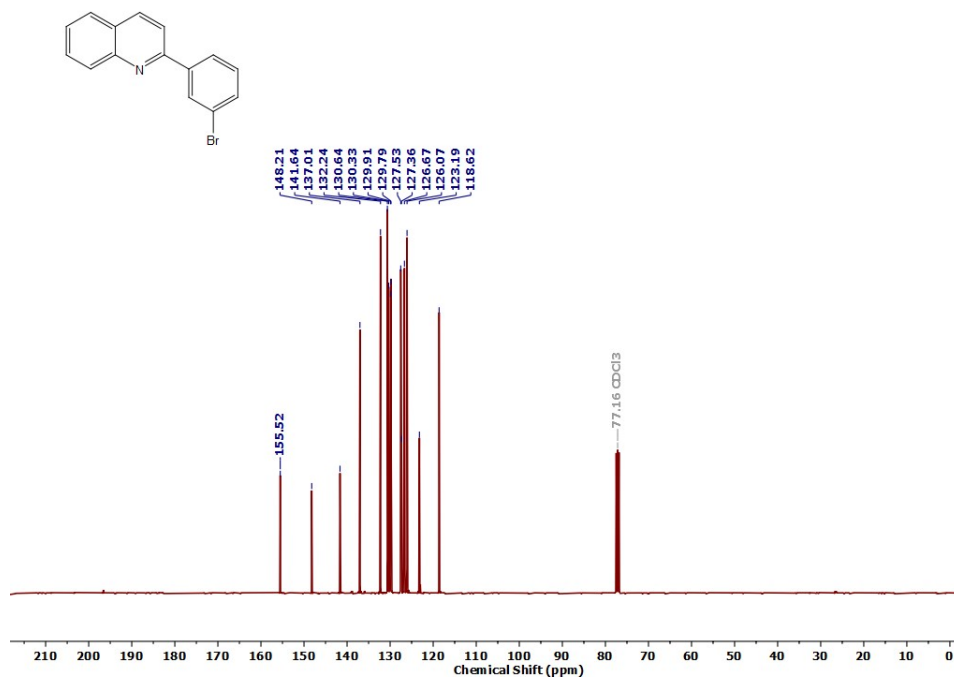
Figure S70: ^{13}C NMR spectrum of **10i**
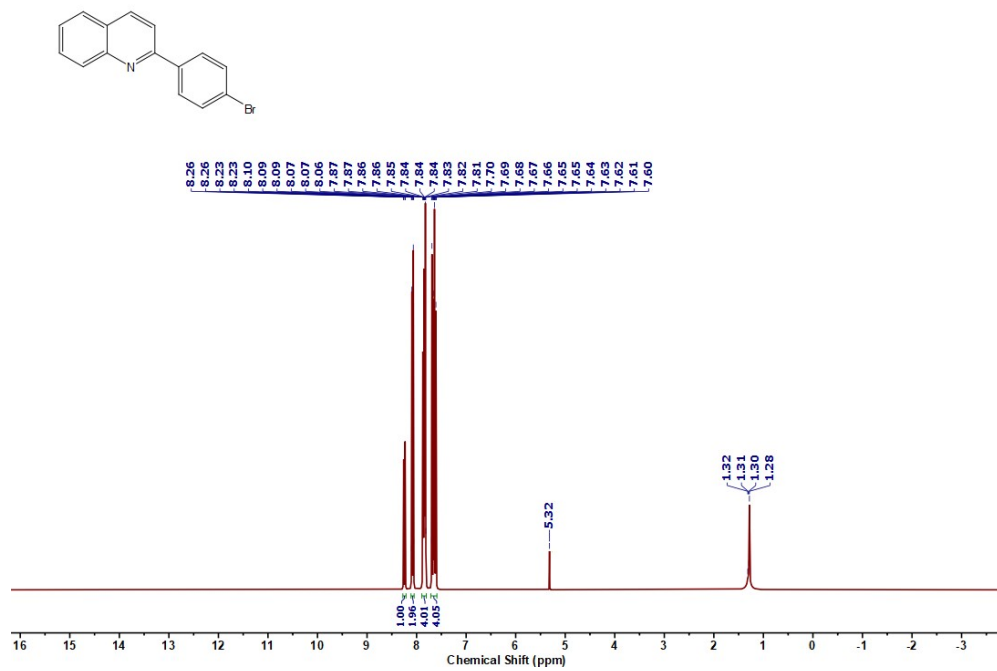
Figure S71: ^{1}H NMR spectrum of **10j**
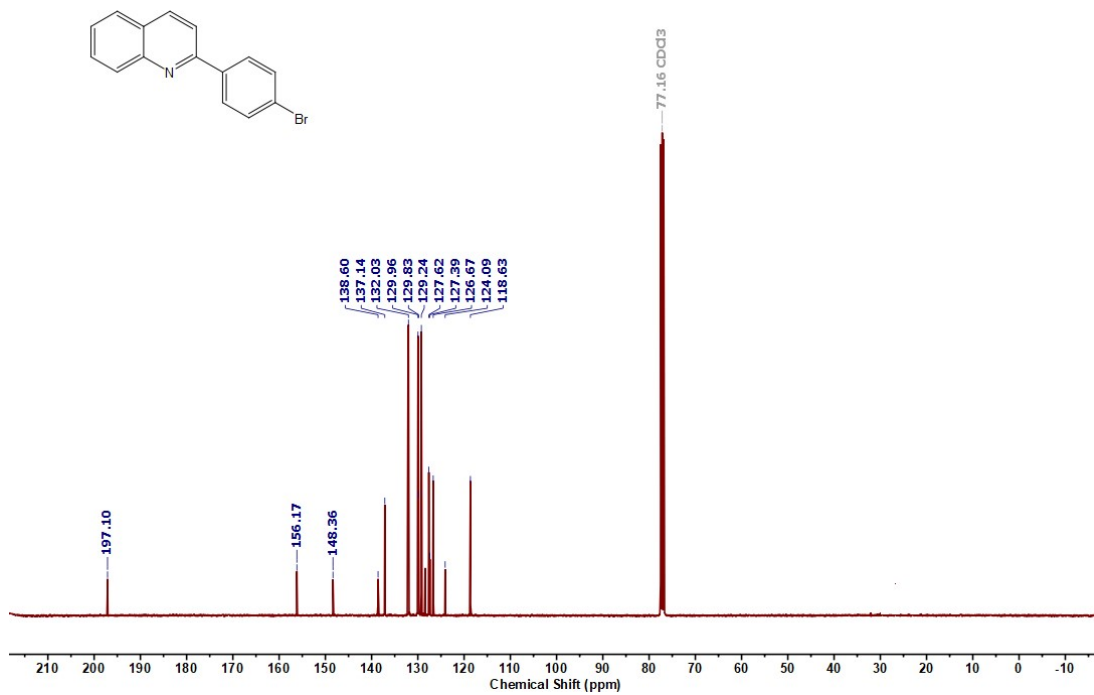
Figure S72: ^{13}C NMR spectrum of **10j**

Figure S73: ^{1}H NMR spectrum of **10k**

Figure S74: ^{13}C NMR spectrum of **10k**

Figure S75: ¹H NMR spectrum of **10l**

Figure S76: ¹³C NMR spectrum of **10l**
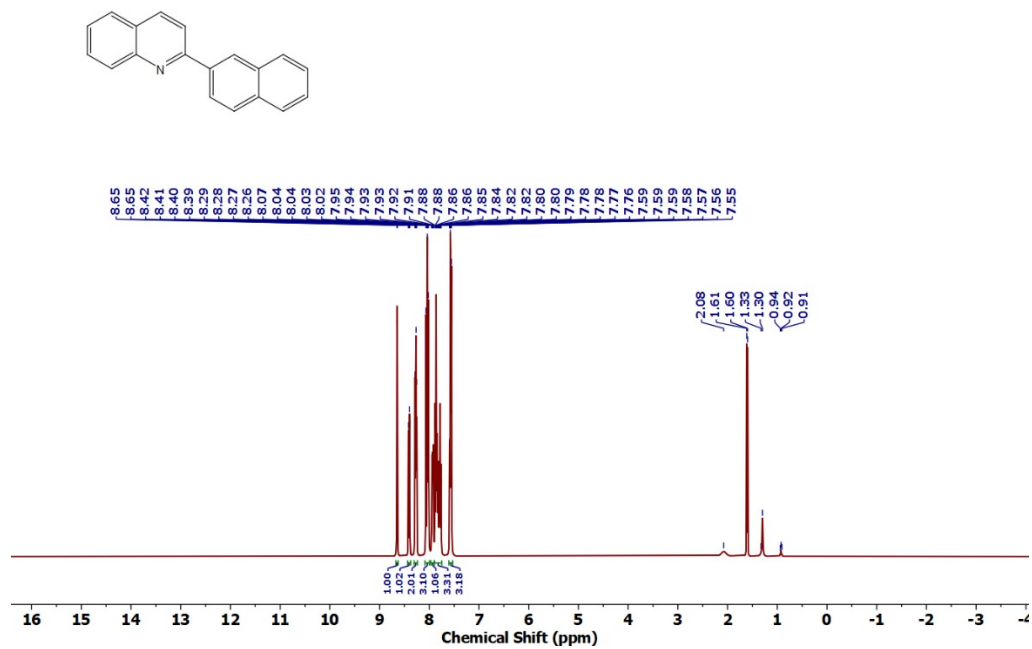
Figure S77: ^{1}H NMR spectrum of **10m**
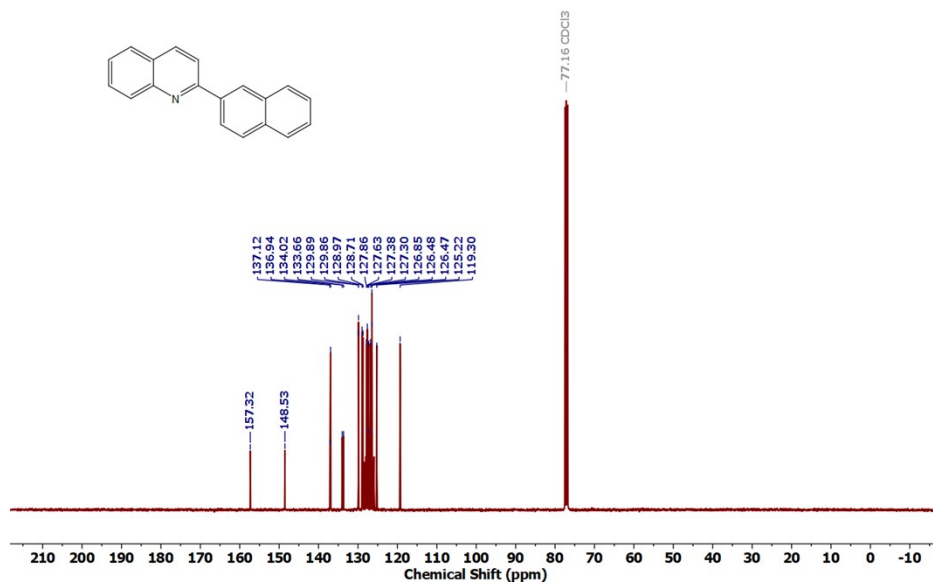
Figure S78: ^{13}C NMR spectrum of **10m**
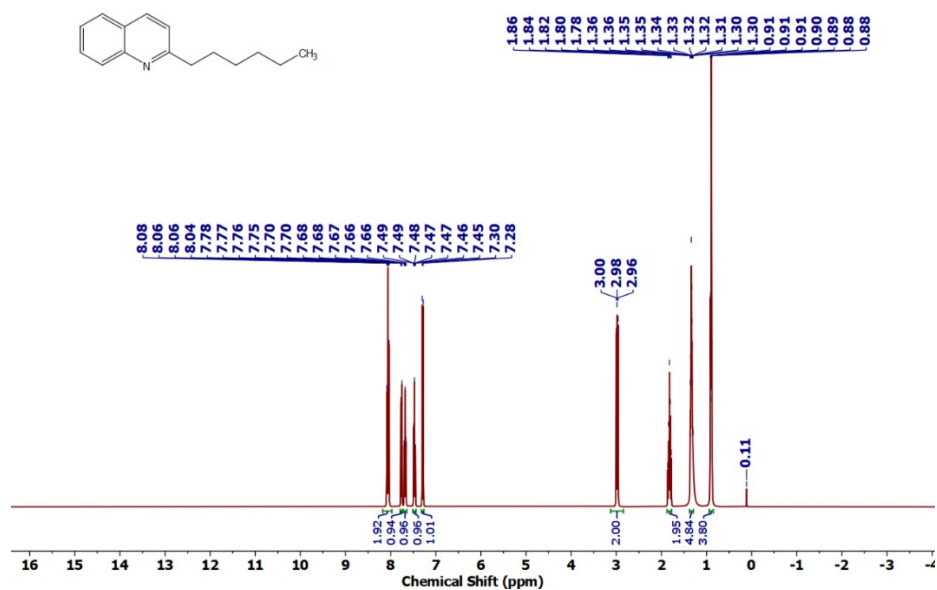
Figure S79: ¹H NMR spectrum of **10n**
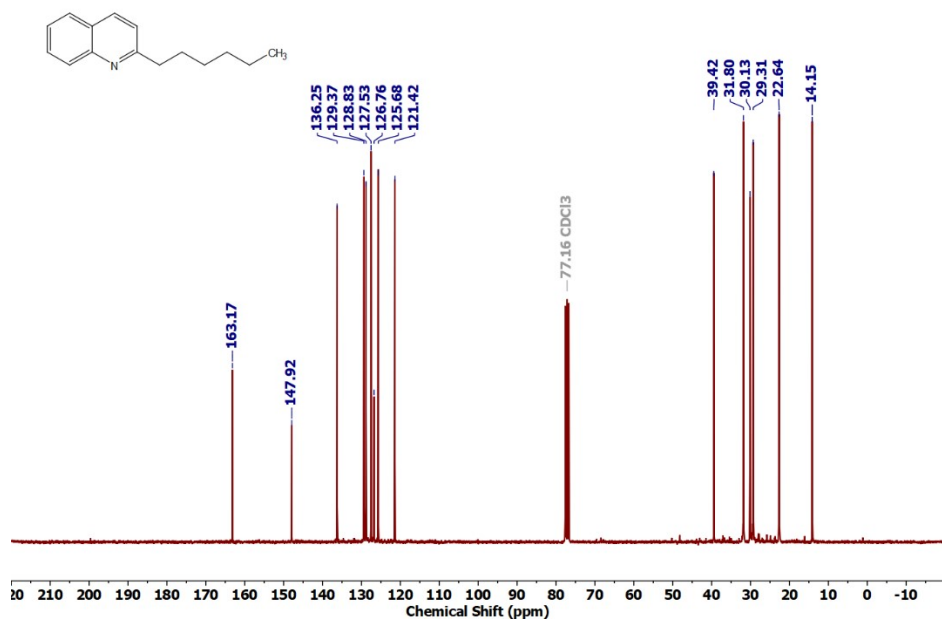
Figure S80: ¹³C NMR spectrum of **10n**

S77
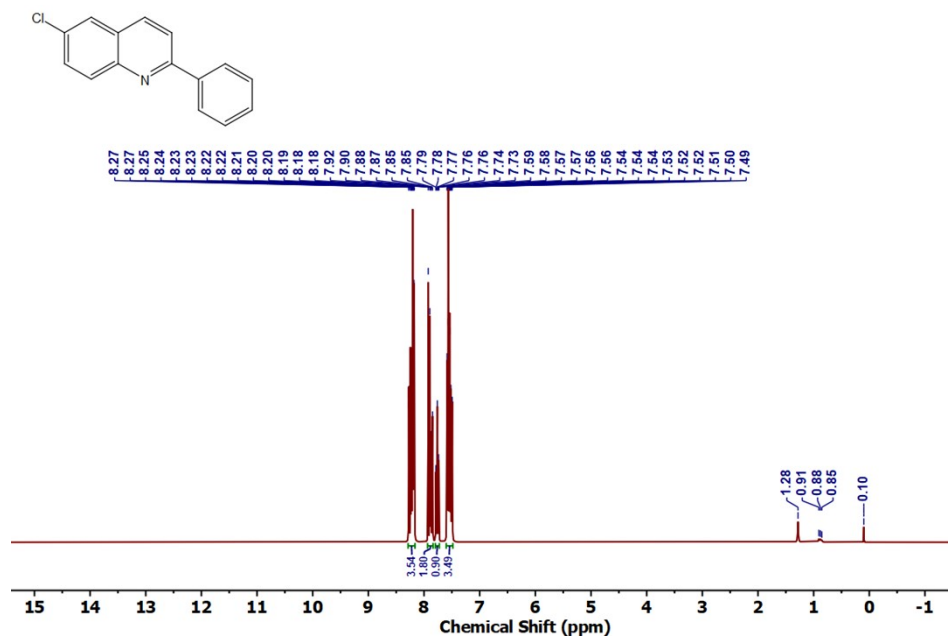
Figure S81: ^{1}H NMR spectrum of **10o**
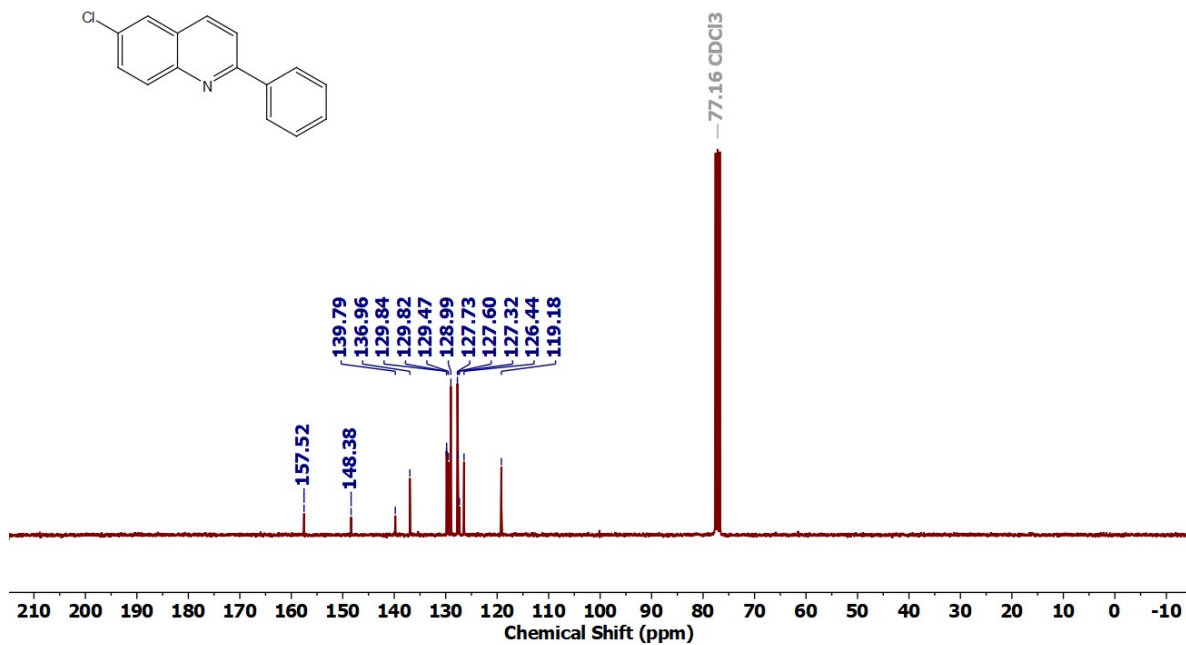
Figure S82: ^{13}C NMR spectrum of **10o**
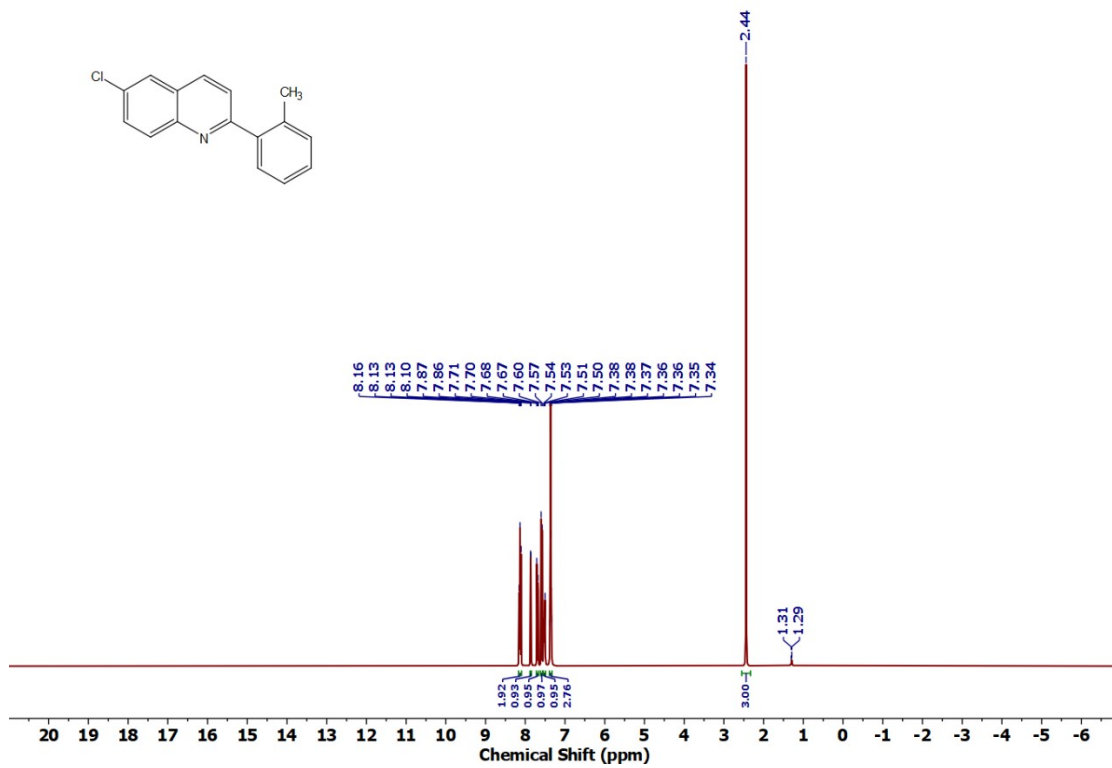
Figure S83: ^{1}H NMR spectrum of **10p**
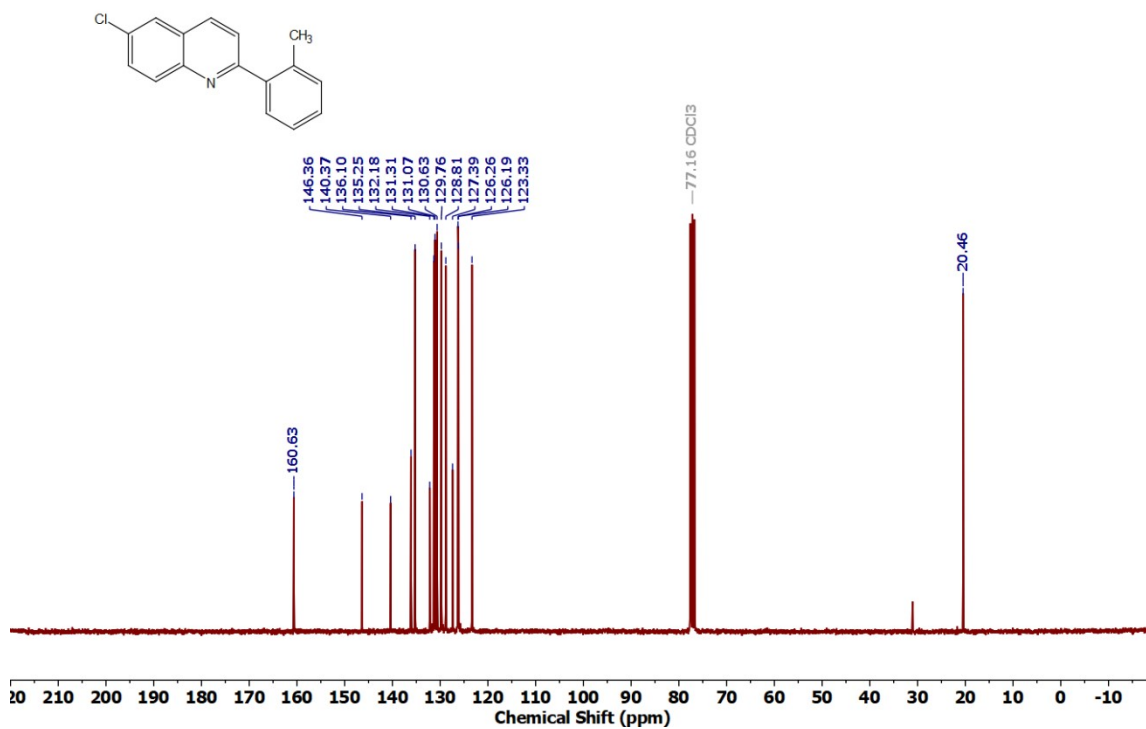
Figure S84: ^{13}C NMR spectrum of **10p**
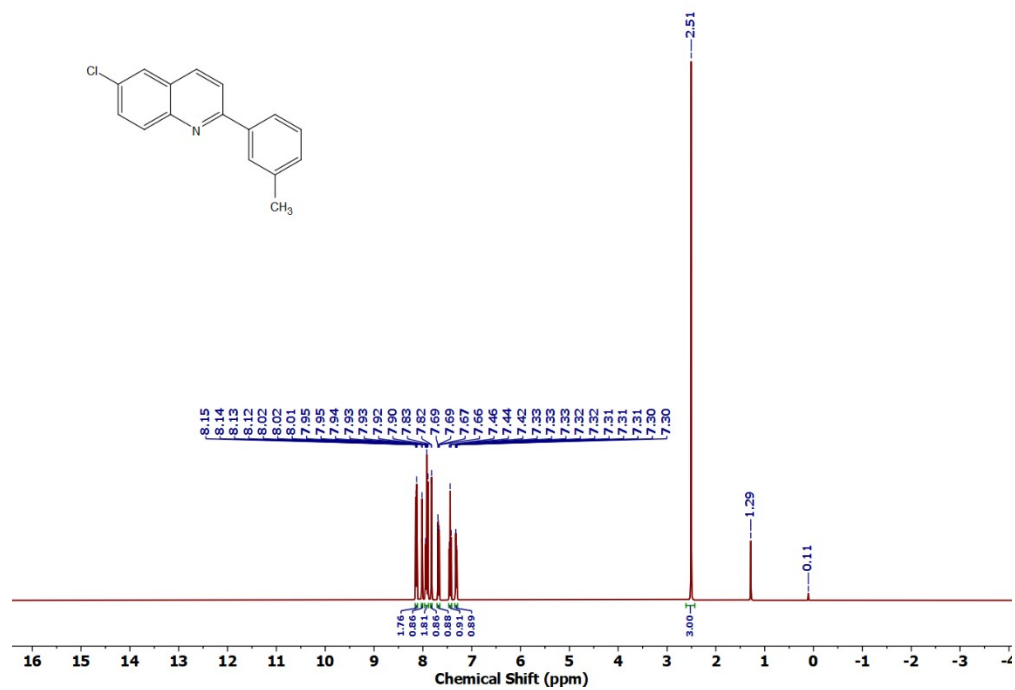
Figure S85: ^{1}H NMR spectrum of **10q**
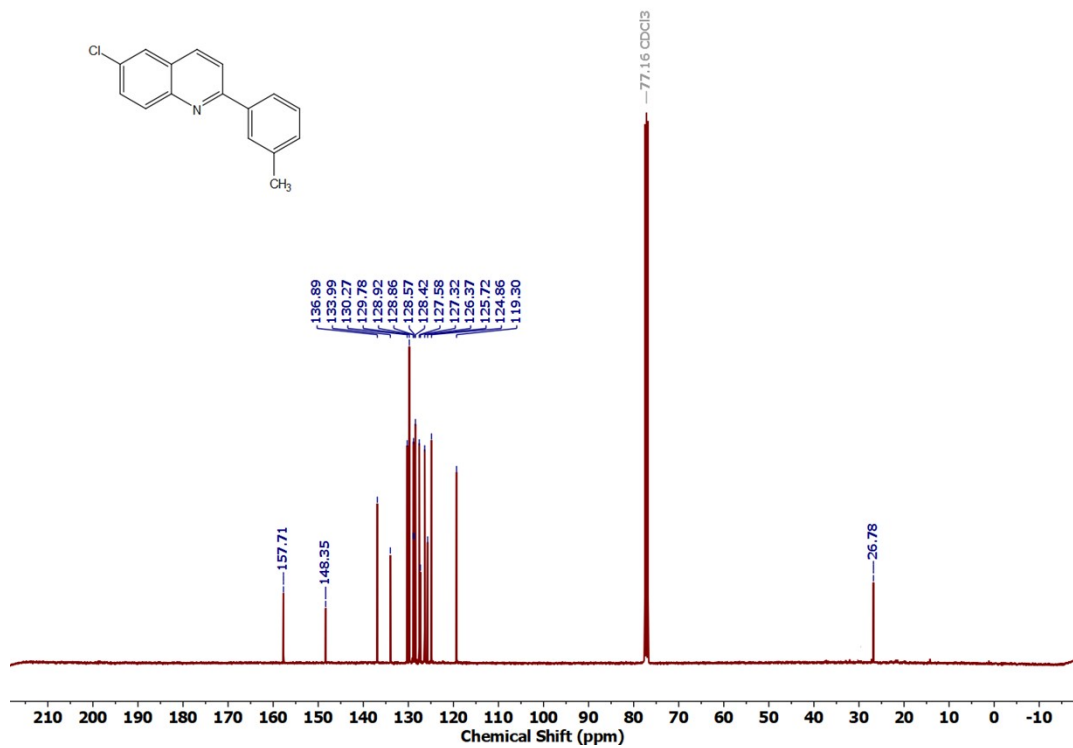
Figure S86: ^{13}C NMR spectrum of **10q**
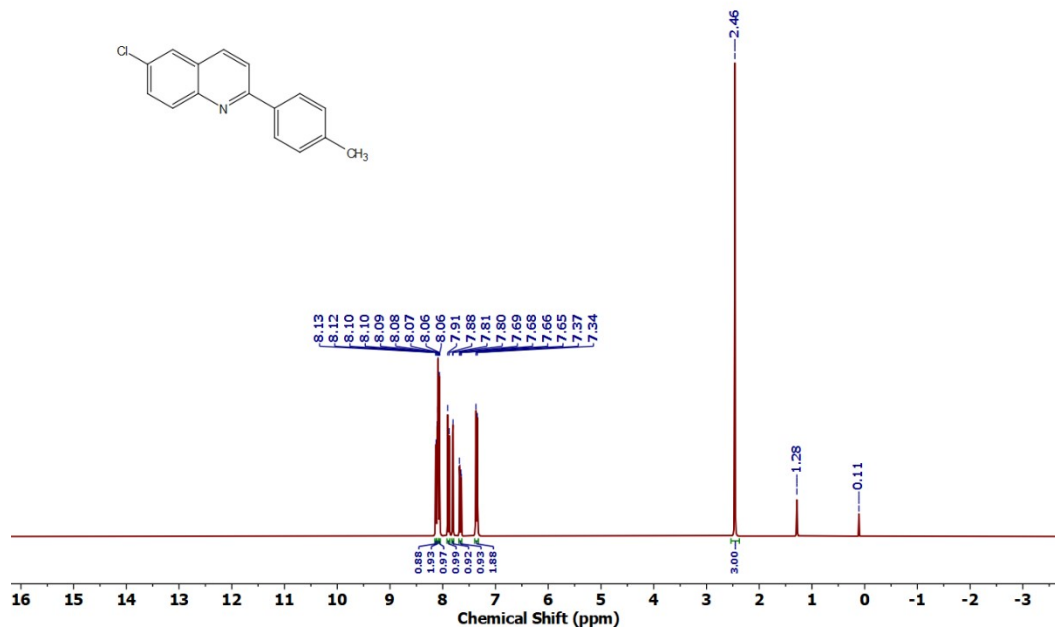
Figure S87: ^{1}H NMR spectrum of **10r**
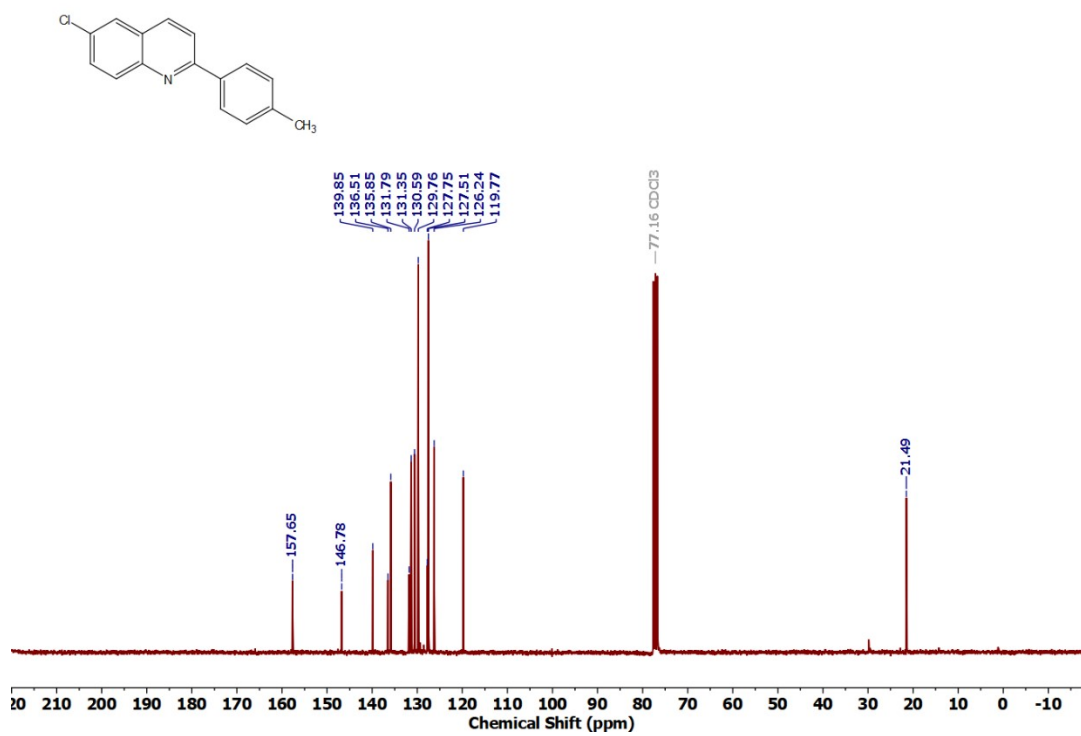
Figure S88: ^{13}C NMR spectrum of **10r**
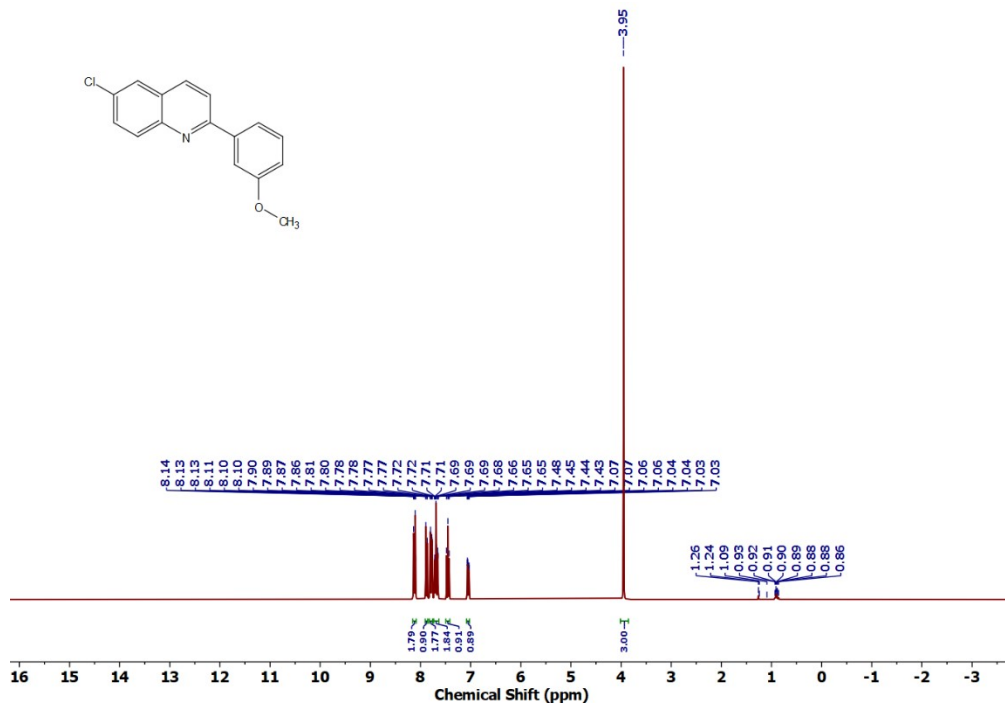
Figure S89: ^{1}H NMR spectrum of **10s**
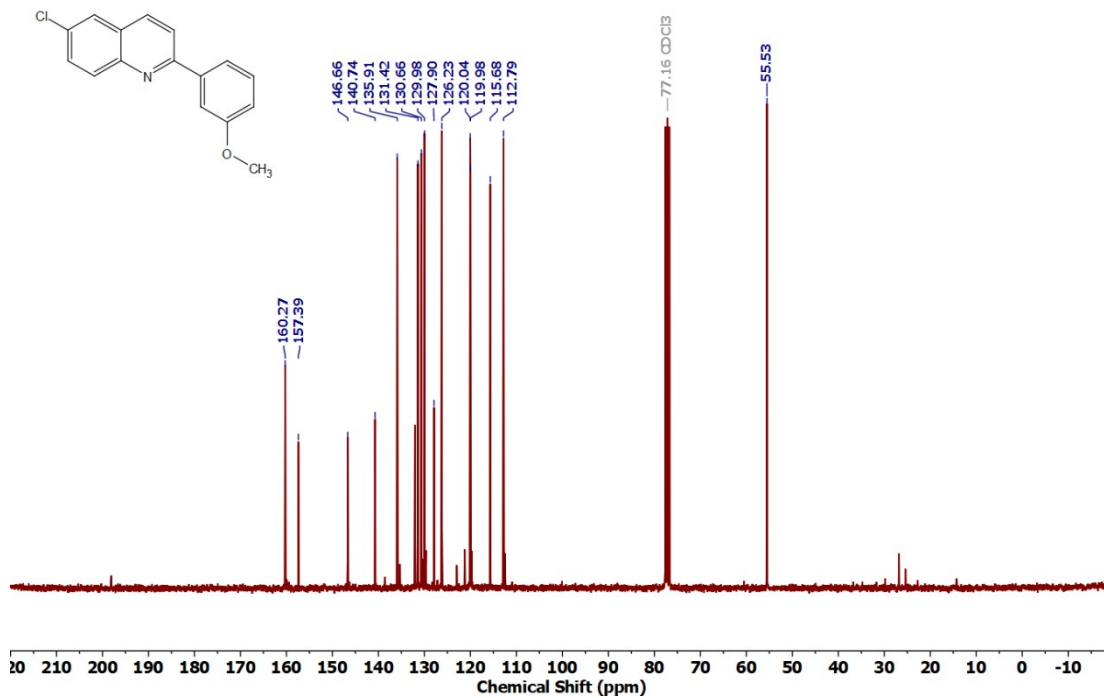
Figure S90: ^{13}C NMR spectrum of **10s**
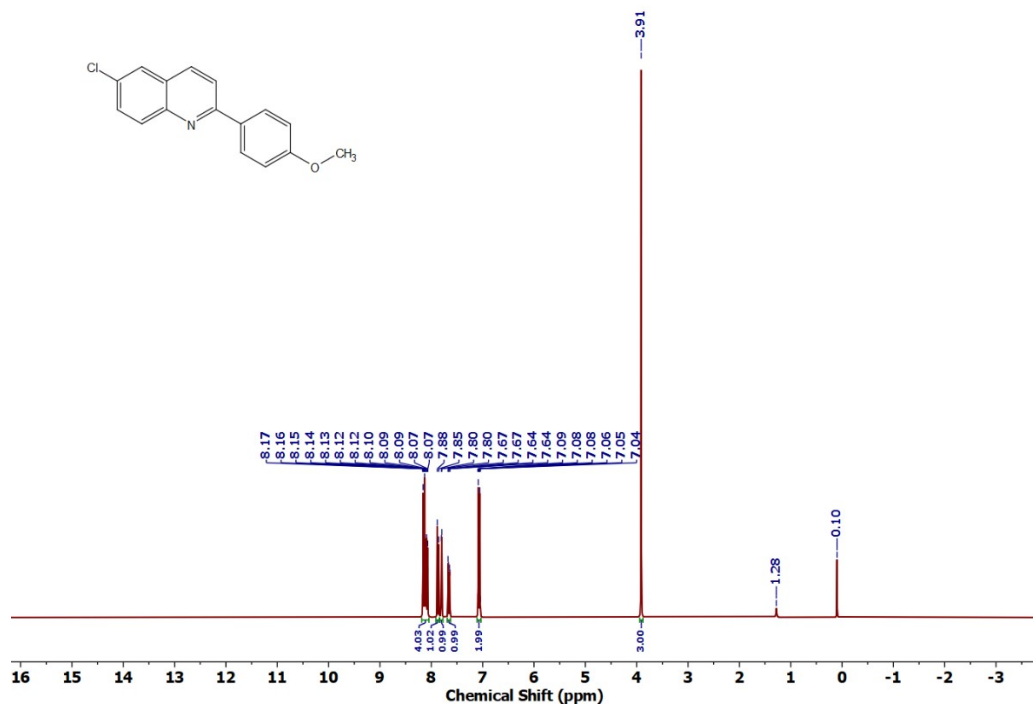
Figure S91: ^{1}H NMR spectrum of **10t**
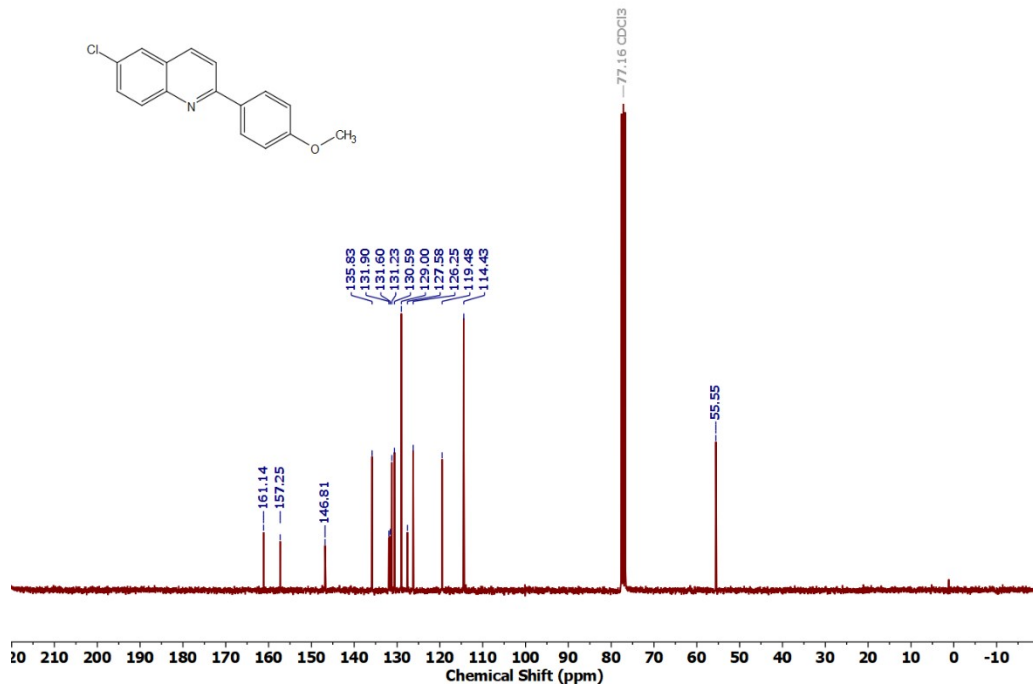
Figure S92: ^{13}C NMR spectrum of **10t**
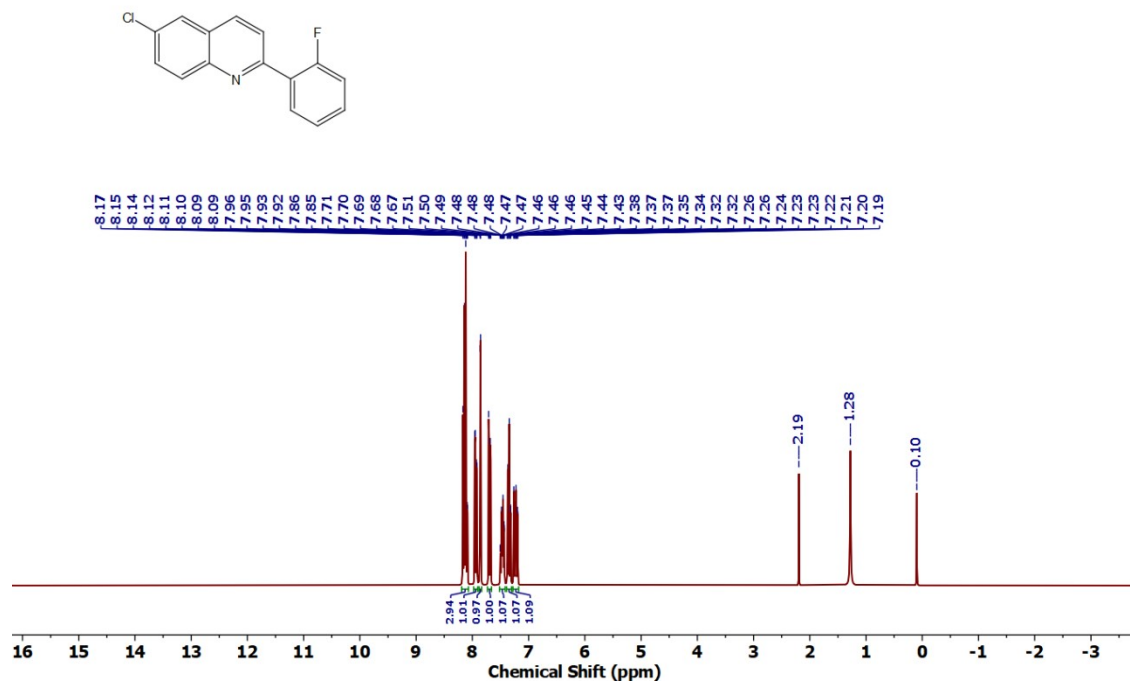
Figure S93: ^{1}H NMR spectrum of **10u**
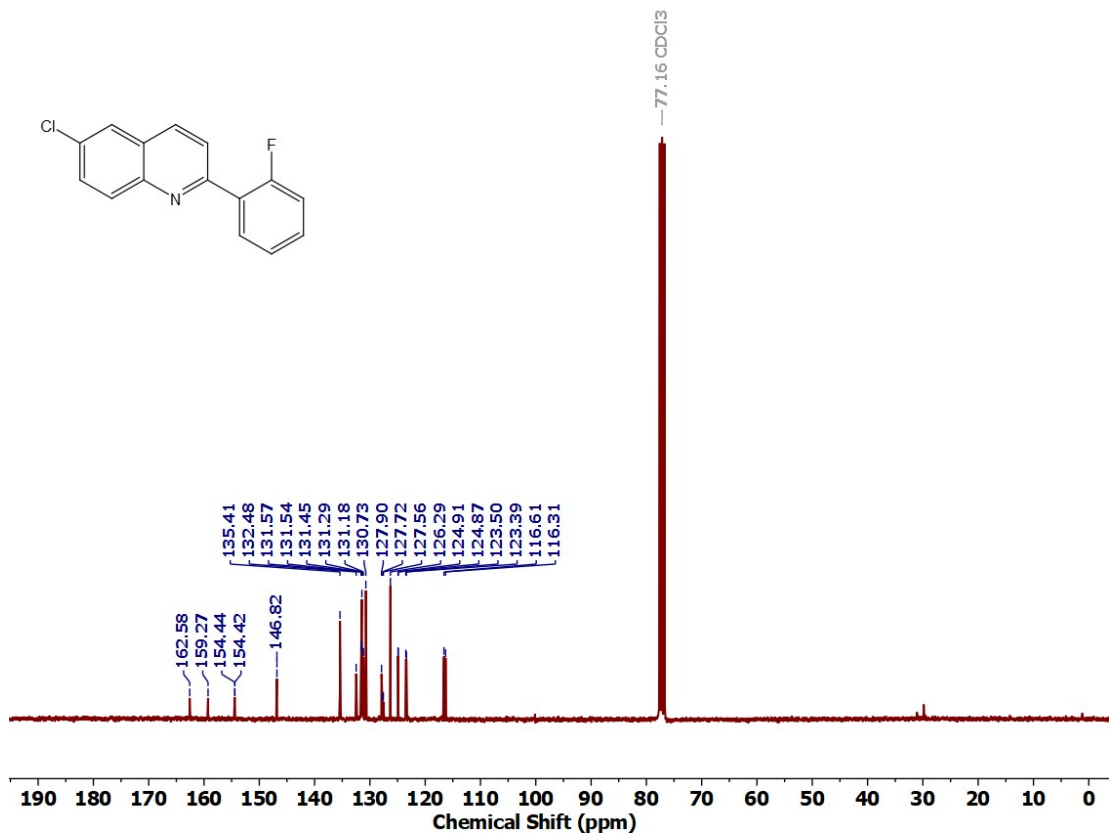
Figure S94: ^{13}C NMR spectrum of **10u**
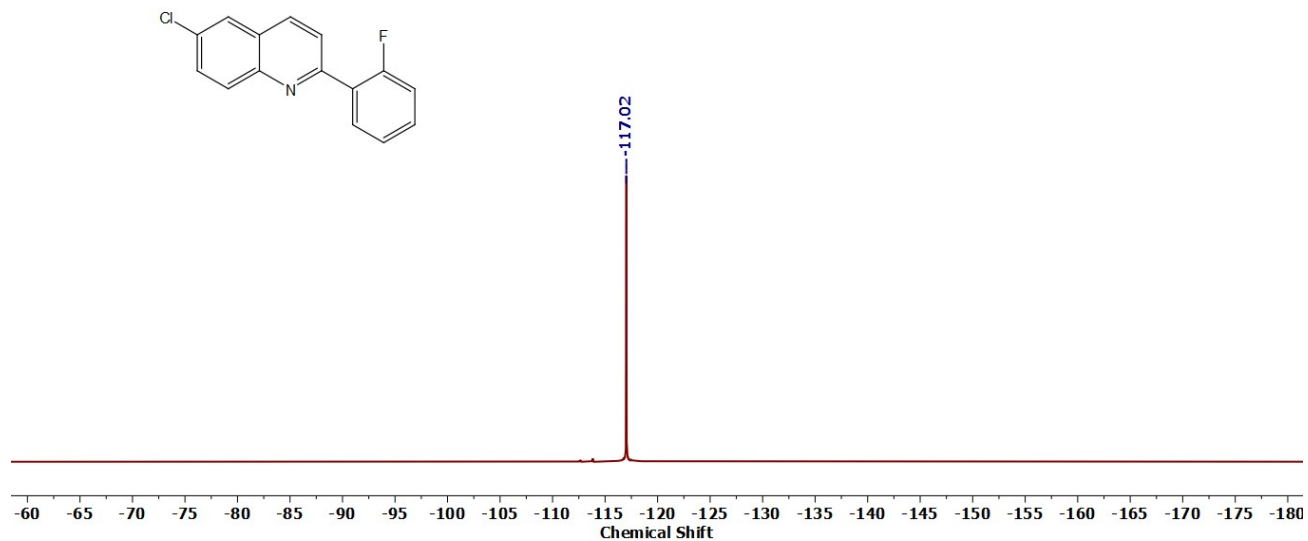
Figure S95: ^{19}F NMR spectrum of **10u**
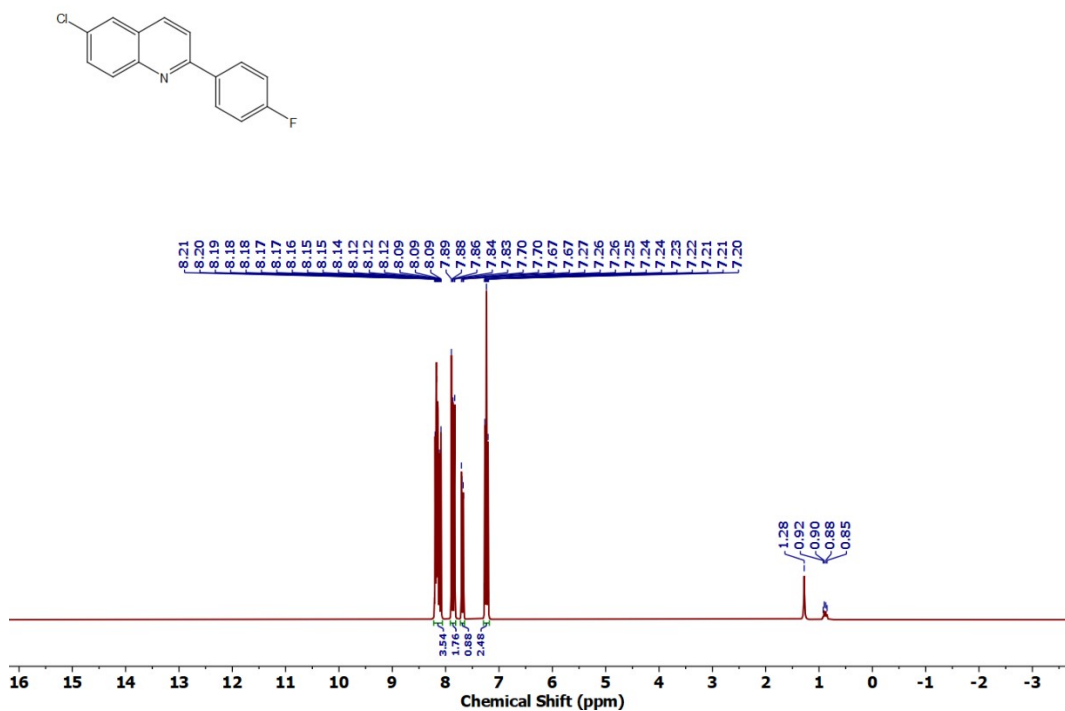
Figure S96: ^{1}H NMR spectrum of **10v**
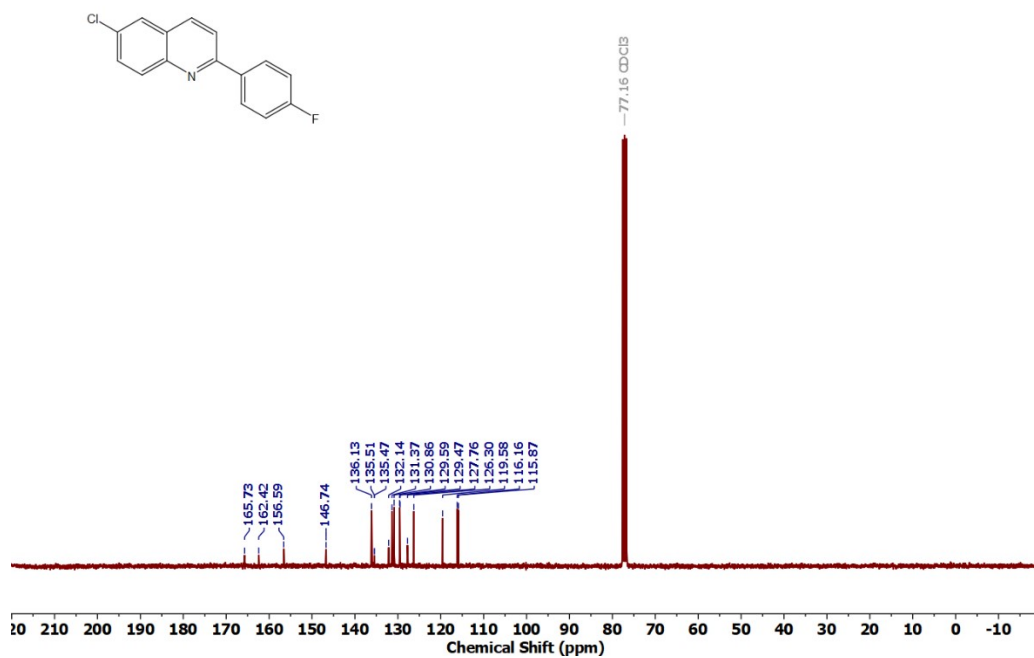
Figure S99: ^{13}C NMR spectrum of **10v**
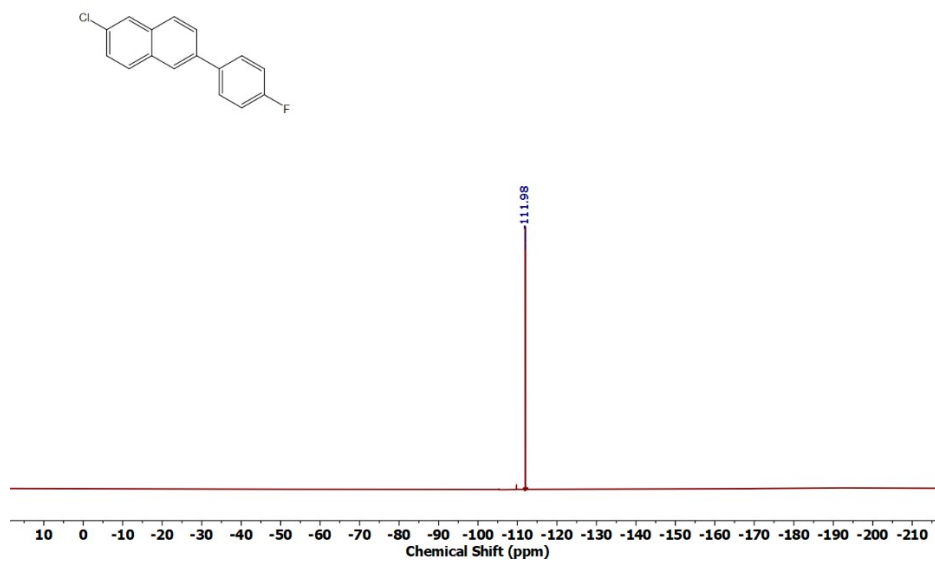
Figure S100: ^{19}F NMR spectrum of **10v**
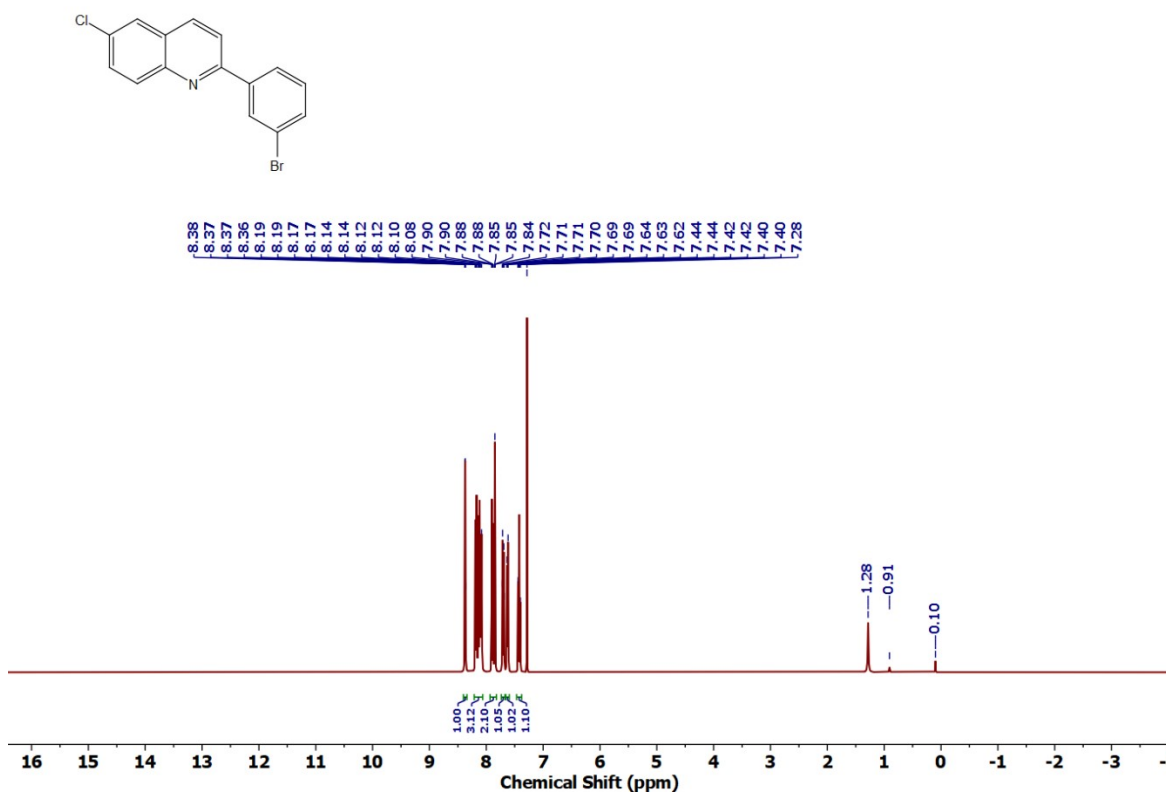
Figure S101: ^{1}H NMR spectrum of **10w**
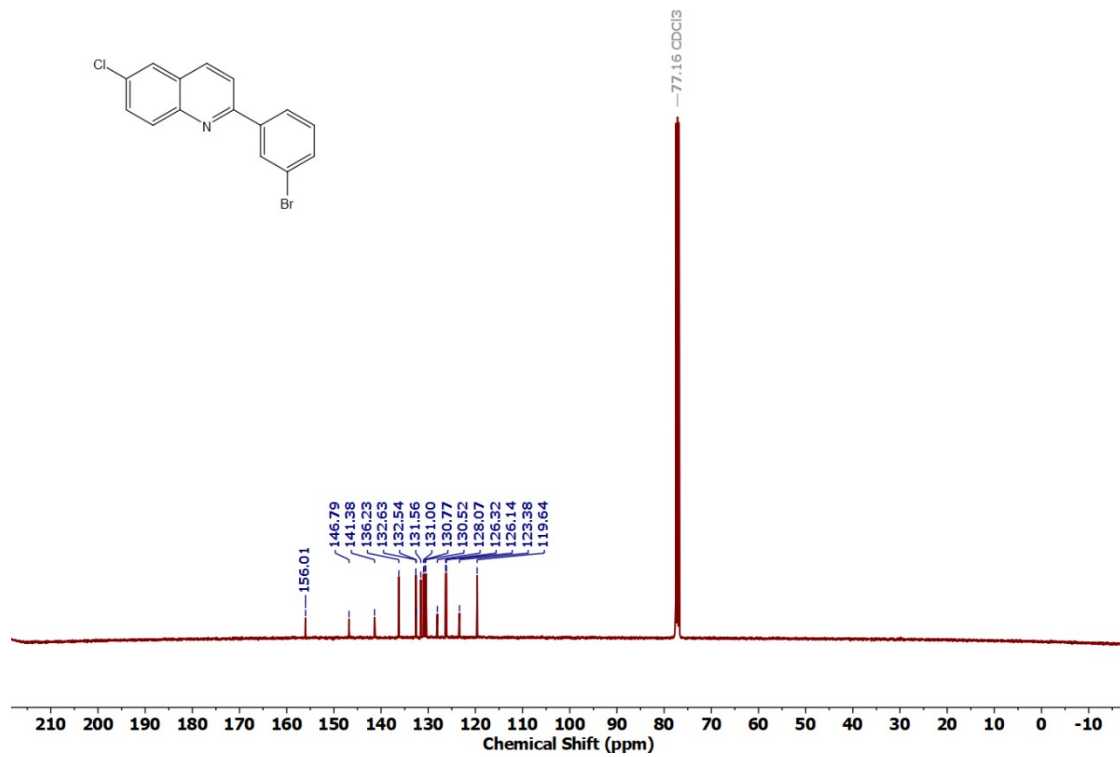
Figure S102: ^{13}C NMR spectrum of **10w**
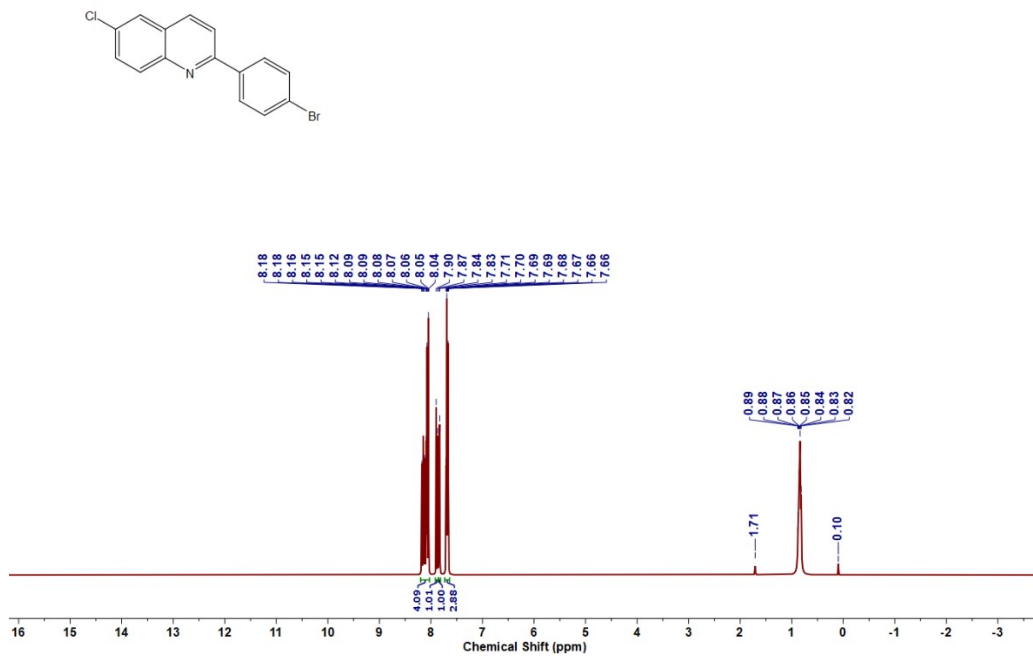
Figure S103: ^{1}H NMR spectrum of **10x**
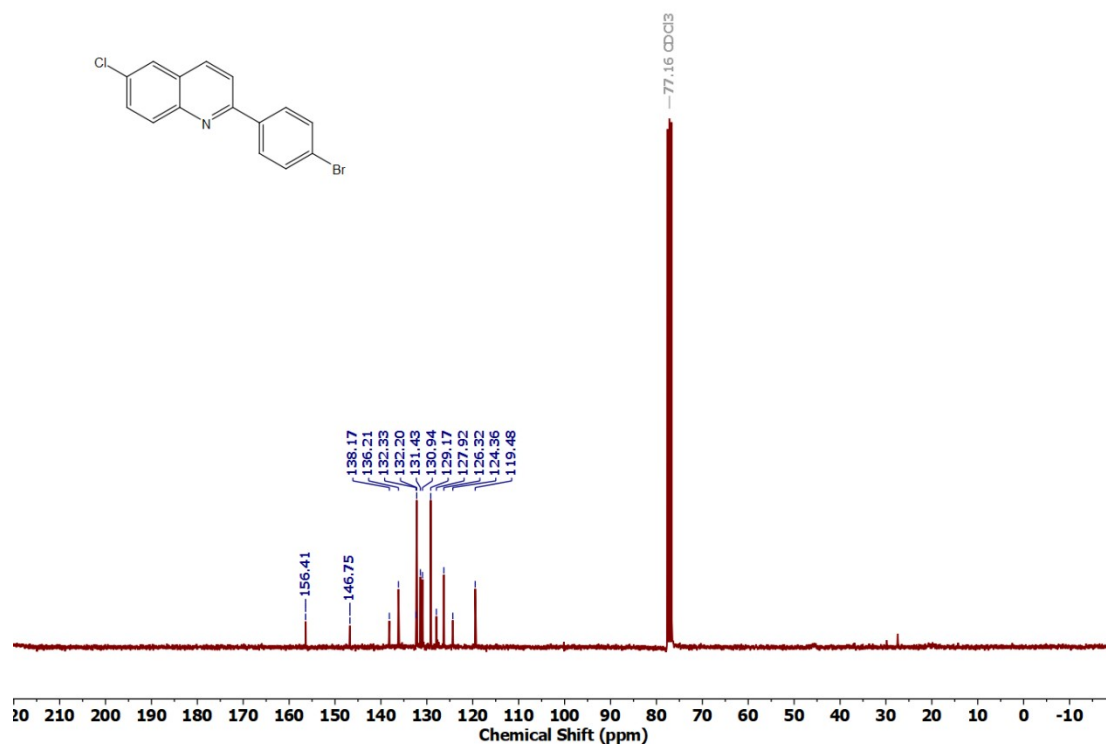
Figure S104: ^{13}C NMR spectrum of **10x**
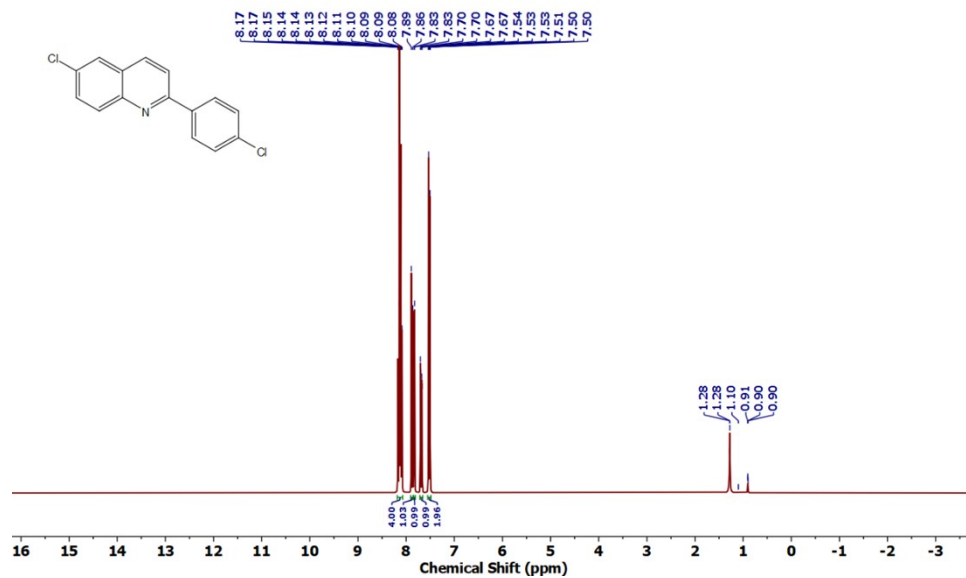
Figure S105: ^{1}H NMR spectrum of **10y**
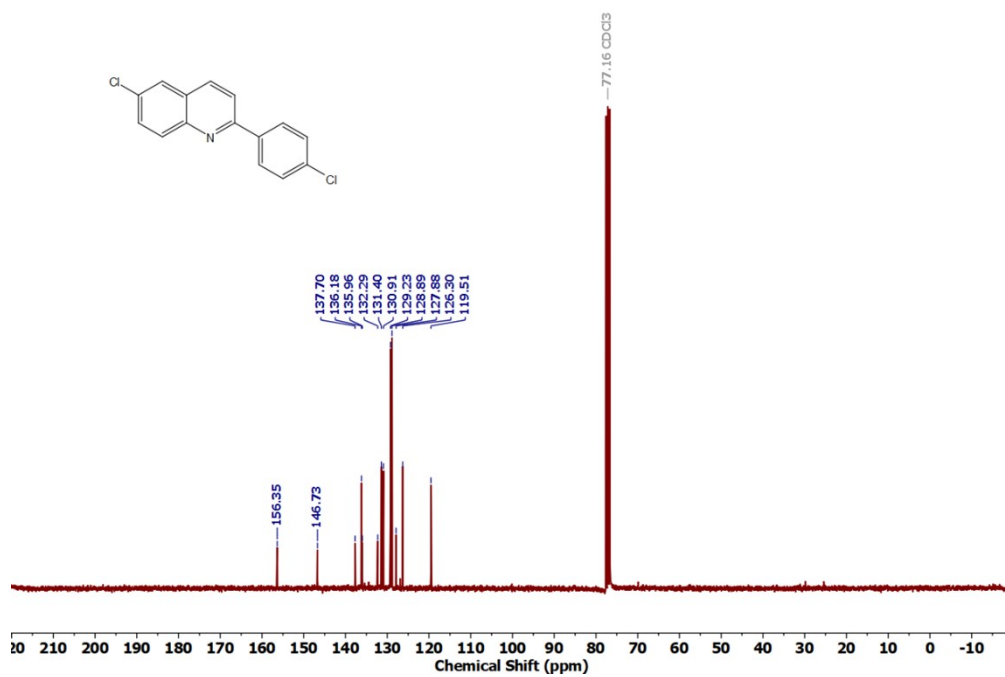
Figure S106: ^{13}C NMR spectrum of **10y**
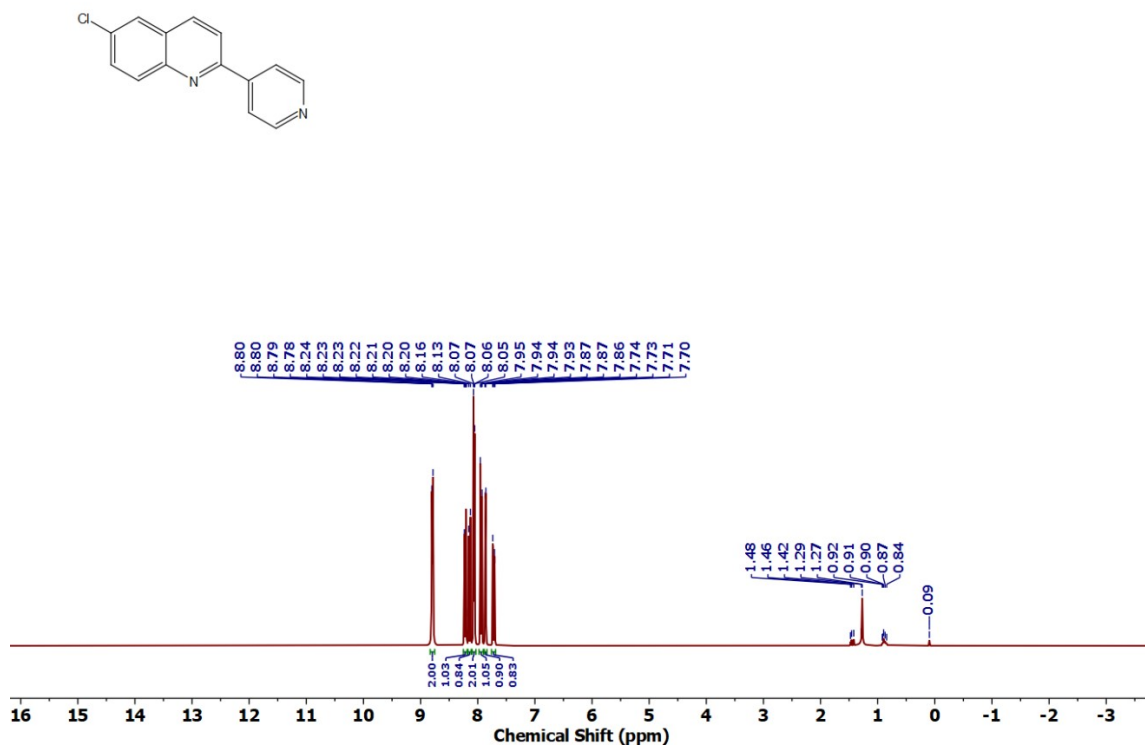
Figure S107: ^{1}H NMR spectrum of **10z**
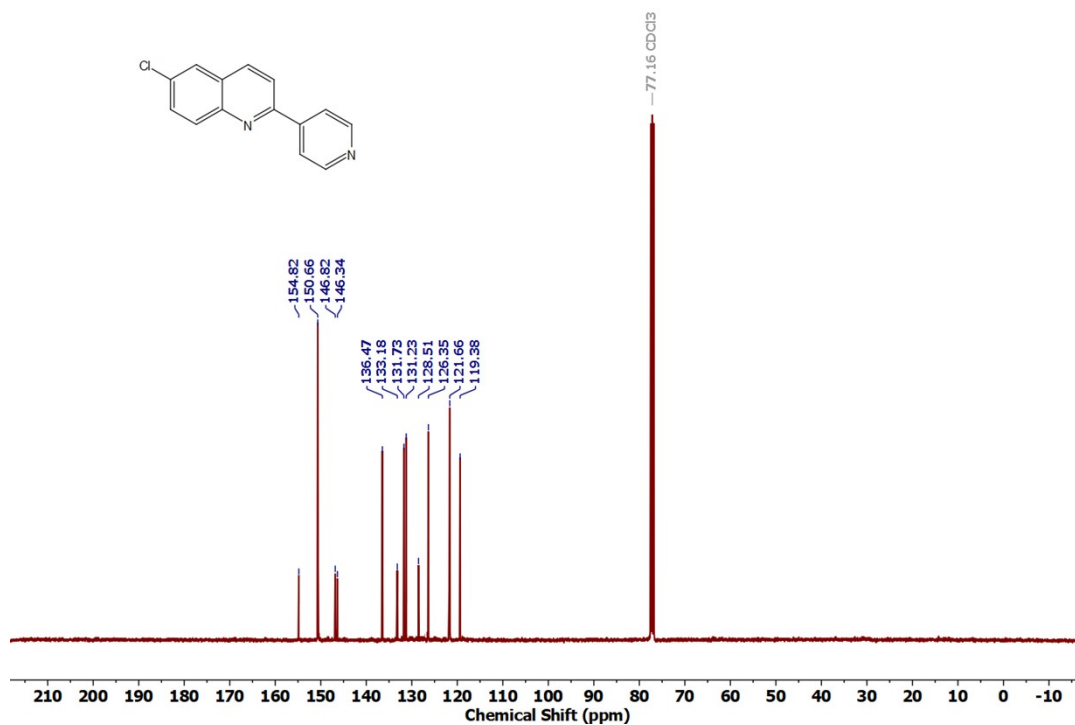
Figure S108: ^{13}C NMR spectrum of **10z**
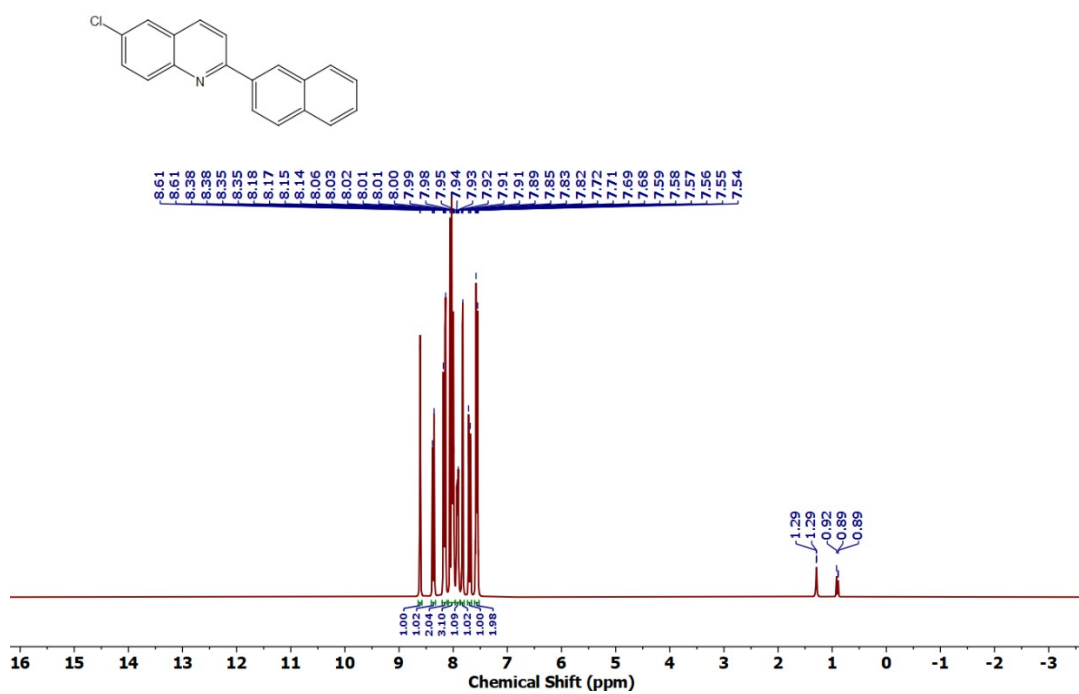
Figure S109: ^{1}H NMR spectrum of **10aa**
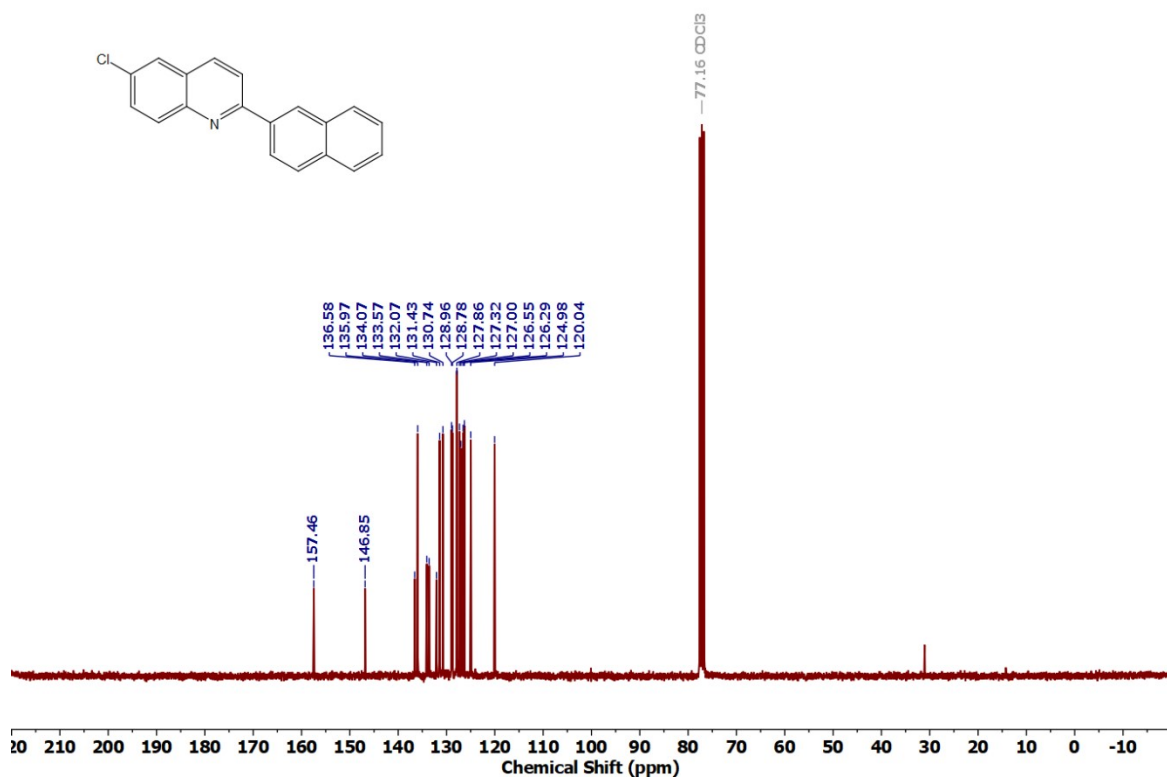
Figure S110: ^{13}C NMR spectrum of **10aa**
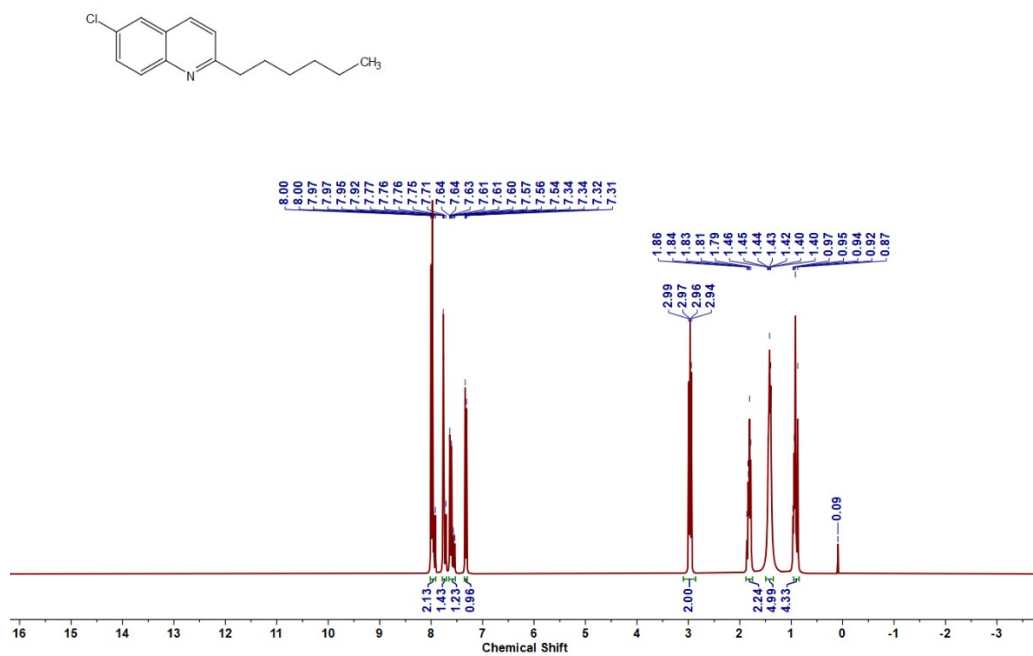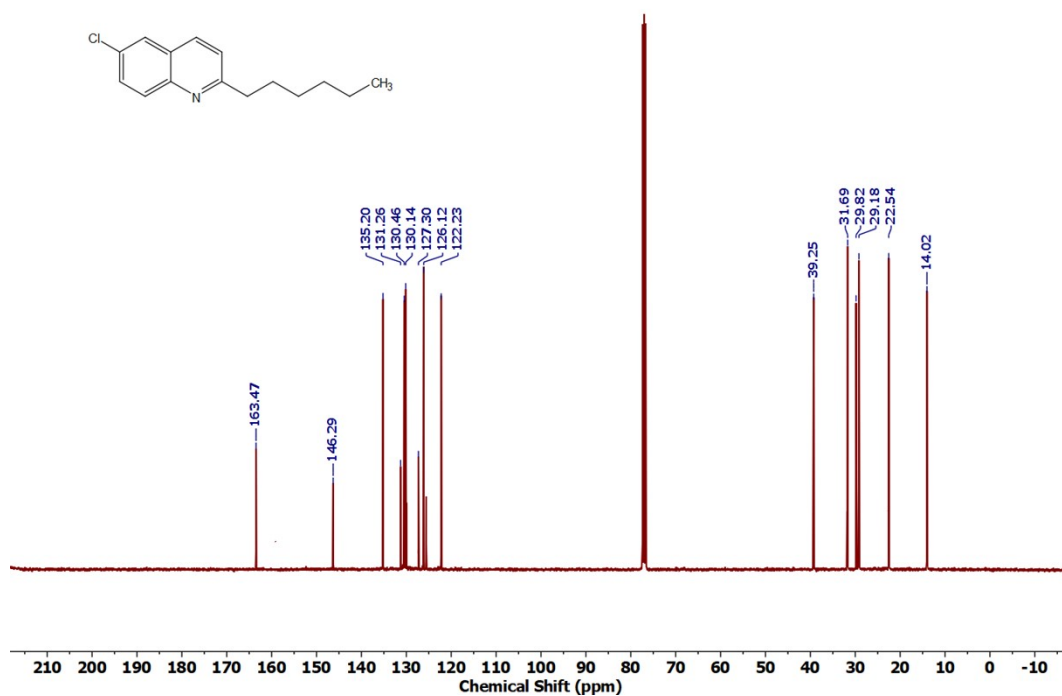

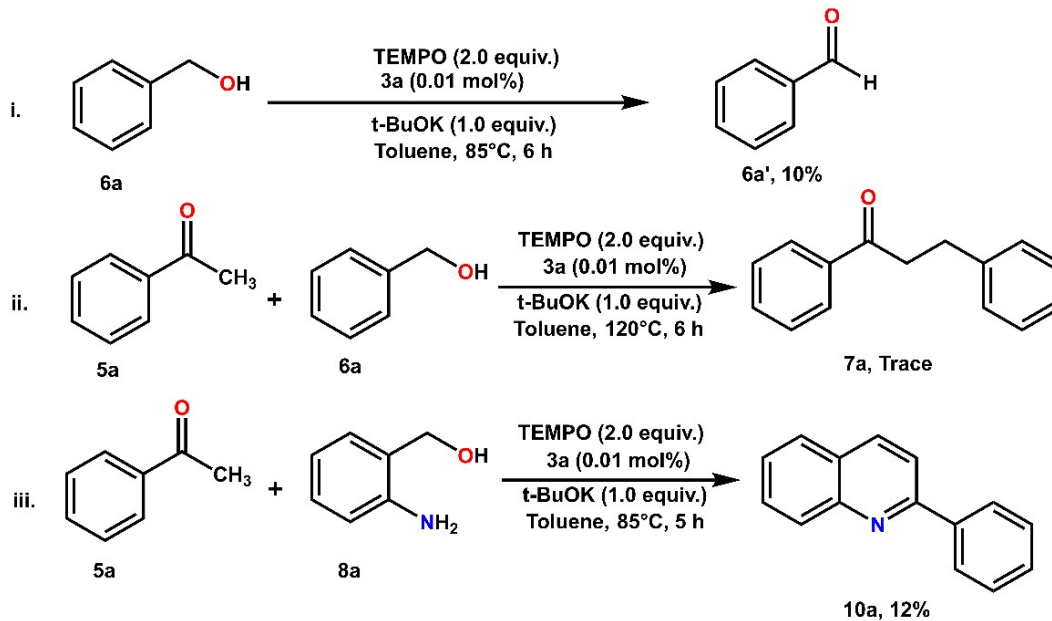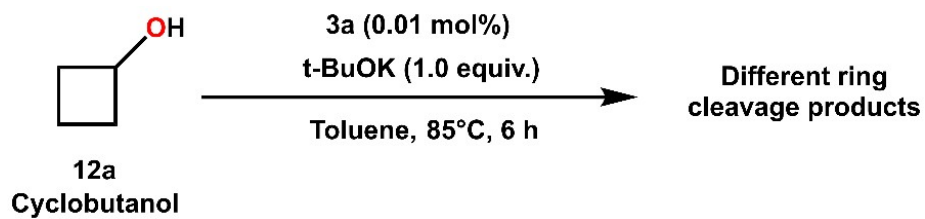**Figure S111:** ^1H NMR spectrum of **10ab**

Figure S112: ^{13}C NMR spectrum of **10ab**

Scheme S1: Investigation of active participation of radical intermediate during catalytic transformation

Scheme S2: Oxidation of radical clock substrate cyclobutanol under optimal condition
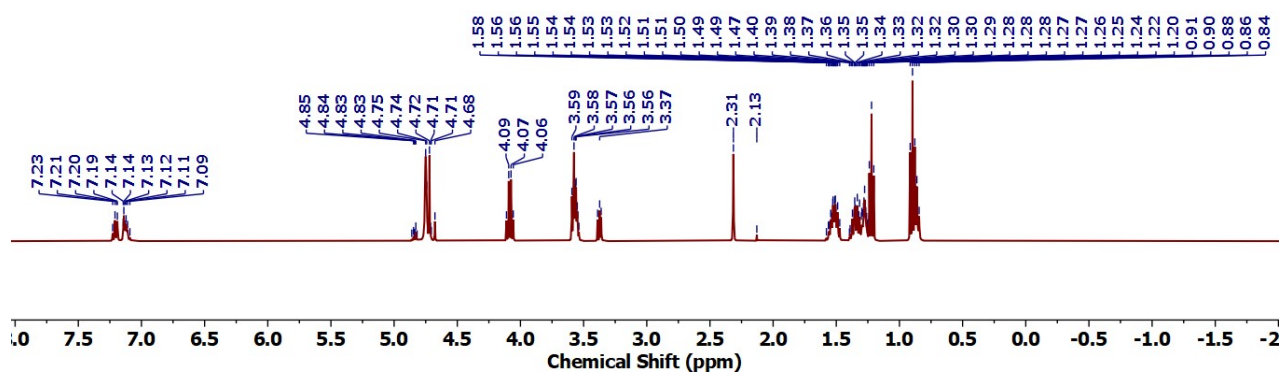

Figure S113: ^{1}H NMR spectrum of reaction mixture of oxidation of cyclobutanol
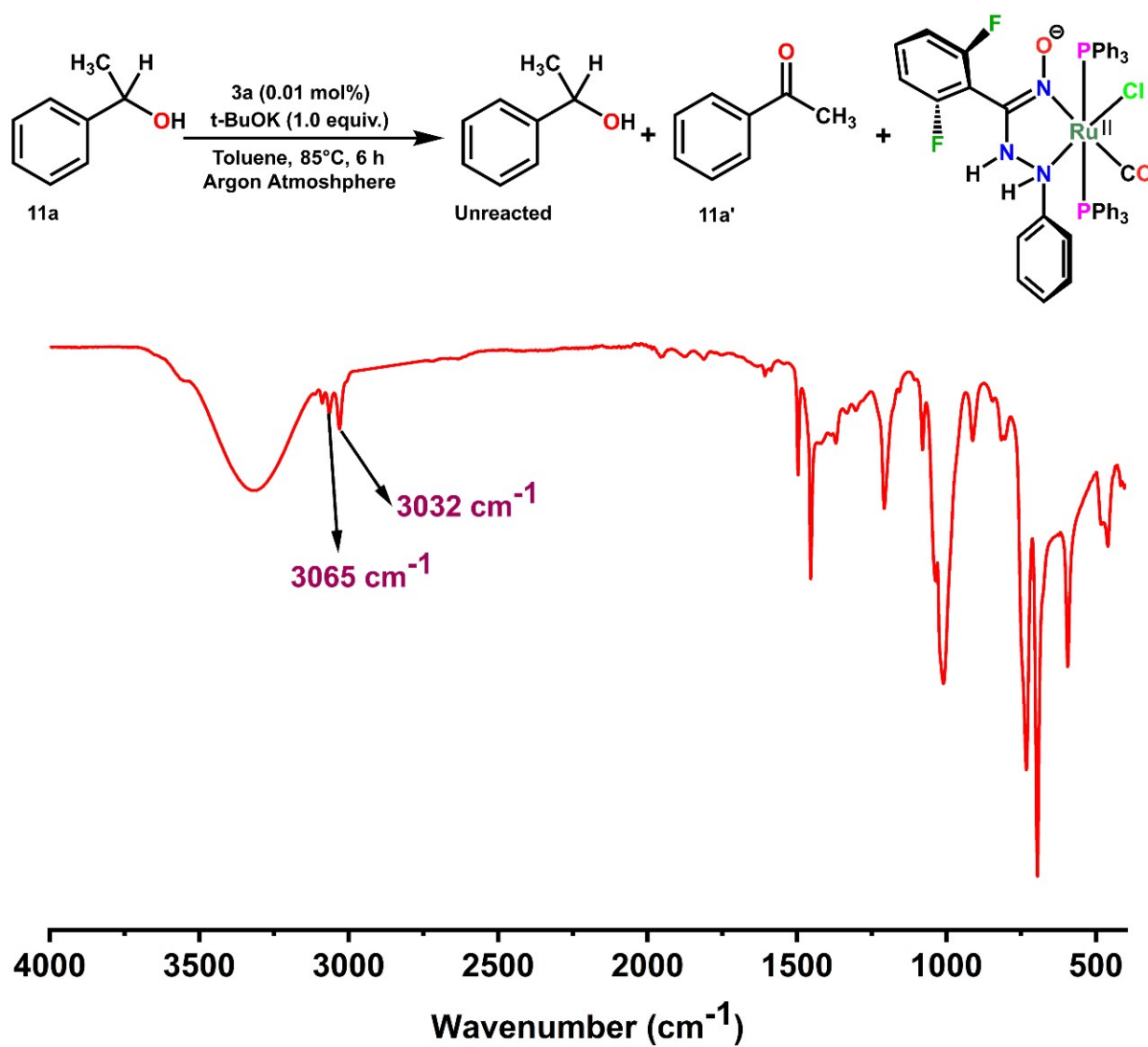
Figure S114: IR spectrum of the reaction mixture involving stoichiometric alcohol dehydrogenation of 1-phenylethanol (**11a**) under argon: involvement of azo/hydrazo redox couple with catalyst **3a**.
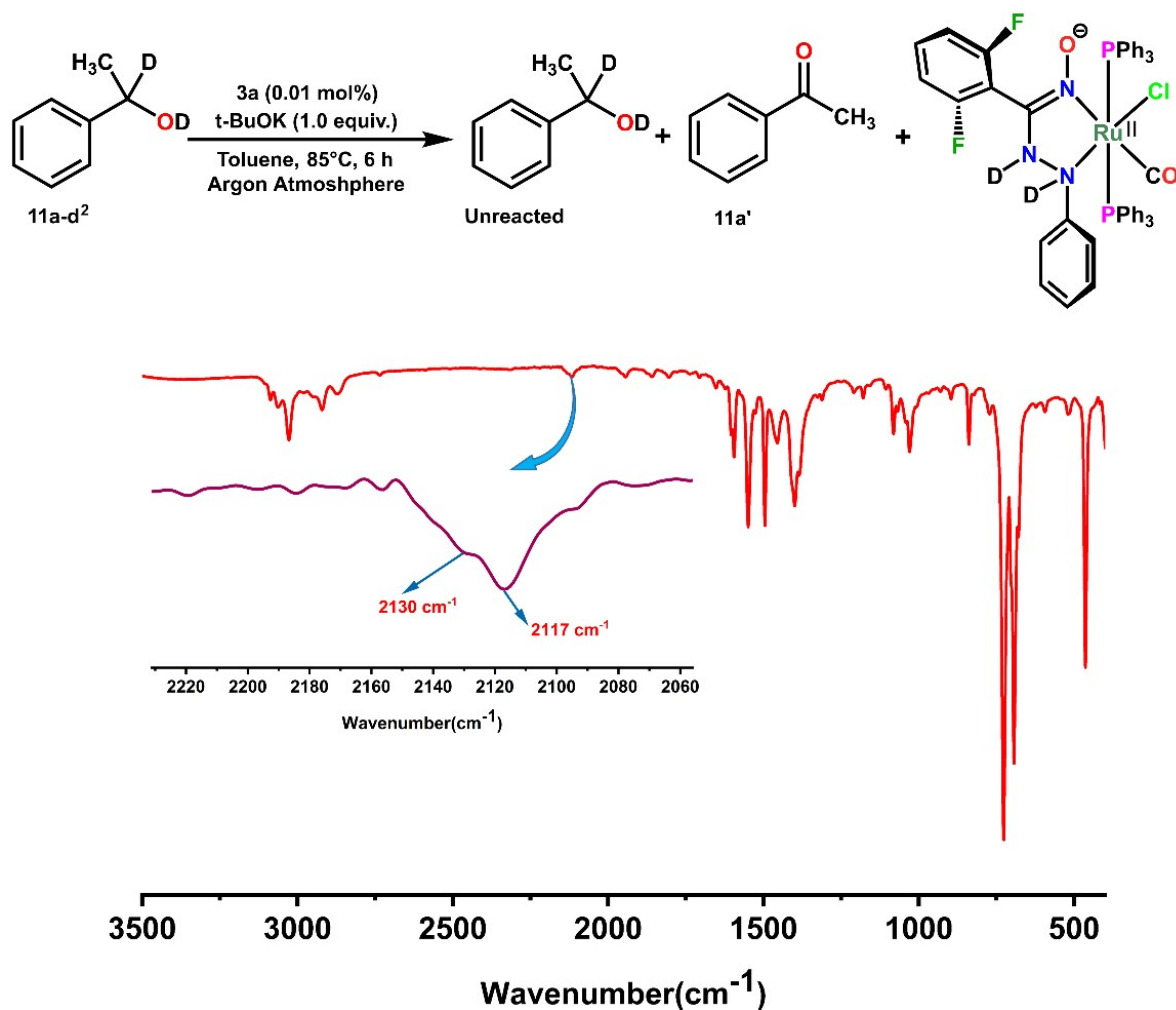
Figure S115: IR spectrum of the reaction mixture involving stoichiometric alcohol dehydrogenation of deuterated 1-phenylethanol (**11a-d²**) under argon: involvement of azo/hydrazo redox couple with catalyst **3a**.

Appendix: Supplementary data

X-ray crystallographic data of **1a**, **2a**, **3a**, **4a**, **10i** and **10t** have been deposited with the Cambridge Crystallographic Data Centre, (12 Union Road, Cambridge CB2 1EZ, UK, United Kingdom; fax: (+44) 1223-336-033; or email: deposit@ccdc.cam.ac.uk) under deposition number CCDC

2303590, 2303589, 2303602, 2303603, 2303607, 2303608 and can be access free of charge the Centre or via its website (http://www.ccdc.cam.ac.uk).

References:

1. SAINT, Data Reduction and Frame Integration Program for the CCD Area-Detector System. Bruker Analytical X-ray Systems, Madison, Wisconsin, USA, 1997–2006.

2. G.M. Sheldrick, SADABS, Program for Area Detector Absorption Correction, Institute for Inorganic Chemistry, University of Göttingen, Germany (1996).

3. G.M. Sheldrick, *Acta Crystallogr. Sect. C: Struct. Chem.*, 2015, **71**, 3-8.

4. O.V. Dolomanov, L.J. Bourhis, R.J. Gildea, J.A.K. Howard, H. Puschmann, *J. Appl. Cryst.*, 2009, **42**, 339-341.

5. A.D. Becke, *J. Chem. Phys.*, 1993, **98**, 5648-5652.

6. C. Lee, W. Yang, R.G. Parr, *Phys. Rev. B: Condens. Matter*, 1988, **37**, 785-789.

7. M. J. Frisch, G. W. Trucks, H. B. Schlegel, G. E. Scuseria, M. A. Robb, J. R. Cheeseman, G. Scalmani, V. Barone, B. Mennucci, G. A. Petersson, H. Nakatsuji, M. Caricato, X. Li, H. P. Hratchian, A. F. Izmaylov, J. Bloino, G. Zheng, J. L. Sonnenberg, M. Hada, M. Ehara, K. Toyota, R. Fukuda, J. Hasegawa, M. Ishida, T. Nakajima, Y. Honda, O. Kitao, H. Nakai, T. Vreven, J. A. Montgomery Jr., J. E. Peralta, F. Ogliaro, M. Bearpark, J. J. Heyd, E. Brothers, K. N. Kudin, V. N. Staroverov, R. Kobayashi, J. Normand, K. Raghavachari, A. Rendell, J. C. Burant, S. S. Iyengar, J. Tomasi, M. Cossi, N. Rega, J. M. Millam, M. Klene, J. E. Knox, J. B. Cross, V. Bakken, C. Adamo, J. Jaramillo, R. Gomperts, R. E. Stratmann, O. Yazyev, A. J. Austin, R. Cammi, C. Pomelli, J. W. Ochterski, R. L. Martin, K. Morokuma, V. G. Zakrzewski, G. A. Voth, P. Salvador, J. J. Dannenberg, S. Dapprich, A. D. Daniels, O. Farkas, J. B. Foresman, J. V. Ortiz, J.

Cioslowski, D. J. Fox, GAUSSIAN 09 (Revision A.01), Gaussian, Inc., Wallingford, CT, (2009).

8. J. Autschbach, T. Ziegler, S.J.A. Gisbergen, E.J. Baerends, *J. Chem. Phys.*, 2002, **116**, 6930-6940.

9.   K.L. Bak, P. Jørgensen, T. Helgaker, K. Rund, H.J.A. Jenson, *J. Chem. Phys.*, 1993, **98**, 8873-8887.

10. T. Helgaker, P. Jørgensen, *J. Chem. Phys.*, 1991, **95**, 2595-2601.

11. E.K.U. Gross, W. Kohn, *Adv. Quantum Chem.*, 1990, **21**, 255-291.

12. M. Cossi, N. Rega, G. Scalmani, V. Barone, *J. Comput. Chem.*, 2003, **24**, 669-681.

13. M. Cossi, V. Barone, *J. Chem. Phys.*, 2001, **115**, 4708-4717.

14. V. Barone, M. Cossi, *J. Phys. Chem. A*, 1998, **102**, 1995-2001.

15. T. Liu, H.X. Zhang, B.H. Xia, *J. Phys. Chem. A*, 2007, **111**, 8724-8730.

16. A. Albertino, C. Garino, S. Ghiani, *J. Organomet. Chem.*, 2007, **692**, 1377-1391.

17. X. Zhou, H.X. Zhang, Q.J. Pan, B.H. Xia, *J. Phys. Chem. A*, 2005, **109**, 8809-8818.

18. X. Zhou, A.M. Ren, J.K. Feng, *J. Organomet. Chem.*, 2005, **690**, 338-347.

19. P.J. Hay, W.R. Wadt, *J. Chem. Phys.*, 1985, **82**, 299-310.

20. P.J. Hay, W.R. Wadt, Ab Initio effective core potentials for molecular calculations. Potentials for the transition metal atoms Sc to Hg, J. Chem. Phys. 82 (1985) 270–283.

21. M.S. Gordon, J.S. Binkley, J.A. Pople, W.J. Pietro, W.J. Hehre, *J. Am. Chem. Soc.*, 1982, **104**, 2797-2803.

22. J.S. Binkley, J.A. Pople, W.J. Hehre, *J. Am. Chem. Soc.*, 1980, **102**, 939-947.

23. N.M. O'Boyle, A.L. Tenderholt, K.M. Langner, *J. Comput. Chem.*, 2008, **29**, 839-845.